2011

ELECTROSPUN POLYMER-FIBER SOLAR CELL

Shinobu Nagata
Virginia Commonwealth University

“ELECTROSPUN POLYMER-FIBER SOLAR CELL”

A dissertation submitted in partial fulfillment of the requirements for the degree of Doctor of Philosophy at Virginia Commonwealth University.

by

SHINOBU NAGATA
Bachelor of Arts, University of Colorado, 2004
Master of Science, Virginia Commonwealth University, 2007

Director: James T. McLeskey, Jr., Ph. D
Associate Professor, Mechanical Engineering

Virginia Commonwealth University
Richmond, Virginia
August, 2011

Acknowledgement

I would like to thank my mentor and advisor Dr. James T. McLeskey for providing me with such vital direction and support throughout this project. His guidance has led me towards new research opportunities and eventually brought me to my next career stage - a research position in California.

I would also like to express my gratitude towards Dr. Chunya Wu for showing me the basics and helping me get acquainted with the lab, Dr. Dimitry Pestov for giving me the most precise and well-observed suggestions for my research , Dr. Gary Tepper for allowing me to collaborate with his lab to perform research on his electrospinning experiment., Dr. Gary Atkinson for guiding me through several equipments at the Virginia Microelectronics center, Mr. Josh Starliper for being a tremendous support and a great friend for years to come, and Dr. Mikhail Reshchikov and Dr. Supryo Bandyopadthay for teaching me many valuable lessons in research which have proven to become critical inputs for my study.

I would like to thank my families and friends for their love and support and to my lab mates whom made my time at VCU enjoyable through the exchange of many discussions about the physics of solar cells.

Finally, I would like to thank the Huynh family and especially Ms. Phuong Huynh for helping me every step of the way toward the final stages of my dissertation. She has diligently helped me count solar fibers, edited my documents, and a significant part of my work would have not been possible without the help of her and her family.

Table of Contents

List of Figures

Abstract

A study of fabricating the first electrospun polymer-fiber solar cell with MEH-PPV is presented. Motivation for the work and a brief history of solar cell is given. Limiting factors to improvement of polymer solar cell efficiency are illustrated. Electrospinning is introduced as a technique that may increase polymer solar cell efficiency, and a list of advantages in the technique applied to solar cell is discussed. Results of electrospun polymer-fiber solar cell, absorption, and its device parameter diagnosis through an equivalent circuit analysis are presented.

1. INTRODUCTION

1.1 Introduction and Motivation

There is a strong demand for renewable energy sources in the world today. The IEA (International Energy Agency) has reported that in the year 2006, 87.1% of electricity in the world was generated from non-renewable resources (coal, nuclear, gas and oil) [1]. Each of these sources can impact the environment in ways such as acid rain, radioactive waste, CO_2 pollution, and imported greenhouse gasses.

In 1956, M. King Hubbert created a theoretical model predicting the peak of oil production to be around year 1965 to 1970 [2]. Many other models were developed predicting the time period of peak oil differing from the Hubbert Peak theory. However all of the models have shown that oil production will decline, and oil is limited in supply. The limitation in supply can lead to an increase in price of gasoline with significant impact to the economy, and cause strain in the nation's electricity such as the 2008 spike in the price of gasoline. Considering that petroleum oil makes up 34.4% of the total primary energy supply along with all the negative impact of non-renewable resources, it is clear that alternatives to non-renewable resources must be investigated.

In response to the energy crisis we face around the world, solar energy is attracting considerable attention as one of next generation energy sources. It has been noted by the U.S. Department of Energy that covering 0.16 % of the earth's surface by 10 % efficient solar cells will provide ~20 TW ($2x10^{13}$ W) of electricity, more than enough to cover the energy demand of the whole planet [3]. With the sun emitting

energy that is virtually unlimited in supply, solar cells have significant potential as a next generation energy source.

The modern solar cell was first demonstrated in 1954 at Bell Labs. It was 6 % efficient and made from crystalline silicon (c-Si) [4]. C-Si solar cells were further developed reaching an efficiency of 14-18 % [5], and more than 95 % of current solar cells in use are c-Si solar cells [6]. In 1974, the amorphous silicon (a-Si) solar cell was invented at RCA Laboratories as an alternative to c-Si device [7]. An a-Si solar cell was made by evaporation of silicon to produce amorphous thin films requiring less material that would lower the cost of solar cell production [8]. The a-Si solar cell has a relatively low 6-8 % efficiency due to high defect densities from evaporation processing. However, the thin film approach used in a-Si solar cell allowed further development utilizing multilayer processing to produce multijunction solar cells, and has led to an efficiency higher than 40 %[9-11] for $Ga_xIn_{1-x}As$ or $Ga_yIn_{1-y}P$ solar cells by stacking different materials to absorb a larger portion of the available sunlight.

Regardless of the significant improvements made in efficiencies of inorganic photovoltaics, they continue to struggle in competing against non-renewable resources due to their high cost. The primary problem is in high energy processing of silicon, and the cost per kilowatt-hour for electricity from Si-based solar cells is as high as $0.25-0.65 /kWh which is roughly 5 times more than the price of electricity produced using fossil fuels [12]. Adding to the high cost of inorganic solar cells, the potential increase in demand for crystalline Si can lead to even higher costs for the devices. One estimate has calculated that for a family consuming 20 kWh/day using 15 % efficient solar cells,

the amount of silicon needed would 10,000 times more than that in a computer [13]. Clearly, a low cost alternative to inorganic solar cells is needed.

Polymer solar cells are a low cost alternative to inorganic solar cells. In addition to the lower cost of polymer solar cells, the use of polymeric materials are known to have several advantages such as lighter weight, and less energy used for large scale production, thanks to solution based processing. Polymer solar cells have significant mechanical flexibility, and are capable of being directly fabricated onto most surfaces including plastics. However, the efficiency of polymer solar cells is still low compared to inorganic solar cells due to poor light harvesting, limited photocurrent generation, and poor charge transport. This dissertation outlines these challenges in polymer solar cells, and will discuss a unique approach of utilizing a technique called electrospinning to resolve these issues. The work is to produce the first ever electrospun polymer-fiber photovoltaic cells.

1.2 Objectives

The objective of this project is to synthesize and characterize polymer-fiber solar cells by electrospinning. It is expected that these new devices will yield increased absorption, improved charge transport and improved charge collection. Increase in these parameters can lead to improved efficiency of the device added to potential lower cost benefits of polymer solar cells. The intention of the dissertation outlined in this proposal is to demonstrate a functioning electrospun polymer-fiber solar cell and characterize its output. The specific goals of the work are fabrication of the first ever polymer-fiber solar cell, and an investigation of triaxial electrospinning as the next step to fabrication of quasi-one dimensional solar cells.

1.3 Dissertation Outline

Chapter 2 presents a background and literature review of organic solar cells. Information on solar radiation and air mass are introduced. Basic characteristics of solar cells are explained. History in development of polymer solar cells is followed. Properties of polymers in organic solar cells are discussed, and different device architectures are discussed with their advantages along with their disadvantages.

Chapter 3 starts with the history of the electrospinning experiment, and its operation. Electrospinning and its application to solar cells are discussed. Some advantages for solar cells made using electrospining are illustrated.

Chapter 4 introduces an unusual occurrence of bimodal fibers in electrospinning. An experiment using a water soluble PTEBS polymer is discussed, and its applicability to solar cells is considered. Significance in humidity for electrospinning is illustrated through an experiment using PTEBS, and its applicability to solar cell synthesis is discussed.

In Chapter 5, three electrospun polymer-fiber solar cell device structures are presented. A bulk heterojunction type polymer-fiber solar cell is considered for its conventional metal-semiconductor-metal structure. Triaxial electrospining is considered for its structural advantages along with its simple solar cell fabrication process. The co-planar bimetallic interdigitated electrode substrate is then introduced for a simple solar cell fabrication process of spin-on device synthesis.

Chapter 6 explains the development of the co-planar bimetallic interdigitated electrode. An experiment is performed with an MEH-PPV:PCBB film spin-coated on

the surface of the electrode. The new electrode substrate is validated from the spin-coated film achieving an efficiency of 3.53×10^{-4} % using an MEH-PPV:PCBM film.

Chapter 7 presents the choices made for the materials used in synthesis of electrospun polymer-fiber solar cell. P3HT and MEH-PPV are compared based on their absorption changes in nanofiber structure, and solvents are chosen from evaluation of photoluminescence spectra. MEH-PPV to PCBM mixture is shown to have better performance for a high weight fraction of PCBM. The amount of PCBM, along with the possible use of PCBB is considered and optimized through electrospun polymer nanofiber morphology.

Chapter 8 presents the performance and morphology of the electrospun polymer-fiber solar cell. Details of the experiment are explained, and an image is shown to prove the fiber morphology of the solar cell. The Current-voltage characteristics of the device are illustrated, and the efficiency of device is estimated from illuminated area of the solar cell, and also from the active area of the solar cell. Based on illuminated area and from the active area of the solar cell, energy conversion efficiencies of 7.92×10^{-10} %, and 3.08×10^{-7} % are achieved, respectively.

Chapter 9 shows the characteristics of the electrospun polymer-fiber solar cell through measurement of absorption. A series of nanofibers prepared using different polymer concentrations are measured for absorption, and show a consistent increase in the amount of red shift. The reason behind this red shift is explained through electrospinning, and its effect in polymer chain structures.

In chapter 10, the device parameters of the electrospun polymer-fiber solar cell are discussed. An efficiency of the device is studied in consideration for the unique device

structure which leads us to conclude that the device efficiency is 3.08×10^{-7} % or better. An equivalent circuit analysis is performed from the current-voltage characteristic equation to understand the relationship between different resistances and fill factor. Chapter 11 concludes with the summary of this work, and future work to be considered for further research in synthesis of electropsun polymer-fiber solar cell.

2. Background and Literature Review

2.1 Solar Radiation

Through series of nuclear fusion reaction of hydrogen and helium, the surface temperature of the sun at 5800 K is hot enough to ionize all elements at this temperature, and emits wide spectrum of radiation. This radiated energy is then either scattered or absorbed on a clear day, and roughly 76% of the incident energy reaches the earth surface (shown in Table 1).

Table 1

Absorption and scattering under typical clear sky conditions			
Factor	Percent absorbed	Percent scattered	Percent of total passing through the atmosphere
Ozone	2%	0%	
Water vapor	8%	4%	
Dry air	2%	7%	
Upper dust	2%	3%	
Lower dust	0%	0%	
Total absorbed or scattered	87%	87%	76%

Considering the atmospheric loss of energy in solar radiation, the amount of radiation can be classified by the air mass coefficient (AM) defined as

$$AM(number) = \frac{1}{\cos\theta}$$

AM0 is the extraterrestrial radiation, AM1 is the vertical incidence of sunlight at the equator at sea level, and AM1.5 is the sunlight radiating through an air mass 1.5 greater than the vertical case [14]. A standard solar radiation has a spectrum around the visible wavelengths from 380 nm to 780 nm as shown in Figure below

Figure 1: http://solardat.uoregon.edu/SolarRadiationBasics.html

2.2 Characteristics of Solar Cells

In characterizing a solar cell, the general interest is in the performance of the device, and its efficiency (η). The efficiency is measured by looking at the ratio between the power input of the incoming light, and the maximum power output of the device. The power output of a solar cell is measured, and characterized by observing the relationship between its current density and voltage known as the J-U curve. With a working solar cell, a J-U measurement will be a curve similar to a photodiode as shown below,

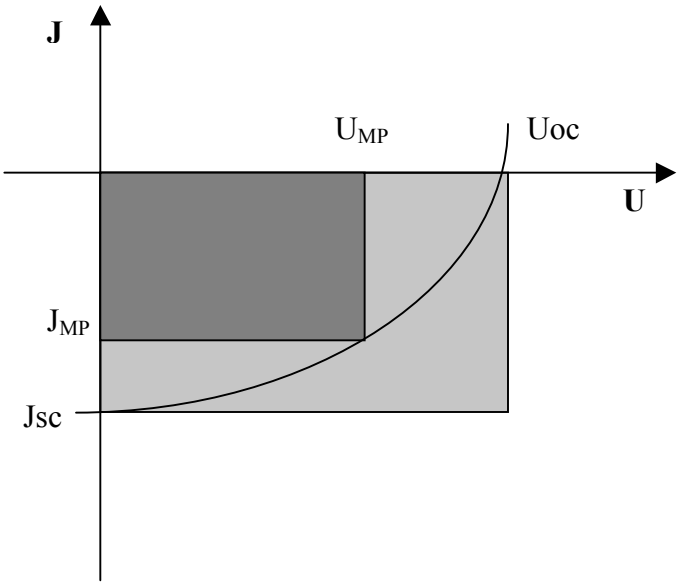

Figure 2: Typical J-U curve of a photovoltaic cell with white light illumination.

A J-U curve of a solar cell will then have a current under short circuit conditions (Jsc), and a voltage under open circuit conditions (Uoc) where these parameters are used to compute the power output, and the power conversion efficiency (η) of a solar cell.

2.2.1 Open Circuit Voltage and Short Circuit Current

When there is no external load on a solar cell, there is a built-in electrical potential between the two terminals of the device under white light illumination, and this is called the open circuit voltage (U_{oc}). U_{oc} is the measure of maximum voltage produced by the device, and it is measured when the load is connected to infinite resistance. The built-in electrical potential V_{oc} will then cause a drift in the photogenerated charges of the device known as the short circuit current (J_{sc}). J_{sc} is the measure of maximum current produced by the device, and it is measured when the load is connected to zero resistance. Using these values, the quality of a device can be characterized by looking at a number called the fill factor (FF).

2.2.2 Fill factor

The ratio between the maximum electrical power, and the theoretical maximum of electrical power estimated from the product of J_{sc} and U_{oc} gives the fill factor (FF) defined as,

$$FF = \frac{P_{Max}}{P_{Theoretical}} = \frac{J_{MP}U_{MP}}{J_{SC}U_{OC}}$$

where J_{MP} and U_{MP} are current density and voltage of maximum electrical power output of the device. Fill factor is essentially a measure of quality of the device, and it can also be seen as the ratio between the dark shaded areas of the J-U curve to the lightly shaded area of the J-U curve (Figure 2). With higher fill factor, the device is able to extract more electrical power from a constant current source with a maximum voltage.

2.2.3 Energy Conversion Efficiency

Solar cell efficiency is a measure of how effectively a device is able to convert the energy of the sun to electricity. Therefore, an efficiency of a solar cell is a ratio between the electrical power output of the cell, and the incident optical power. Solar cell efficiency η is then given by,

$$\eta = \frac{J_{MP}U_{MP}}{P_{light}} = \frac{(FF)J_{SC}U_{OC}}{P_{light}} \qquad [14]$$

2.3 Polymer Solar Cells

2.3.1 History

Single organic layer (e.g., tetracene) solar cells were the first reported in the late 1960s and early 1970s, and consisted of an organic layer sandwiched between a low-work-function metal layer (aluminum) and a high-work-function metal (gold) as shown in Figure 3 [15-19] ,

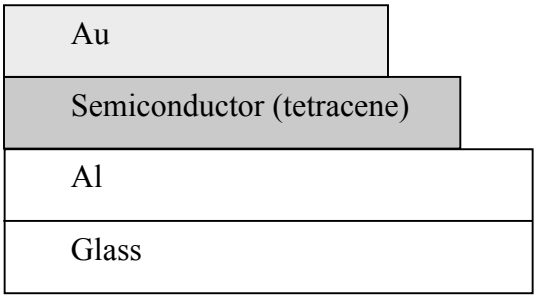

Figure 3: Single organic layer (e.g., tetracene) solar cells.

In 1977, Shirakawa et al introduced doped polyacetylene as a new class of conducting polymers in which the electrical conductivity can be systematically and continuously varied over a range of eleven orders of magnitude [20]. Since that time, electronic devices such as OLEDS and polymer solar cells have been the subject of extensive research. Polymer solar cells utilize two materials working in pairs: a light absorbing polymer donating an electron to an electron acceptor.

For homojunctions, growth of a thin oxide layer on the low-work-function material was recognized as an electron acceptor in 1983, where it formed a metal-insulator-semiconductor (MIS) structure Schottky-type photodiodes demonstrating a photovoltaic effect [21]. Extremely low efficiencies of these devices (~10^{-4}%) [16] led

to research in testing wide array of materials by different research groups. However, the efficiencies of homojunction organic solar cells remained below 1% [21].

Breakthrough advances in organic solar cells were made first by Harima et al in 1984, and Tang in 1986 with the introduction of two-component organic photovoltaic cell [22,23]. A power conversion efficiency of 1% under AM2 illumination was achieved through the use of zinc phthalocyanine (ZnPc) and porphyrin derivative (TPyP) thin films [22], and also with copper phthalocyanine (CuPc) and a perylene tetracarboxylic (PV) derivative [23]. Figure 4 shows the device layout of two-layer organic photovoltaic cell by Tang.

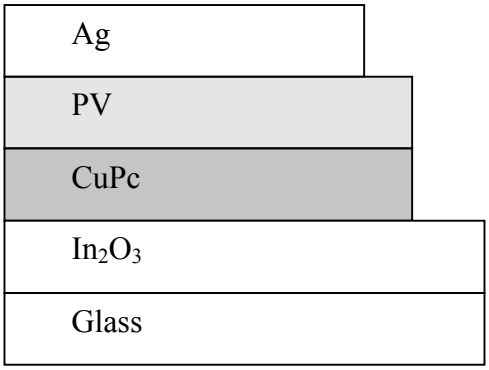

Figure 4: Two organic layer solar cells.

Through research on these heterojunction polymer solar cells, the charge transfer at the interface between two materials were found to be energetically favorable with distinct electron donor and acceptor layers [24].

2.3.2 Properties of polymers in Organic photovoltaics

For organic solar cells, the most common polymers have included the poly(phenylenevinylenes) such as MEH-PPV and the polythiophenes such as: poly(3-

undecyl-2,2 '-bithiophene) or P3UBT and poly(3-hexylthiophene) or P3HT. These conjugated polymers have semiconducting characteristics resulting from their alternating single (σ-bonds) and double carbon-carbon bonds (σ-bond and π-bond combination). With delocalized π-bonds over the entire molecule, the overlapping p_z orbitals formulate two orbitals that are called a bonding (π) orbital and an antibonding (π*) orbital. These two orbitals are the source of semiconducting properties of conjugated polymers where π-orbital are the highest occupied molecular orbitals (HOMO) with lower energy, and π*-orbitals are the lowest unoccupied molecular orbitals (LUMO) of higher energy. The difference in these two orbitals energy levels are the source of a polymers band gap, and their optical properties such as photon absorption and emission. HOMO/LUMO levels and band gap of various polymers are summarized in Table 2 below.

Table 2: HOMO/LUMO levels and band gaps of various polymers.

Conjugated polymers	LUMO (eV)	HOMO (eV)	Band gap (eV)	Reference
P3OT	-2.85	-5.25	2.4	[25][26]
MEH-PPV	-3	-5.3	2.3	[27]
MDMO-PPV	-2.8	-5.0	2.2	[28]
PTEBS	-2.8	-5.0	2.2	[29-32]
P3HT	-3.2	-5.2	2.0	[33]
PPE-PPV(DE21)	-3.6	-5.6	2.0	[34]
APFO Green 2	-3.6	-5.6	2.0	[35]
PPE-PPV(DE69)	-3.56	-5.46	1.9	[34]
PTBTB	-3.73	-5.5	1.77	[36,37]
P3DDT	-3.55	-5.29	1.74	[34]
PBEHTB	-3.6	-5.3	1.7	[38]
PB3OTP	-2.75	-4.2	1.45	[39]
PBEHTT	-3.6	-5.0	1.4	[40]
APFO Green 1	-3.9	-5.14	1.24	[41,42]
PTBEHT	-4.0	-5.2	1.2	[40]

2.3.3 Architecture

2.3.3.1 Bilayer heterojunction devices

In 1992, Sariciftci et al showed that the MEH-PPV polymer had an ultrafast photoinduced electron transfer reaction to C_{60} [43]. C_{60} or Buckminsterfullerene, is a form of carbon, which stores up to 6 electrons, and is able to work as a strong electron acceptor [44]. Other common acceptors include TiO_2 [32] and CdSe [45]. Sariciftci et al later fabricated an organic solar cell as a planar heterojunction device consisting of successive layers of MEH-PPV, C_{60}, and gold deposited onto indium/tin oxide (ITO) coated glass substrates as shown in Figure 5 below [46].

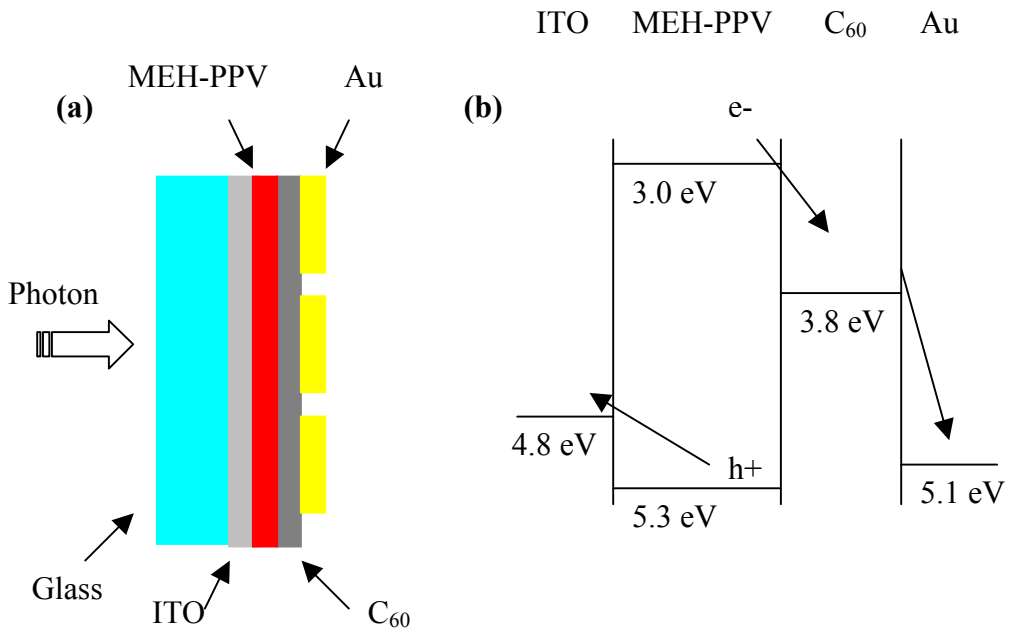

Figure 5: (a) Schematic, and (b) flat band energy-level diagram for ITO/MEH-PPV/C_{60}/Au device.

Polymer solar cells work as follows: when light is absorbed by an organic semiconductor (e.g. MEH-PPV), it generates a mobile excited state consisting of a tightly bound

electron-hole pair known as the Frenkel exciton [47]. The electron-hole pair for most conjugated polymers is generally known to have a binding energy of 0.3 eV – 0.4 eV [48,49]. With the energy level offset being greater than the exciton binding energy, the electron-hole pair is separated at a polymer (MEH-PPV)/electron-acceptor (C_{60}) interface where the holes will then travel through the polymer ($\mu \sim 1.1\times10^{-7}$ cm^2/Vs for MEH-PPV [27]) to the anode (ITO), and the electrons will travel through the energetically favorable C_{60} by hopping ($\mu=2\times10^{-7}$ m^2/Vs [50]) and toward the Au cathode. This process is shown in Figure 6 as a circuit diagram.

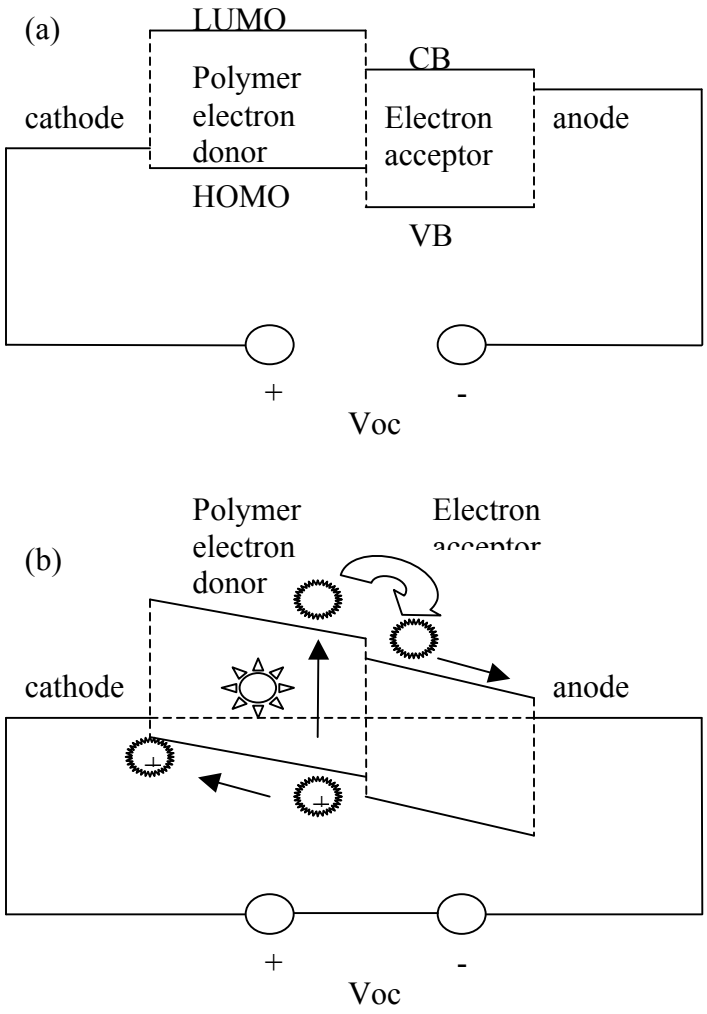

Figure 6: Bilayer structure device band diagram of an open circuit mode (a), and a short circuit mode (b).

Since its discovery, C_{60} has been the electron acceptor of choice for polymer solar cells, and one of the primary focuses in organic solar cell has been an engineering of interface between electron donor polymer, and the electron acceptor.

2.3.3.2 Bulk heterojunction devices

A bilayer device is limited by small interfacial area where the electron-hole pair separation occurs. In order to overcome this challenge, the bulk heterojunction device

was conceived in 1994 by Yu et al [51] as an alternative. MEH-PPV sensitized with C_{60}(MEH-PPV:C_{60}) in a Xylene solution was fabricated in a sandwich configuration as shown in Figure 7.

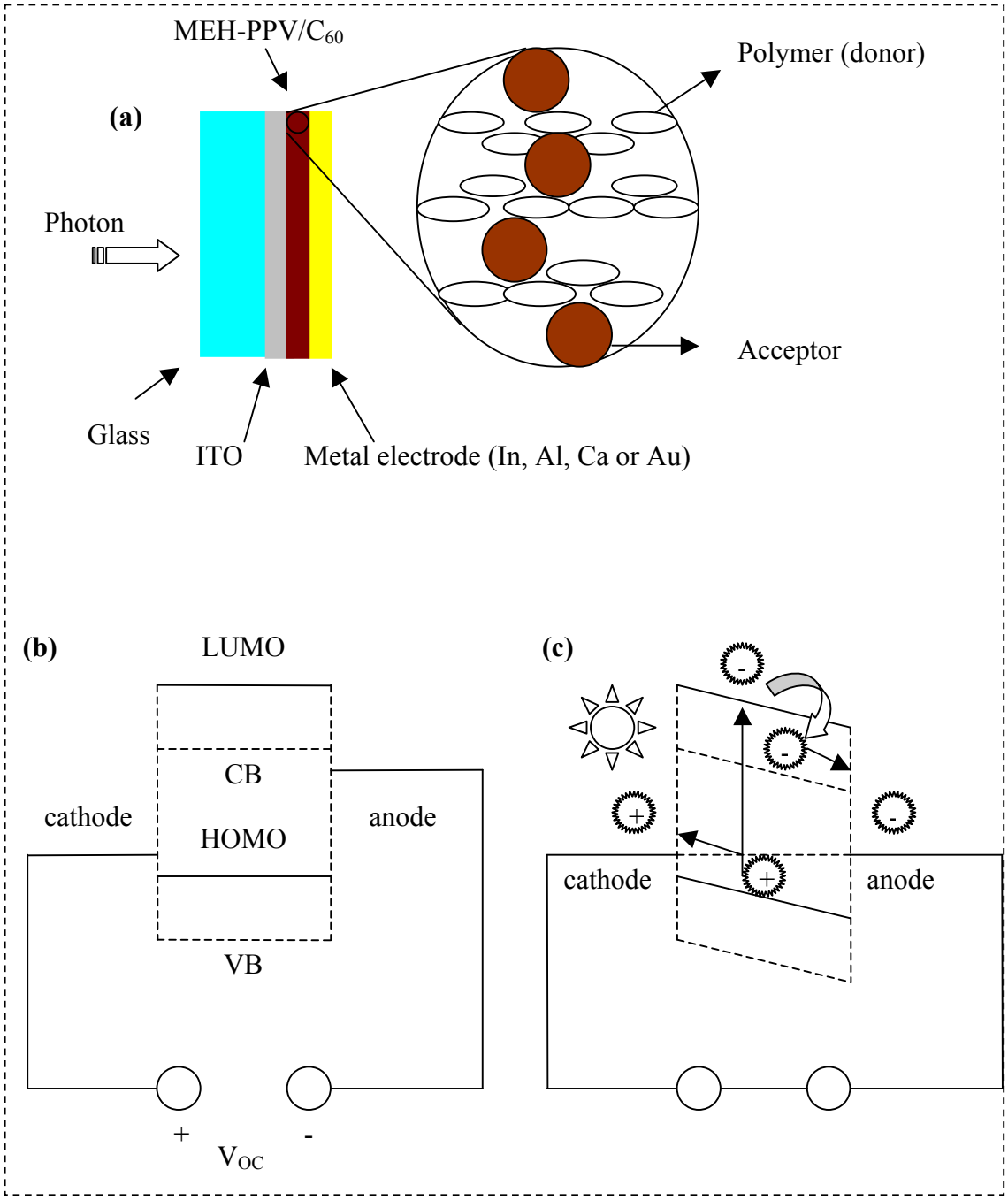

Figure 7: Bulk heterojunction solar cells schematic drawing (a), band diagram of an open circuit mode (b), and of closed circuit mode (c).

Yu et al compared their device with a pure poly(3-octyl thiophene), P3OT, homojunction. The MEH-PPV:C_{60} bulk heterojunction device showed slightly higher photosensitivity compared to the pure P3OT device. With the P3OT device, photosensitivity increased with light incident through the ITO glass. This was explained as carrier generation and transport dominating the device performance at the cathode interface.

For a mixture of polymer with C_{60}, a discrepancy was found between calculated external quantum efficiency (EQE) and the results suggested from photoluminescence (PL) quenching [52]. This indicated a problem in charge transport through the active layer for bulk heterojunction devices, and the concentration of polymer and C_{60} becomes important in establishing two percolation networks for the generated electron/hole pairs of the active layer.

The first step in processing light into electric current in organic solar cells is the absorption of a photon to produce an exciton. However, organic solar cells suffer from poor light harvesting since they tend to be only efficient in the blue region of the solar spectrum, and not in the red. Most organic semiconductors have relatively large bandgaps (> 2 eV) [53], and 1.4 eV has been reported to be the optimal value for better light harvesting [54]. Development of low bandgap polymer has been proven to be difficult [40] although recent efforts have made progress in this area [37]. Instead, other approaches to increase light harvesting have been demonstrated such as increasing absorption of fullerene component of the organic solar cell by replacing C_{60}-PCBM with C_{70}-PCBM [40].

Excitons formed through light absorption in organic solar cells have a lifetime of approximately 10^{-9} s [55]. If an exciton fails to dissociate within its diffusion length of 4-20 nm [56], the energy is lost due to charge recombination. This loss in energy can be avoided through the use of bulk heterojunction structure where it has been shown that the charge transfer from conducting polymers to C_{60} is 10^3 times faster than the decay of photoexcitations [57]. However, with C_{60} dispersed throughout the bulk heterojunction medium, the concentration of the electron acceptor becomes a critical factor in formation of interpenetrating network for efficient collection of carriers. Yu et al [57] studied the performance of their MEH-PPV:PCBM device for 1:1, 1:3, and 1:4 weight ratio respectively. The resulting carrier collection efficiency (η_c), and energy conversion efficiency (η_e) are shown in the figure below.

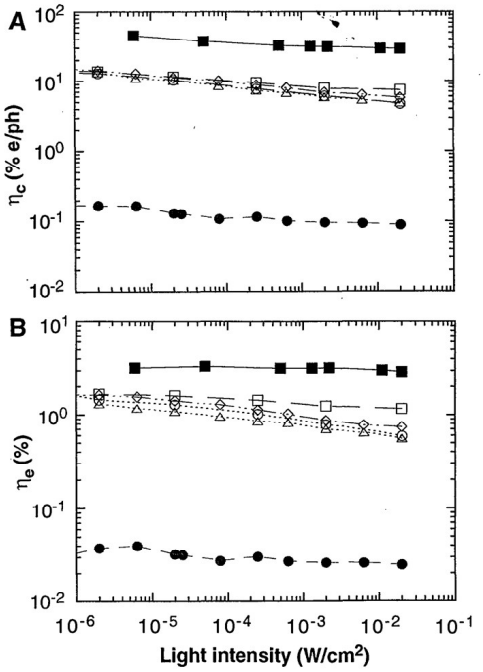

Figure 8: η_c (Carrier collection efficiency) (**A**) and η_e (Energy conversion efficiency) (**B**) of Ca/MEH-PPV:[6,6]PCBM(1:4)/ITO (solid squares); Ca/MEH-PPV:[6,6]PCBM(1:1)/ITO (open squares); Al/MEH-PPV:[6,6]PCBM(1:1)/ITO (diamonds); Ca/MEH-PPV:[5,6]PCBM(1:1)/ITO (open circles); Ca/MEH-PPV:C_{60}(3:1)/ITO (triangles); and Ca/MEH-PPV/ITO (solid circles) [57].

Bulk heterojunction devices made from a 1:4 ratio by weight for MEH-PPV:PCBM mixtures had the highest η_c and η_e among other mixtures. Later studies by Kim et al showed that below 20% PCBM in the MEH-PPV:PCBM mixture by weight (4:1) was below the percolation threshold, and an interpenetrating networks for PCBM form at 50% (1:1) and above [52].

In summary, the challenges to improvement of polymer solar cells include, charge transport through the active layer, light harvesting, and charge recombination. In a conjugated polymer solar cell, these challenges can be met by decreasing the length of charge transport, red shifting the absorption spectrum, and by providing an interpenetrating network of an electron acceptor. All of these maybe accomplished by transforming the conventional solar cells of two-dimensional structure to a quasi-one-

dimensional structure. A technique for producing a quasi-one-dimensional structure is discussed in Chapter 3.

3. ELECTROSPINNING

3.1 History

The fundamental concept of electrospinning otherwise known as "electrostatic spinning," dates back to as early as 1934, when Formhals published a series of patents for an experimental setup in production of polymer filaments using electrostatic force [58]. His setup consisted of an electrode placed inside a polymer solution, with the charged solution then jetting out of a metal spinnerette, and evaporating to form polymer filaments at the grounded collector. Through continued research and development of electrospinning, the technique has found its way into filtration, biomedical, protective clothing, electrical and optical, and many other applications [58]. With its ability to produce nanoscale fibers, due to a surge of interest in nanotechnology over the recent years, the number of publications in the area of electrospinning has continued to grow as can be seen from Figure 9 below.

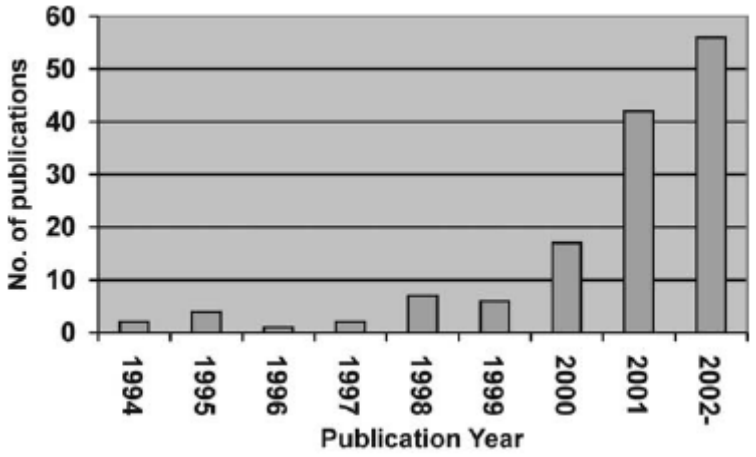

Figure 9: Comparison of the annual number of scientific publications since the term of "electrospinning" was introduced in 1994. (Data analysis of publications was done using the SciFinder Scholar search system with the term "Electrospinning", as at 18 October 2002) [58].

In addition to the ability to produce electrospun nanofibers, advances in the experimental setup have been made in producing with aligned nanofibers, and utilizing multi capillary techniques[59].

3.2 Operation

In electrospinning, a polymer solution is charged with an AC or DC voltage, and the polymer solution forms a jet of polymer fibers which will be collected at the nearest grounded object (Figure 10).

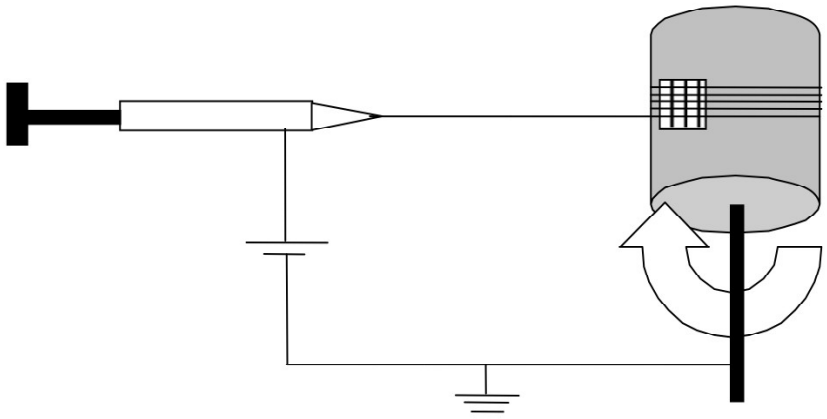

Figure 10: Schematic diagram of the Electrospinning set up.

In some cases, a grounded object can be a conductive rotating drum. With control of the drum speed, it has been demonstrated that the velocity of the reel surface can be adjusted to closely match the speed of the drawing fiber to assist in alignment of the nanofibers [60]. A sample substrate can then be mounted on top of the rotating drum to form aligned polymer-fiber photovoltaics. Other methods of fiber alignment include the use

of an auxiliary field, a thin wheel collector with a sharp edge, frame collector, and etc [58].

Not all materials can be electrospun. In 1987, Hayati et al showed the significance of liquid conductivity for an electrospinning solution. As opposed to insulating liquids, conducting liquids have produced unstable streams, and have been proven difficult to electrospin [61]. For this reason, the majority of research in electrospinning has been done with non-conducting polymeric solutions. Table 3 below shows a list of polymers and the corresponding solvents used in previous research done in electrospinning.

Table 3: Electrospun Polymers and its corresponding solvents [62].

Polymer	Solvent
Cellulose acetate	Acetone
Acrylic resin (96% acrylonitrille)	DMF
a) Polyethylene oxide b) Polyvinyl alcohol c) Cellulose acetate	a) Water/chloroform b) Water c) Acetone
a) Poly(2-hydroxy ethyl methacrylate) b) Polystyrene c) Poly (ether amide)	a) Formic acid and Ethanol b) Dimethyl Formamide and Diethyl Formamide c) Hexa fluoro 2-propanol
Polyethylene oxide (PEO)	Water
Polyethylene terephthalate	Mixture of dichloromethane and trifluoroacetic acid
Polyaniline / PEO blends	Chloroform
Polyether urethane	Dimethyl acetamide
Poly-L-lactide (PLLA), Polycarbonate (PC), Polyvinylcarbazole	Dichloromethane
Polystyrene	Tetrahydrofuran (THF)
Polybenzimidazole (PBI)	N, N_Dimethyl Acetamide (DMAc)
Nylon 6 and Nylon 6 + montmorillonite (NLS)	1,1,1,3,3,3-hexa fluoro-2-Propanol (HFIP) and DMF

a) Polyethylene oxide (PEO) b) Polycarbonate (PC) c) Polyurethane (PU)	a) Isopropyl alcohol (IPA) b) DMF and THF c) DMF
Polyvinyl chloride	THF, DMF
Polyurethane	DMF
Polycaprolactone	Acetone
Styrene-Butadiene-Styrene (SBS) triblock copolymer	75% THF and 25% DMF
Poly-L-Lactide	Dichloromethane
Poly (methyl methacrylate-random) PMMA-r-TAN	Mixed solvent of Toluene and DMF
Polyethylene-co-vinyl acetate (PEVA), Poly lactic acid (PLA) and blend of PEVA and PLA	Chloroform
Poly (p-phenylene terephthalamide) (PPTA) (Kevlar 49 from Dupont)	95-98 wt % Sulphuric acid
Polyethylene terephthalate (PET) and Polyethylene naphthalate (PEN)	
Silk like polymer with fibronectin functionality (SLPF)	Formic acid / hexafluoro isopropanol
Polyurethane and PEO	Tetrahydrofuran and Dimethylformamide

Electrospinning is able to produce nanofibers only for viscoelastic materials that can undergo strong deformations while being cohesive enough to support the stresses developed during pulling [58]. However, various methods have been applied to materials which are difficult to electrospin such as the conjugated polymers commonly used for fabrication of solar cells. In the development of nanofiber structured electronic devices which require these non-electrospinnable materials, other polymers are incorporated into the electrospinning process through mixing or co-axial electrospinning.

Conjugated polymers used to make solar cells and conducting liquids are generally not viscoelastic enough for electrospinning. One method often employed to

allow electrospinning of these otherwise non-electrospinnable materials is the mixing an electrospinnable polymer to the non-electrospinnable solution. P3HT is a conjugated polymer which is difficult to electrospin because it crystallizes quickly and blocks the electrospinning nozzle. In order to electrospin P3HT, Lee et al prepared a series of samples with an electrospinnable high molecular weight poly (ε-caprolactone) (PCL) polymer mixed into P3HT solution dissolved in anhydrous chloroform ($CHCl_3$, Aldrich)[63]. The weight ratio of the P3HT:PCL blended solution was varied from 90:10 to 50:50 (w/w), and PCL content of the P3HT:PCL nanofibers was completely removed by dipping a sample into trifluoro-ethylene (TFE) for 20 min. Nanofiber morphology was retained when the mixing ratio of PCL was more than 90:10 as can be seen from the SEM images shown in Figure 11.

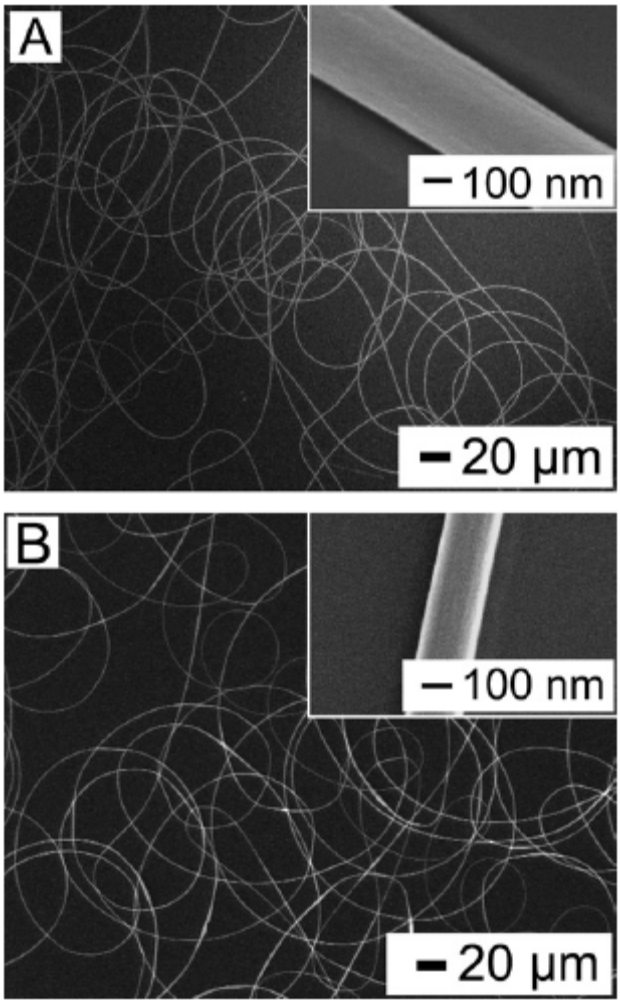

Figure 11: SEM images of blended fibers of P3HT and poly(ε-caprolactone) (PCL) using a single nozzle: (A) P3HT:PCL (80:20, w/w) and (B) P3HT:PCL (50:50, w/w). The insets are higher magnification images of the fibers[63].

Also for nanofibers after removal of PCL,

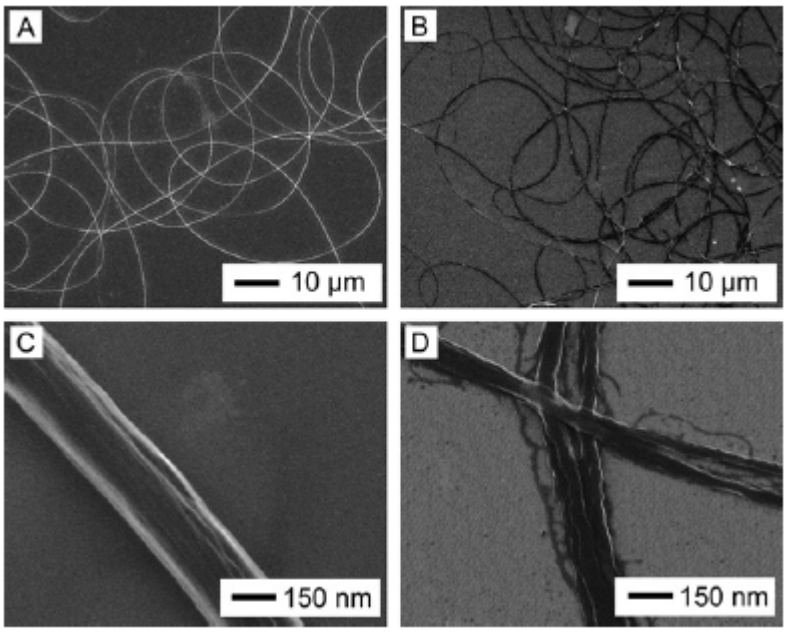

Figure 12: SEM images of Electrospun blend fibers of P3HT and PCL taken after selectively removing PCL: (A,C) P3HT:PCL (80:20, w/w) and (B,D) P3HT:PCL (50:50, w/w)[63].

After the removal of PCL, the electrospun P3HT nanofiber was able to maintain not only its nanofiber structure, but also its electrical properties. The mobility measurement for a 20 wt% PCL nanofiber showed degradation of one order of magnitude, $\mu = 0.0012\ cm^2V^{-1}s^{-1}$, while a 50 wt% PCL nanofiber showed two-order of magnitude degradation with $\mu = 0.00047\ cm^2V^{-1}s^{-1}$[63]. Although there was some level of degradation in their electrical properties, mixing of a high molecular weight electrospinnable polymer has proven itself to be a good method for nanofiber structured electronic devices.

Coaxial electrospinning (Figure 13) is another method that is able to produce nanofibers from conjugated polymer solutions of low viscoelasticity.

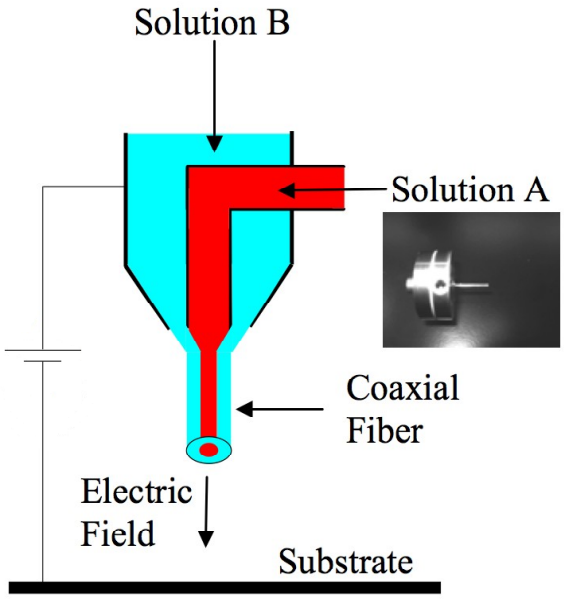

Figure 13: Schematic of Coaxial Electrospinning device (inset is a photograph of the needle).

To prevent mixing of solutions A and B, it is favorable to use two immiscible solvents for the two solutions. An electric field is applied for an electrospinnable outer solution B to form a coaxial jet, and inner solution A is fed through the jet with an infusion pump. If solution B is chosen to be a spinnable polymer solution and solution A is a conjugated polymer solution, the collected coaxial fibers can be immersed in the same solvent used to prepare solution B to wash away the outer polymer to leave a conjugated polymer nanofiber. Successful nanofibers have also been synthesized with solution B as a pure solvent for conjugated polymer solution A. To electrospin pure P3HT nanofibers, Lee et al used Chloroform as solution B to prevent fast crystallization of P3HT solution from the solution A nozzle [63]. Figure 14 below shows the SEM image of P3HT nanofibers produced from Chloroform/P3HT coaxial electrospinning experiment.

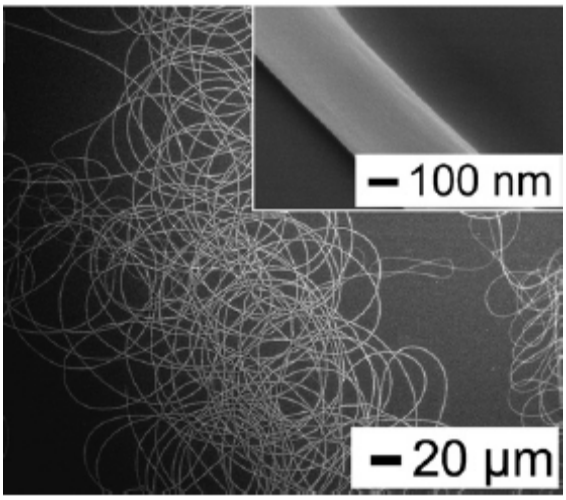

Figure 14: SEM images of P3HT fibers with a coaxial nozzle with solvent assistance. The inset is a higher magnification of the fiber [63].

Using coaxial electrospinning with solvent assistance, good nanofiber morphology is maintained using the conjugated polymer P3HT. Whether with an electrospinnable polymer or with a pure solvent, coaxial electrospinning is a powerful technique for synthesizing conjugated polymer nanofibers.

There are other ways to utilize coaxial electrospinning such as making solution A an electrospinnable polymer solution B the non-electrospinnable conjugated polymer. This method of inverted coaxial electrospinning has an advantage in that it does not require the removal of the electrospinnable polymer to access the electronic properties of conjugated polymer because it is exposed at the surface of the coaxial nanofiber. Zhao et al in 2007 were successful in using this inverted coaxial electrospinning method with PVP as the core, and the conjugated polymer MEH-PPV as shell in synthesizing a conjugated polymer nanofiber[64]. Figure 15 below are images of the MEH-PPV shell coaxial nanofiber.

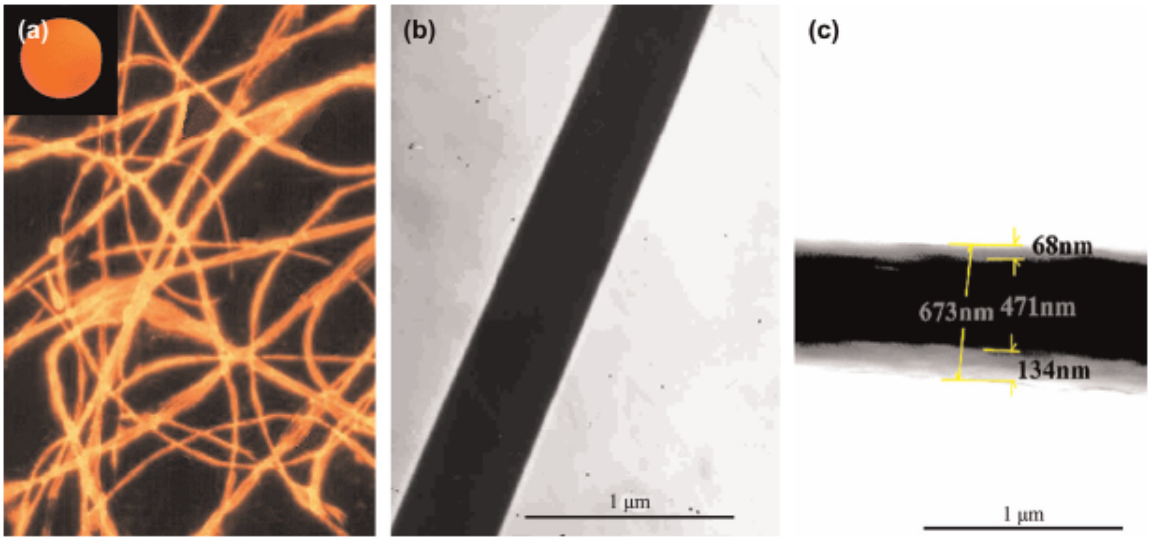

Figure 15: (a) A fluorescence microscope image of PVP/MEH-PPV fibers (inset is the spin cast MEH-PPV film), (b) TEM image of PVP fiber and (c) TEM image of the PVP/MEH-PPV fiber[64].

Good morphology was observed in MEH-PPV shell coaxial nanofiber. However, a significant blue shift was observed in the PVP/MEH-PPV nanofiber which can be damaging for its use in polymer electronics. Possible causes for the blue shift include nano-effect of the thin MEH-PPV fiber, and also the possibility of PVP diffusing into MEH-PPV shell to serve as a nanospacer to prevent π-π stacking [64].

As it is evident from coaxial electrospinning, the nozzle tip used for electrospinning is often a main factor in determining the morphological structure of the electrospun nanofiber. By incorporating a multi-channel nozzle in electrospinning, Zhao et al successfully prepared nanofibers of multi-channel multi-tubular structures [65]. Their multi-channel nanotubes were prepared from electrospinning $Ti(OiPr)_4$ with poly(vinyl pyrrolidone) for their outer shell, and paraffin oil for their inner fluid. Figure 16 below is an SEM image of the multi-channel tube nanofibers.

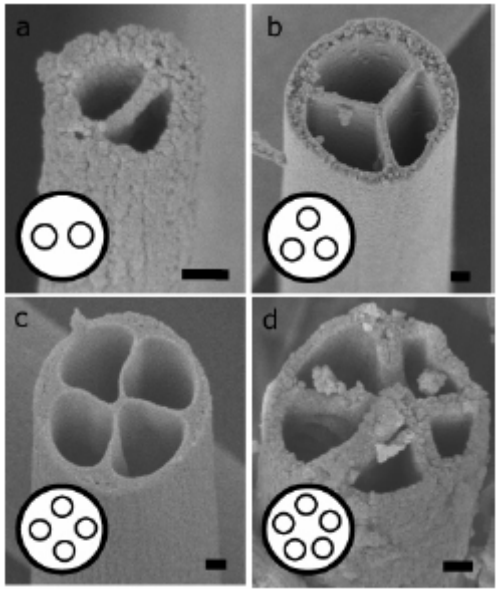

Figure 16: SEM images of multi-channel tubes with variable diameter and channel number. (a-d) Corresponding to tube with channel number from two to five. The inset in each figure shows the cross section illustration of spinneret that was used to fabricate the tube. The as-prepared tubes accord very well with the corresponding spinneret. Scale bars are 100 nm[65].

The collected fibers were calcined to remove the organics from the nanofibers, and the SEM image shows how multi-tubular structure was able to form according to the electrospinning spinneret. Other forms of electrospinning spinneret are the multi-axial structures such as those prepared by Joo et al [66]. The TEM image below is a cross section of triaxial nanofibers where both the innermost and outermost layers are silica, and the middle layer is the self assembling PS-B-PI block co-polymer with isoprene volume fraction of 0.28 (SI-28).

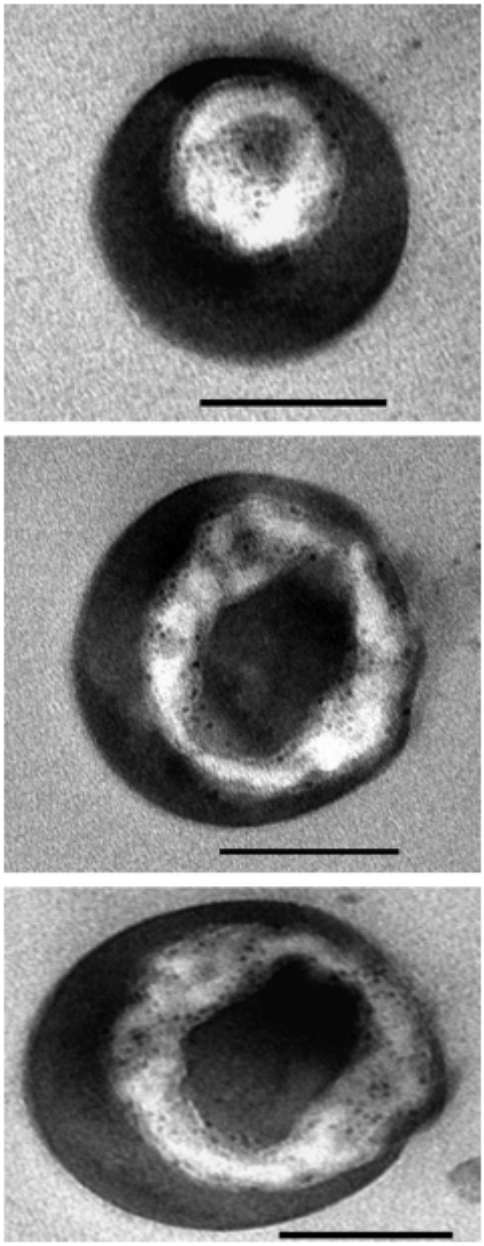

Figure 17: TEM images of cross sections of triaxial nanofiber with least (Top image) to highest (Bottom image) loads of SI-28/magnetite nanoparticles sandwiched between two silica layers. The samples are annealed at 150°C for 72 h. The scale bar is 100 nm [67].

The TEM image clearly shows the triaxial structure of the nanofiber. Electrsopinning proves to be a highly customizable technique with multi-tubular to multi-layered nanofiber structures. Its ability to mold nanofibers into different structures presents it self with a possibility for applications such as diodes, drug delivery systems, and etc.

3.3 Application of Electrospinning to Solar Cells

Most solution-based electronics can be electrospun into nanofiber structures. This is because a non-electrospinnable solution can be electrospun simply by the addition of an electropinnable polymer, and this allows for various possibilities in nanofiber electronics. Polyaniline is a conductive polymer widely used for electrodes, capacitors, and batteries. An experiment was carried out by Norris et al [67], where a conductive solution of Polyaniline mixed with 10-camphorsulfonic acid (PAn.HCSA) was used for electrospinning. Electrospinning failed to produce pure PAn.HCSA nanofibers due to low viscosity and surface tension not allowing for a stable drop at the capillary tip. However, electrospinning of PAn.HCSA nanofiber was made possible by adding a small fraction of PEO to the chloroform based solution. Figure 18 below is an SEM image of the PEO doped PAn.HCSA electrospun nanofiber.

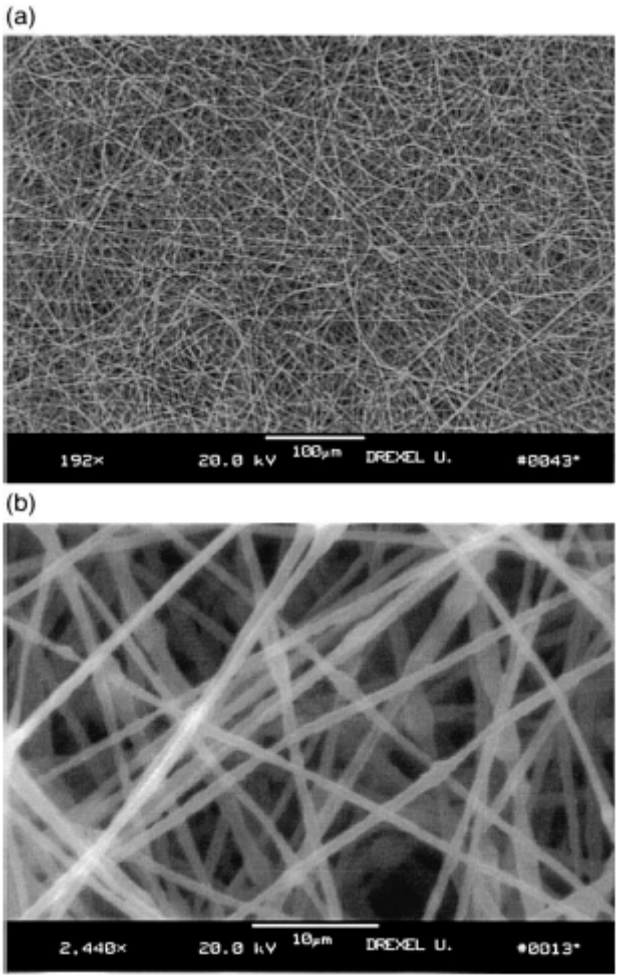

Figure 18: SEM micrographs of the Electrospun fibers from a 2 wt.% PAn.HCSA/2 wt.% PEO solution dissolved in chloroform at 25 kV at (a) **192 and (b) 2440 magnification [67].**

PAn.HCSA being a conductive solution, the change in its conductivity by the formation of the nanofiber structure was studied. Figure 19 compares the conductivity of a cast film to electrospun nanofibers with increasing concentration of PAn.HCSA in a blended solution.

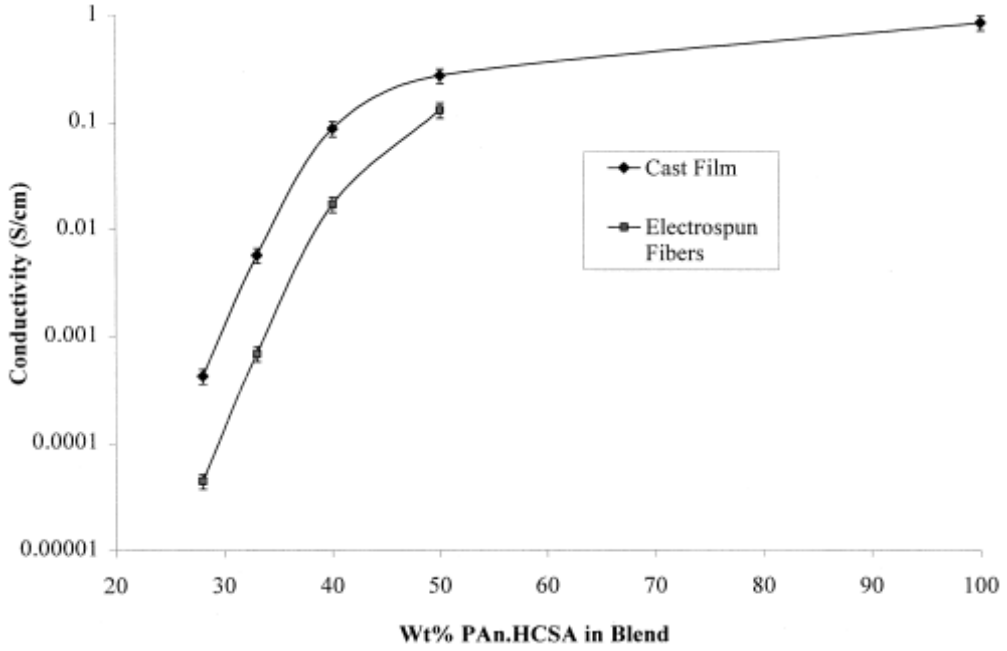

Figure 19: Electrical conductivity of the PAn.HCSA/PEO blend Electrospun fibers and cast films prepared from the same solution [67].

The graph shows that there is a similar trend in conductivity with increasing PAn.HCSA concentration. However, the conductivity of the electrospun fibers is significantly lower, and this is attributed to the four point probe system measuring the conductivity by the volume and not by individual fibers. By measuring individual fibers, it is expected that the conductivity of electrospun fibers will be comparable to conductivity of cast film. Synthesis of conductive nanofiber has been demonstrated. However, no significant change was observed in electronic properties of the PAn.HCSA nanofibers as opposed to its cast film.

Chuangchote et al observed some advantages in using a TiO_2 nanoparticle/nanofiber electrode for their dye sensitized photoelectrochemical cell [68]. An electrospinnable PVP polymer was added to the methanol solution with Titanium butoxide, and acetylacetone for electrospinning. SEM images along with its UV-visible

absorption spectra for both TiO_2 nanoparticle and nanoparticle/nanofiber eletrode are presented below.

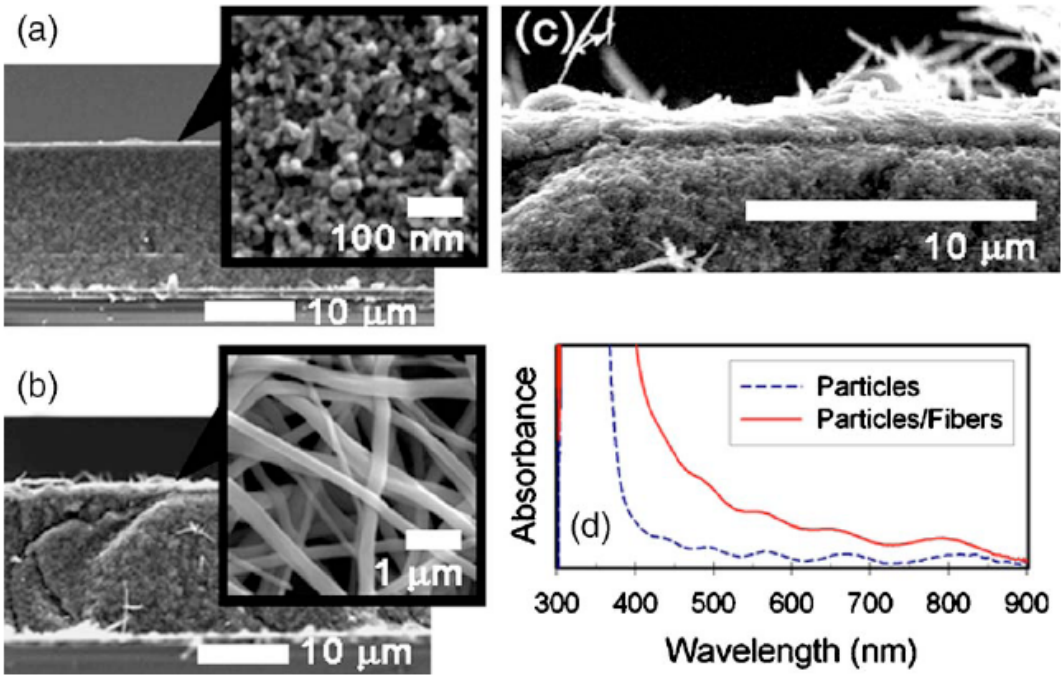

Figure 20: SEM images of (a) nanoparticle electrode and (b) nanoparticle/nanofiber electrode. (c) Connection part between nanoparticles and nanofibers in nanoparticle/nanofiber electrode. (d) UV-visible absorption spectra of both types of electrodes [68].

As opposed to the PAn.HCSA nanofibers, TiO_2 nanoparticle/nanofiber showed an increase in absorption. Performance of both TiO_2 nanoparticle and nanoparticle/nanofiber solar cells are summarized in Table 4 below.

Table 4: Photovoltaic properties of the DSCs investigated [68].

Samples	Thickness of particle layer (μm)	Area (cm^2)	J_{sc} (mA/cm^2)	V_{oc} (V)	FF	η (%)
Nanoparticles	8.4	0.25	14.0	0.70	0.68	6.69
Nanoparticles/nanofibers	8.4	0.25	15.9	0.71	0.68	7.10
Nanoparticles	15.5	0.25	16.1	0.69	0.67	7.47
Nanoparticles/nanofibers	15.5	0.25	17.9	0.69	0.66	8.14
Nanoparticles	15.5	0.052	18.5	0.67	0.75	9.25
Nanoparticles/nanofibers	15.5	0.052	22.4	0.64	0.72	10.3

With increased light absorption, dye sensitized photochemical cells of TiO_2 nanoparticle/nanofiber electrodes improve efficiency when compared with a nanoparticle device. Depending on the solution used for electrospinning, nanofiber structure of a solution can bring positive effect in electronic properties of the fabricated device.

Sundarrajan et al recently reported photovoltaic cells from conjugated polymer nanofibers [69]. A coaxial electrospinning technique was utilized with a blend solution of P3HT/PCBM in chloroform/toluene (3.5/1 wt.-%) for the core, and 10 wt.-% PVP in chloroform/ethanol (1/1 wt.-%) for the shell. The coaxial fibers were collected on fluorine-doped tin oxide (FTO) plate. After etching away the PVP shell by soaking in an ethanol solution for ~20 min, the nanofiber mat was then covered with an aluminum (Al) sputtered FTO substrate and clamped using binder clips as shown in Figure 21.

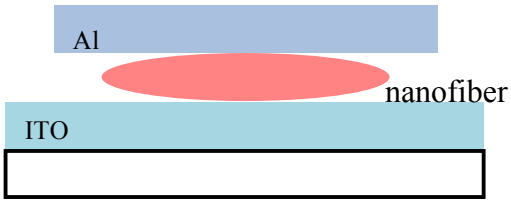

Figure 21: Sundarajan et al Solar cloth device structure**.**

Figure 22 shows the morphology of the electrospun nanofiber after PVP etching**.**

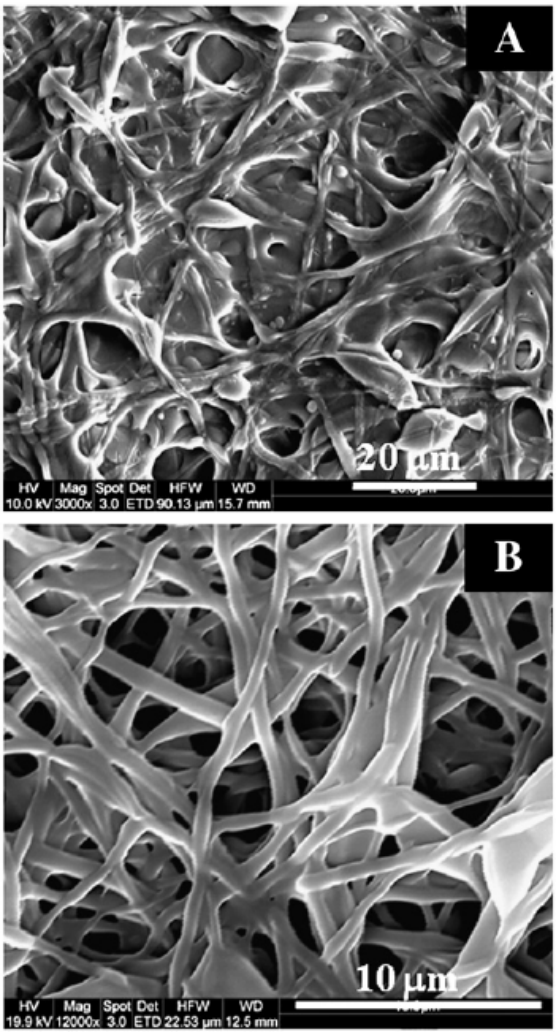

Figure 22: SEM images of the fibers after washing the PVP template [69].

Similar to the TiO_2 nanofibers of Chuangchote et al [68], the observed P3HT/PCBM nanofibers showed a slight redshift in their absorption spectrum as shown in Figure 23 below.

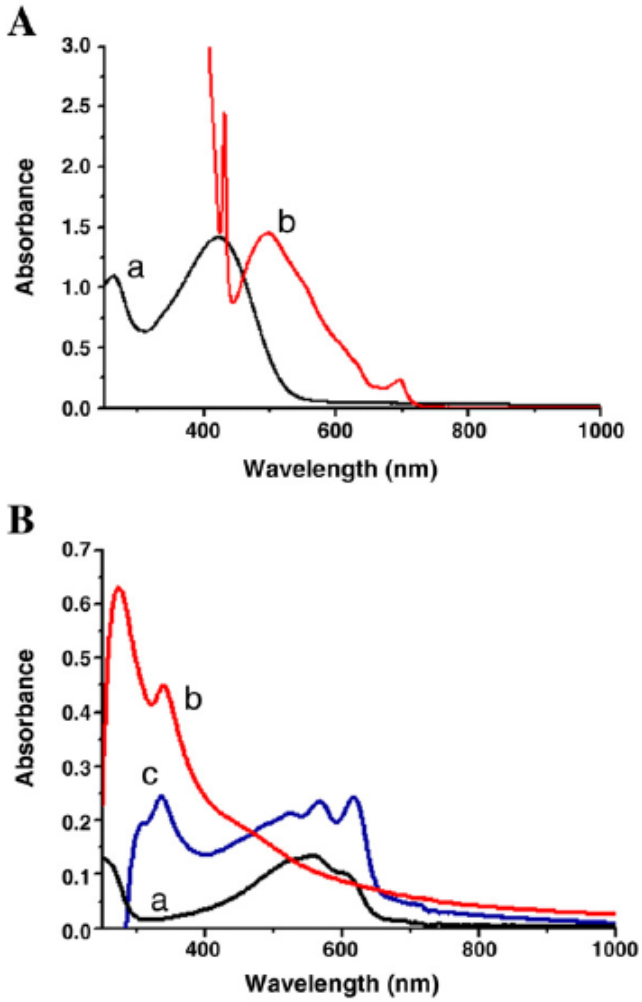

Figure 23: Traces a and b in Panel A show the absorption spectra of the solutions of pure P3HT and PCBM, respectively. Traces a and b, respectively, in panel B show the corresponding spectra of their thin films. Absorption spectrum of the solar cloth is depicted in trace c [69].

The absorption spectra of P3HT/PCBM nanofibers showed the most red shift with respect to P3HT of other structures. The red shift is explained as a result of stretching of the polymer chains [70], and an extra 10 nm red shift from electrospinning in comparison to P3HT thin film shows how electrospinning can be a very effective method for increased absorption. However, even with a structurally increased light harvesting ability, the electrospun P3HT/PCBM nanofiber yielded a relatively low photovoltaic efficiency of

8.7×10^{-8}. Current to voltage characteristic of Sundarrajan's electrospun nanofiber solar cell is shown below in Figure 24.

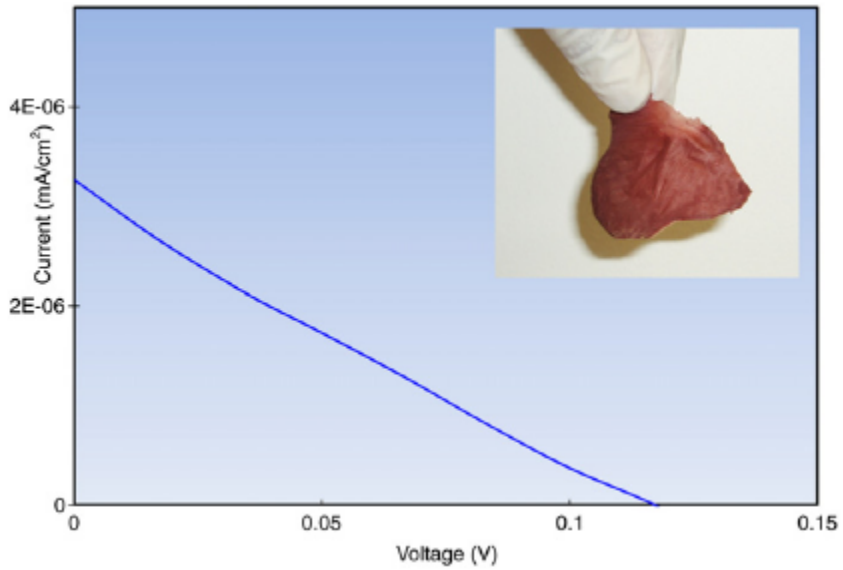

Figure 24: J – V graph of the P3HT/PCBM solar cloth measured under 1 Sun conditions. Inset shows a picture of the solar cloth fabricated using electrospinning [69].

Short circuit current Jsc, open circuit voltage (Uoc), and fill factor (FF) of the electrospun solar cell were measured at 3.2×10^{-8} mA/cm^2, 0.12 V and 22.1 respectively. A significant drawback in Sundarrajan's electrospun solar cell comes from its device structure, where the P3HT/PCBM nanofiber serving as the active layer of the device is actually a thick mat of ~5 µm. Because of low charge carrier mobility of P3HT/PCBM, a 5 µm active layer is too thick for an efficient charge transfer for its sandwiched device structure between Aluminum and FTO. For better implementation of nanofibers to solar cells, different device structures needs to be taken into consideration.

3.4 Advantages of Electrospun Nanofibers for Solar Cells

There are several advantages to conjugated polymer nanofibers formed through electrospinning. Studies of changes in the optical properties of conjugated polymer

nanofibers were performed by Babel et al [71]. Blends of MEH-PPV/poly(3-hexylthiophene) (P3HT), and MEH-PPV/poly(9,9-dioctylfluorene) (PFO) were coaxially electrospun with poly(vinylpyrrolidone) (PVP) as their shell in the core-shell structure of nanofibers. For each solution, series of binary blends weight percentage of MEH-PPV with P3HT (20, 30, 40, 50, 60, and 70 wt % MEH-PPV) and PFO (5, 14, 28, 44, and 55 wt % MEH-PPV) were prepared. The resulting absorption and photoluminescence measurements for the MEH-PPV/P3HT solution are shown in figure below.

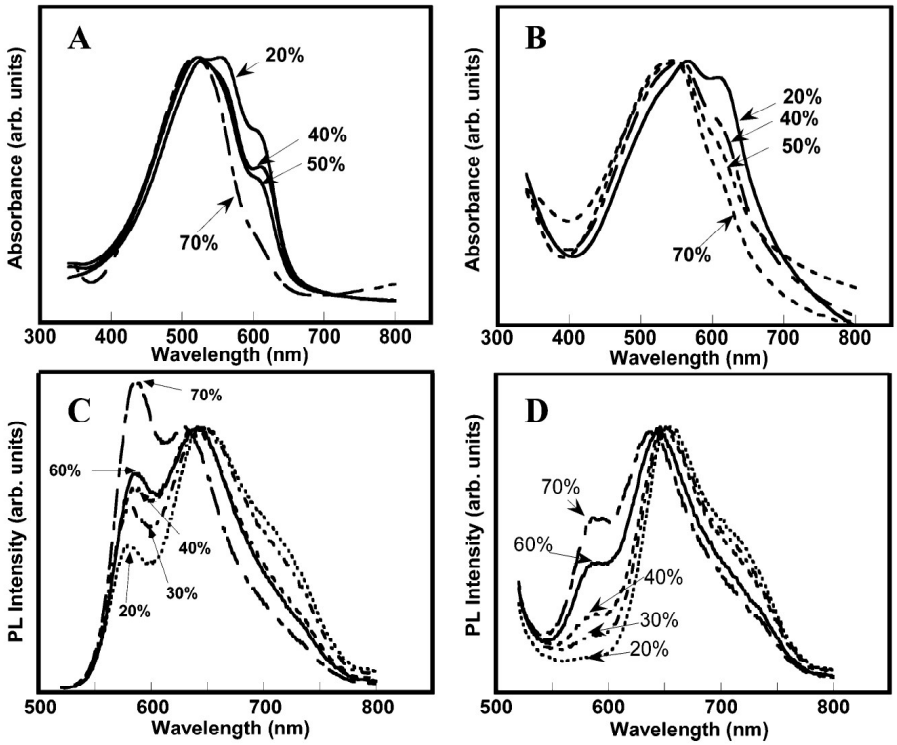

Figure 25: Optical absorption (A, B) and photoluminescence emission (C, D) spectra of MEH-PPV/P3HT blend nanofibers (B, D) and spin-cast thin films (A, C). The number on each curve is the wt % of MEH-PPV [71].

Comparing the thin films to electrospun nanofibers, a red shift in the MEH-PPV absorption peaks from 520 nm to 550 nm were observed. As explained earlier, the red shift is considered to be an effect due to stretching of the polymer chains leading to

extension of the π-conjunction length [72]. In studying the PL spectra, intensity decrease with increase in P3HT concentration was observed suggesting an efficient energy transfer from MEH-PPV to P3HT. Clear differences observed between the 20 wt % blend thin film and the 20 wt % nanofiber imply an enhanced interaction between MEH-PPV and P3HT from their confined nanostructures compared to bulk thin film.

Similar results were obtained with MEH-PPV/PFO blend but with a larger red shift of 50 nm for the MEH-PPV peak. However, due to structural nature of the MEH-PPV/PFO nanofibers, no significant increase in energy transfer from MEH-PPV to PFO was observed. Figure 26 are SEM, and TEM images of MEH-PPV/PFO blend nanofibers with different concentration of MEH-PPV.

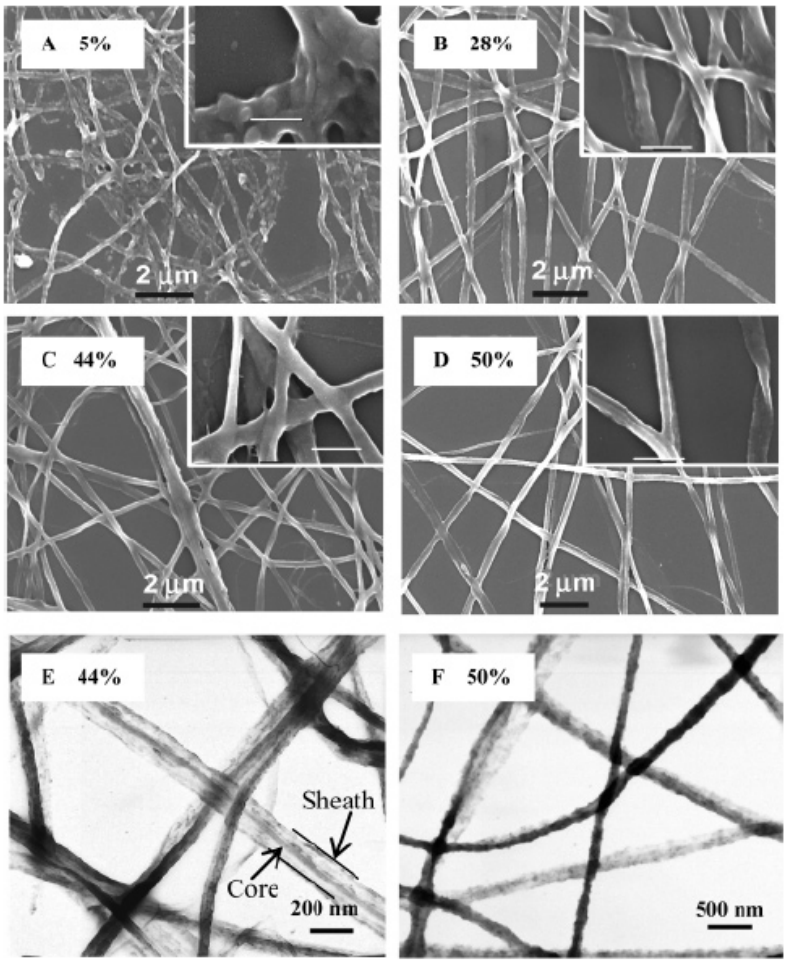

Figure 26: Morphology of Electrospun MEH-PPV/PFO blend nanofibers SEM images (A-D) and TEM images (E,F) with different concentrations of MEH-PPV. The scale bars in the inset are 500 nm [71].

The MEH-PPV/PFO blend nanofibers maintained core-shell structures or continuous bundles of individual nanofibers resulting in less interfacial surface area between the two polymers, and this explains the lack of significant increase in energy transfer in comparison to MEH-PPV/P3HT nanofibers. However, the reduced interfacial surface area can cause restriction in orientation of the polymer chains, and thus the most amount of red shift observed for the PFO polymer. Unlike electrospun MEH-PPV and PFO fibers, no red shift in the P3HT absorption peak was observed in their experiment.

One unique feature of photovoltaic device fabrication from electrospinning is in its application of electric field. Application of an electric field is an essential part of the electrospinning technique, and a study was done by Padinger et al [73] showing the effects of electric current in preparation of a photovoltaic device. Figure 27 are current to voltage curves of P3HT/PCBM solar cells prepared in different fabrication process.

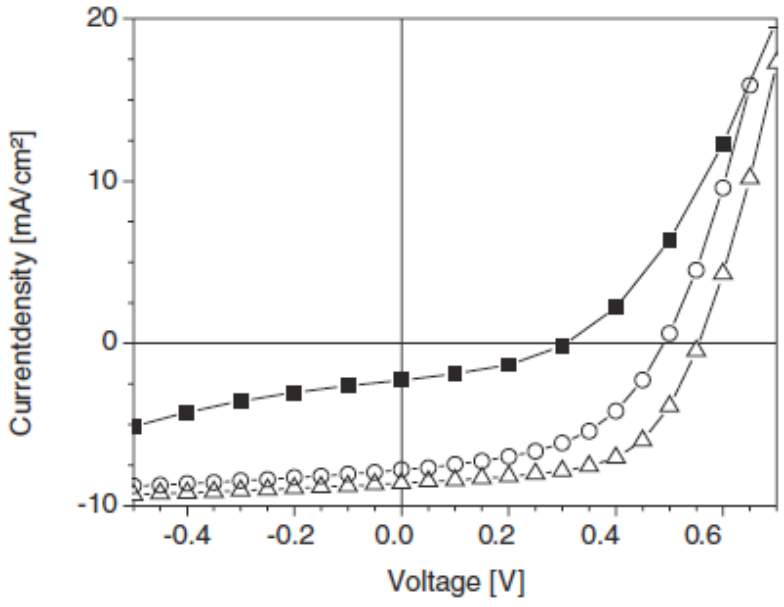

Figure 27: Current-voltage (I-V) curves of P3HT-PCBM solar cells under illumination with white light at an irradiation intensity of 800 Wm^{-2}: as-produced solar cell (filled squares), annealed solar cell (open circles), and cell simultaneously treated by annealing and applying an external electric field (open triangles) [73].

Annealing, and simultaneous application of an external voltage have shown to improve the efficiency of P3HT/PCBM solar cell. Increase in open-circuit voltage can be explained by burning of the shunt resistance, and an increase of short-circuit current shows mobility enhancement of charge carriers in the photoactive layer. Annealing of the polymer film has been known to help crystallize the polymer structure for better device performance [74]. With an electric field, there is an additional orientational effect that takes place, which is presumed to help in enhancement of mobility. Considering this orientational effect with an electric field, electrospinning could be a simple way to implement mobility enhancement for bulk heterojunction photovoltaics.

4. Electrospinning of water soluble polymer PTEBS

Sodium poly[2-(3-thienyl)-ethoxy-4-butylsulfonate] (PTEBS) is a water-soluble thiophene polymer semiconductor, which has been used as electron donor to prepare environmentally friendly water-soluble polymer thin film solar cells [32]. For an initial attempt in fabrication of an electrospun polymer-fiber solar cell, PTEBS was combined in an aqueous solution with PEO and then electrospun into fibers in order to study its electrospinning properties and the effect of fiber diameter on optoelectrical properties. The result was the discovery of a new method for producing bimodal fibers via electrospinning [75].

While electrospun mats exhibiting varying and even bimodal size distributions have been produced [76-78], chemically and physically distinct fibers have not been previously electrospun from a single homogeneous solution. Gupta and Wilkes reported "bi-component" fibers of poly(vinyl chloride)/segmented polyurethane (PVC/Estanew) and poly(vinyl chloride)/poly(vinylidiene fluoride) (PVC/PVDF), but the bi-component fibers were produced from two different polymer solutions using side-by-side technology [79].

PTEBS solutions were prepared both with and without ammonium hydroxide (NH_4OH). Both solutions were dissolved in deionized water at a concentration of 1.5%. The PTEBS solution without NH_4OH was then magnetically stirred for 14 days. For the PTEBS solution with NH_4OH, 20 mg of NH_4OH was added per 1 ml of PTEBS solution immediately after the DI water was mixed with PTEBS. Because the NH_4OH accelerates the dissolution, the PTEBS solution with NH_4OH was magnetically stirred for only 3 days. PEO with molecular weight of 2,000,000 g/mol was then added to these

two PTEBS solutions at a concentration of 20 mg per 15 mg PTEBS and stirred for one day.

Following preparation, both solutions were electrospun using a high voltage DC power source (Spellman CZE 1000R) [80,81]. The infusion rate of the solution was controlled using a Harvard Apparatus PHD 2000 syringe pump. The electrospun fibers were collected on a substrate mounted on a rotating hexagonal drum with a speed of ~1725 rotations per minute. All of the fibers were electrospun at an infusion rate of 1 **µ**l/min and with a needle tip to substrate distance of 10 cm. The electrospinning voltage was set at a value slightly above that required to get stable jet: 4.5 kV for the solution without NH_4OH and 6.5 kV for the solution with NH_4OH. The morphology was characterized using an optical microscope (Olympus BX60) and transmission electron microscopy (TEM) (Jeol JEM-1230). The absorption spectra were measured with UV/VIS spectrometer (Perkin Elmer Lambda 40). A high speed video camera (Photron FASTCAM-PCI R2) was used to observe the formation of the Taylor cone and jet.

Figure 28 show the typical morphology of the electrospun fibers made from the PTEBS/PEO solution without and with NH_4OH.

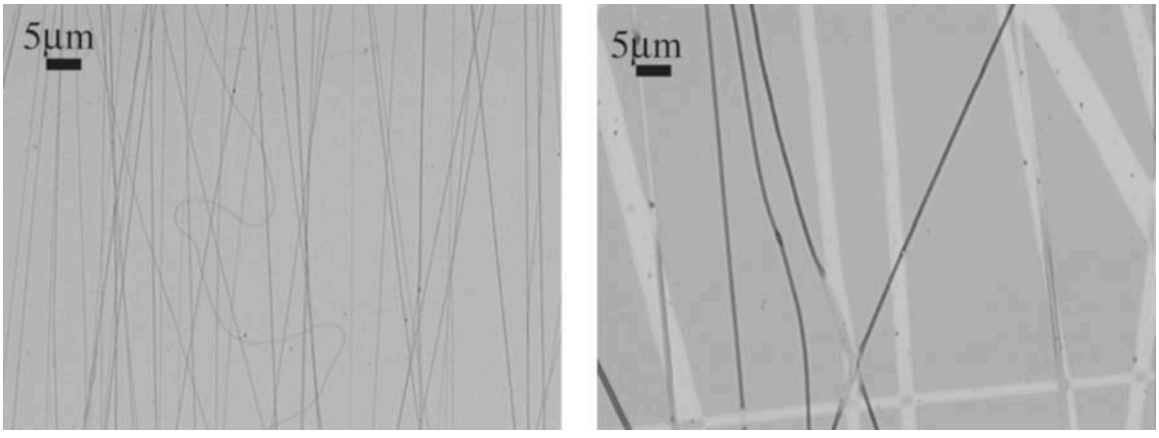

Figure 28: Microscope photo of the electrospun PTEBS/PEO fibers: (a) The unimodal PTEBS/PEO nanofibers without NH_4OH. (b) The bimodal PTEBS/PEO fibers with NH_4OH.

The PTEBS/PEO fibers prepared without NH_4OH show a unimodal morphology where all the fibers have almost the same diameter and color (Figure a). By contrast, the fibers made from the PTEBS/PEO solution with NH_4OH produced two different kinds of fibers in a bimodal morphology: large diameter white fibers and small diameter black fibers. Regardless of the infusion rate, the electrospinning voltage, and the distance between the needle and the substrate, and even if PEO with different molecular weights (400k, 1M and 2M) were used, the fibers made from PTEBS/PEO solution with NH_4OH always produced a bimodal distribution.

Figure 29 shows TEM images of the unimodal and bimodal fibers.

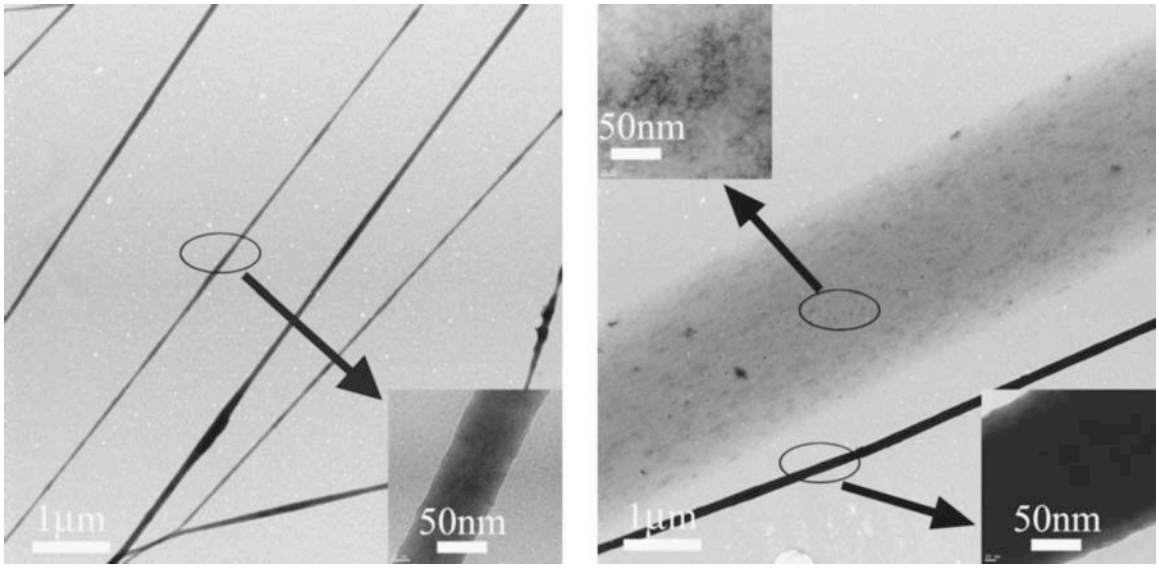

Figure 29: TEM images of the unimodal and bimodal fibers. (a) Unimodal (the inset is the highest definition TEM image). (b) Bimodal (the top left inset is the highest definition TEM image of the big fiber, the bottom right inset is the highest definition TEM image of the small fiber).

The insets are the highest definition TEM images. The diameter of the unimodal fibers (Figure a) is around 60 nm. The highest definition TEM image reveals a composite morphology consisting of tiny irregular dark domains embedded in a white fiber.

For the bimodal fibers (Figure b), the diameter of the small fibers is about 200 nm while the diameter of the large fibers is more than 1 μm. The high definition TEM image of the small fibers is still very dark under the same contrast and brightness. It has been shown that the presence of sulfur in a polymer can result in a darker contrast under TEM [71]. PTEBS contains sulfur and therefore, the TEM images of the bimodal fibers suggest that the small black fibers contain more PTEBS in comparison to the 4 large white fibers.

PEO is also soluble in chloroform [62] whereas PTEBS is not. This was confirmed by spinning PEO fibers and then annealing them at 80 °C in a chloroform atmosphere. The pure PEO fibers were completely dry-washed away. By contrast, a thin film of PTEBS showed no change under the same conditions. In order to verify that the small fibers contain more PTEBS, the bimodal fibers were annealed at 80 °C in chloroform atmosphere. As shown in Figure30, the large white fibers disappeared after annealing for 20 hours, while the small black fibers were left intact on the glass substrate.

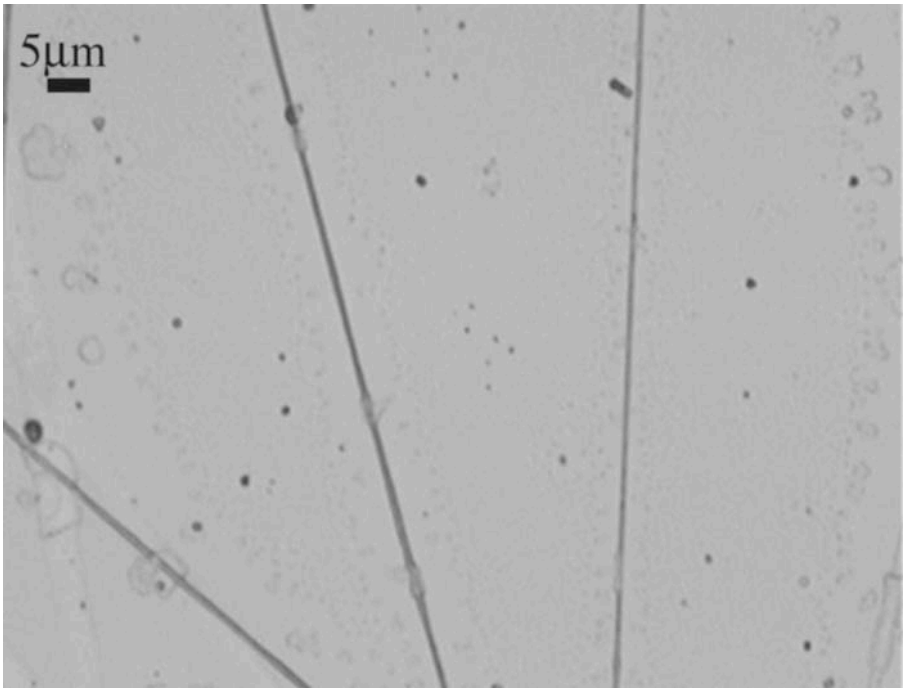

Figure 30: Microscope photo of bimodal PTEBS/PEO fibers taken after annealing at 80°C in chloroform atmosphere. The large white fibers have disappeared.

These results are consistent with the TEM observations and confirm that the small and large diameter fibers are chemically as well as physically distinct.

A high speed CCD camera was used to observe the Taylor cone during the electrospinning process. We observed that only one Taylor cone was formed and only one jet emerged from the tip of the Taylor cone in both the unimodal and bimodal cases. When NH_4OH was replaced with NaOH, bimodal fibers were also obtained. Therefore, we believe the formation of bimodal fibers of chemically distinct polymers may be related to the presence of OH- radicals in the electrospinning solution. We also found that the conductivity of a pure PTEBS thin film was increased by about one order of magnitude when made from a solution containing NH_4OH. The higher electrical conductivity indicates that more PTEBS molecules were ionized when using NH_4OH. The negatively charged PTEBS ions, unlike PEO, should move against the direction of the electric field. We believe that the different polarity and electrophoretic mobility of PTEBS and PEO leads to separation within the cone-jet region and the formation of chemically distinct fiber segments. The electric fields employed in the electrospinning process are comparable to the fields used in electrokinetic processes such as gel electrophoresis, but to our knowledge electrokinetic chemical separation has not been previously reported in electrospinning.

Figure 31 shows the absorption spectra of the unimodal PTEBS/PEO nanofibers.

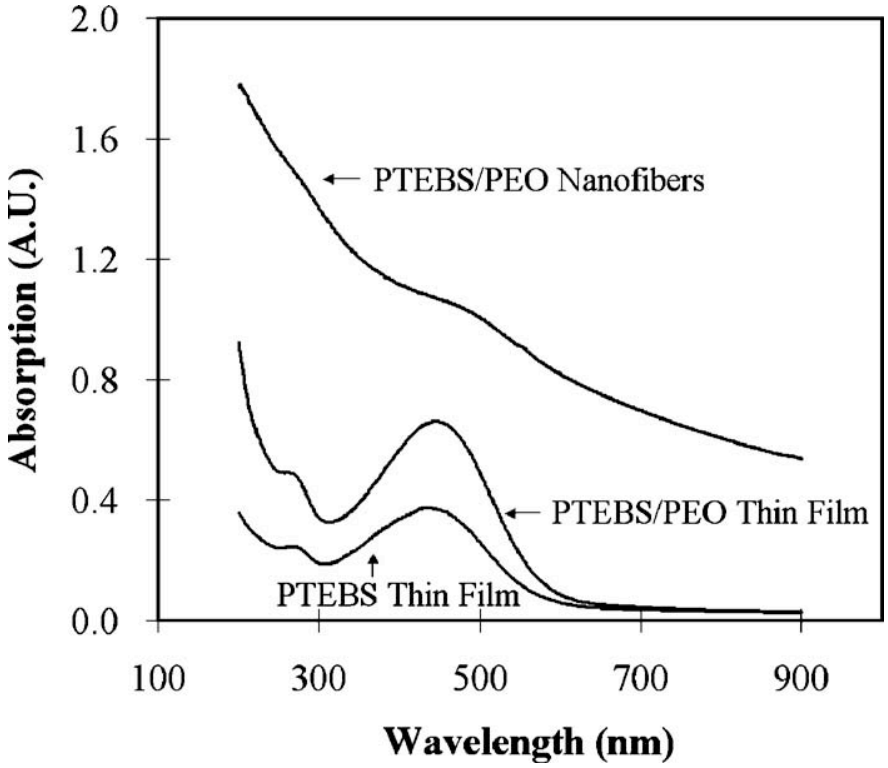

Figure 31: Absorption spectra of a pure PTEBS thin film, a PTEBS/PEO thin film, and unimodal PTEBS/PEO nanofibers.

In order to eliminate the influence of the absorption of the substrate in the UV region, quartz slides were used as substrates to collect the electrospun fibers. Moreover, a quartz slide was used as the reference for the absorption measurement. The absorption spectrum was significantly changed with the structure change from thin film to nanofibers. Unlike the spin coated thin films of pure PTEBS and PTEBS/PEO, the absorption spectrum of the unimodal PTEBS/PEO fibers does not have an obvious peak around 460 nm.

The observed difference in the optical absorption spectra of the 60 nm composite fibers may be produced by the nanoscale PTEBS domains disorderly embedded in PEO (Figure a). The nanoscale PTEBS domains (with a band gap of 2.0 eV) are embedded within the transparent wide band gap PEO forming an assembly of organic quantum dots.

It is well-established that the optical properties of semiconducting quantum dots can be different than the optical properties of bulk material and the PTEBS/PEO composite nanofibers appear to have unique optical characteristics in comparison to their bulk or thin film counterparts.

The optical absorption of the larger bimodal PTEBS/PEO fibers was almost the same as that of a spin coated PTEBS/PEO composite thin film . We believe that this is due to the much larger (200 nm and 1 μm) diameters of the bimodal fibers, which are too large to produce any optical changes in the polymers.

4.1 Humidity and Electrospinning

Electrospinning from an aqueous PTEBS/PEO solution without NH_4OH resulted in the formation of a mat of composite nanofibers with relatively uniform size distribution and an optical absorption spectrum different than that of the bulk material. Electrospinning from an aqueous PTEBS/PEO solution with NH_4OH resulted in the formation of a mat of chemically and physically distinct fibers; large diameter white (PEO) fibers and small diameter black (PTEBS) fibers.

However, composite nanofibers are known to show a blue shift in their optical emission spectrum. For example, the electronic properties of MEH-PPV/SBA-15 composite nanofibers were characterized by Madhugiri et al where the emission spectra of the nanofibers are shown in Figure 32 [82].

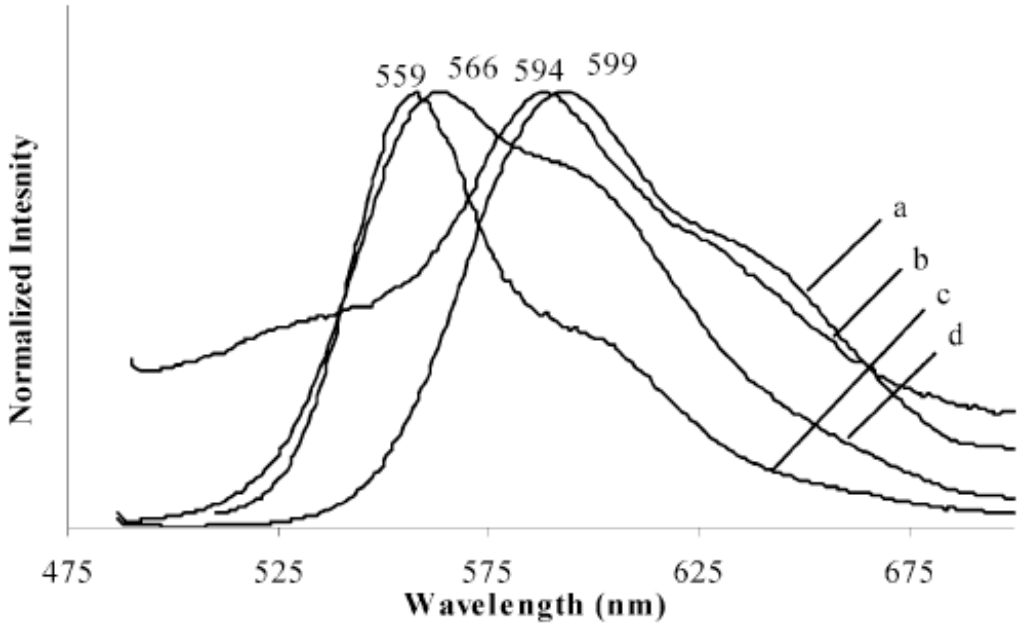

Figure 32: Comparative emission spectra of (a) MEH-PPV film, (b) MEH-PPV fibers, (c) MEH-PPV solution (10-7 M solution in 1,2-dicholorethane), and (d) MEH-PPV/SBA-15 composite fibers [82].

A blue shift of an emission spectrum for a MEH-PPV/SBA-15 composite fibers was observed with respect to MEH-PPV film and MEH-PPV fibers. Although the composite fiber still shows a red shift in comparison to the MEH-PPV solution due to less spatial separation of the polymer chains, preventing polymer chain aggregation can lead to a decrease in π-π stacking, and interchain electron delocalization for higher emission energies. By mixing the surfactant SBA-15, the polymer aggregation of MEH-PPV is reduced, and a blue shift for the MEH-PPV/SBA-15 is observed.

In preparation of an organic solar cell, a blue shift of the polymer absorption can decrease its performance. In contrast to the blue shift shown in composite nanofibers, coaxial electrospinning can be used to avoid a decrease in π-π stacking, and to cause a red shift in PTEBS nanofibers. To demonstrate this, coaxial PTEBS fibers were fabricated.

For this experiment, a 1.5% concentration of PTEBS in de-ionized water was used as a core solution, and a 2.5% concentration of 200000 g/mol PEO dissolved in

Chloroform was used as the outer solution to perform coaxial electrospinning. The coaxial electrospinning was performed with the PTEBS solution infusion rate at 4.5 μl/min, and the PEO solution infusion rate at 40 μl/min. The distance from the coaxial needle tip to the grounded substrate was kept at 28 cm with a DC voltage of 16 kV, and the collected fibers were washed using an ethanol vapor in a 65°C oven for an hour to remove the PEO coatings of the collected coaxial nanofibers. Figure 33 is an image of PTEBS/PEO coaxial nanofibers taken from an optical microscope at 100× magnification.

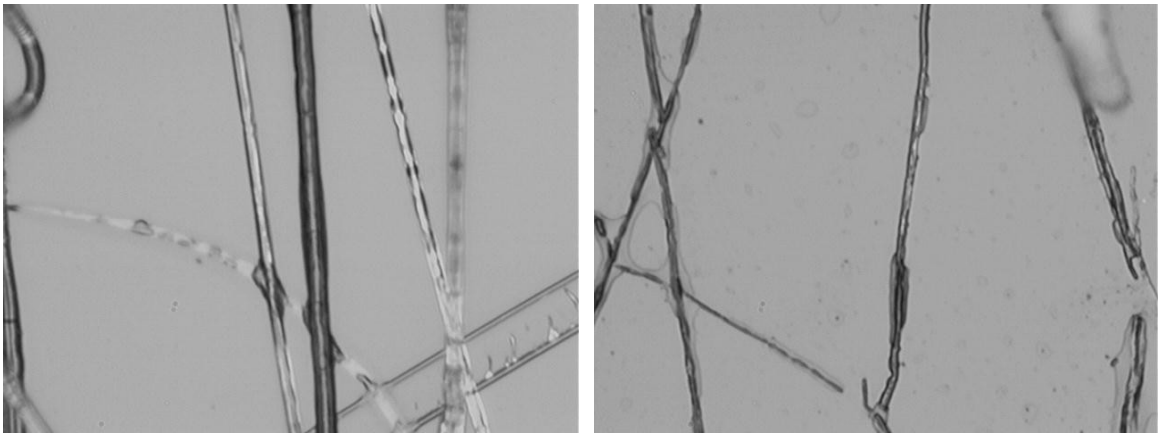

Figure 33: 100× Optical microscope image of (Left image) PTEBS/PEO coaxial nanofibers, and (Right image) PTEBS nanofiber extracted from ethanol vapor washing of PTEBS/PEO coaxial nanofibers.

The contrast in the coaxial nanofiber image shows a clear coaxial structure of the PTEBS/PEO nanofibers. After washing in ethanol vapor, the residual nanofibers are those of PTEBS due to insolubility of PTEBS in ethanol as opposed to high solubility of PEO. Although no extensive steps to characterize the collected nanofibers were taken, the role of humidity in electrospinning was clearly demonstrated. This experiment was performed under 14.1% humidity. Figure 34 below shows an experiment performed under the same electrospinning condition, but with 27 cm distance for the left image, and 29.5 cm distance for the right image where the humidity was recorded as high as 47%.

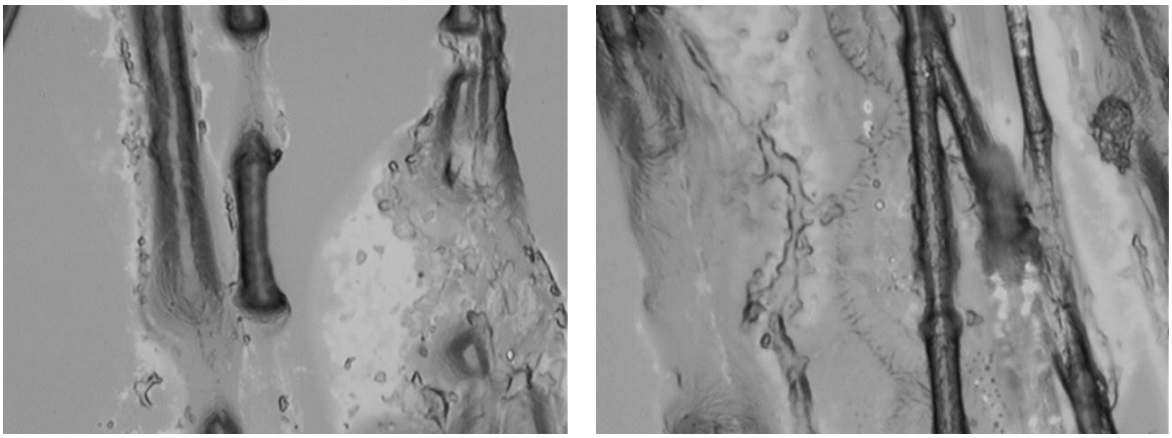

Figure 34: 100× Optical microscope image of (Left image) PTEBS/PEO coaxial nanofibers with 27 cm needle to substrate distance, and (Right image) PTEBS/PEO coaxial nanofibers with 29.5 cm needle to substrate distance with 47% humidity.

In the high humidity condition, the image shows a discontinuous nanofiber structure where the outer PEO solution is unable to contain the core PTEBS solution. PTEBS being dependent in atmospheric humidity, coaxial electrospinning of PTEBS proves to be a difficult experiment due to its inconsistency of collected nanofibers. Through our research in other donor materials, MEH-PPV has shown to have much more stability in coaxial electrospinning, and the following chapters will discuss the fabrication of electrospun polymer-fiber solar cells based on MEH-PPV/PCBM mixture.

5. Electrospun polymer-fiber solar cell structure

The objective of this project is to take advantage of the qualities of electrospun nanofibers in order to improve the performance of polymer solar cells. If a solution of donor/acceptor mixture is fabricated into a nanofiber structure with electrospinning, anode and cathode metals of different work functions are the pieces needed in preparation of a solar cell device. To demonstrate the feasibility of this idea, three different placements of electrodes have been considered for fabrication of electrospun polymer-fiber solar cells.

5.1 Bulk heterojunction type polymer-fiber solar cells

Within a history of organic solar cells, its device structure has typically consisted of a two dimensional sandwich structure where an active layer was deposited onto a transparent conducting substrate, and a counter electrode was evaporated on an exposed surface of the active layer. With electrospinning, an active layer fibers may be collected onto a transparent conducting electrode, and a counter electrode evaporated on the exposed surface of electrospun nanofibers. This device structure is shown in Figure 35 where FTO is used for the transparent conductor, and gold is the counter electrode metal is evaporated onto the electrospun nanofiber surface. This is essentially the device structure fabricated by Sundarrajan et al [69] and described in Chapter 3.

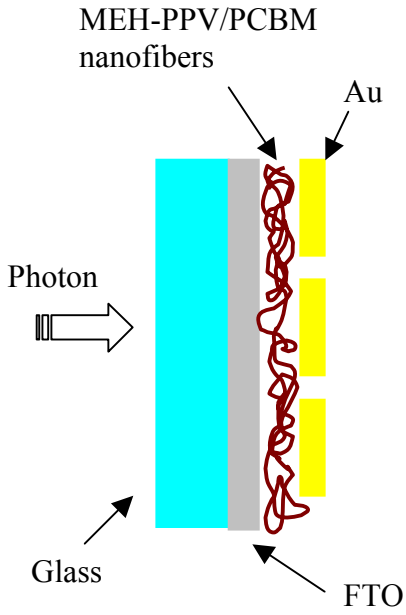

Figure 35: Schematic diagram of FTO/MEH-PPV:PCBM nanofiber/Au device.

For an active layer film deposited onto a transparent conductor, one structural advantage to this design is in its ability to incorporate a hole blocking layer between a conductor and an active layer which has been shown to significantly increase the performance of organic solar cells. To add a hole blocking layer between a conductor and an electrospun polymer-fiber active layer, a hole-blocking layer must be prepared prior to the polymer fiber collection. However, coaxial electrospinning often requires washing of outer shell polymer to establish a connection between the conjugated polymer of the core, and this process can often interfere with the hole blocking layer film. In addition, there is a possible short circuit from an evaporated metal piercing through the polymer fiber openings. To avoid the short circuit of the two electrodes, thicker fiber matt of active layer nanofiber maybe considered, yet this will only produce a repeated problem encountered by Sundarrajan where a thicker fiber matt leading to poor performance of the device due to low charge carrier mobility of the active layer [69]. Due to these

problems encountered in for sandwich structure of electrospun polymer-fiber solar cells, other structures are considered for the fabrication of electrospun polymer-fiber device.

5.2 Triaxial electrospinning of polymer-fiber solar cells

Triaxial electrospinning has been reported for organic LEDs [83], and the same structure offers several potential advantages for organic solar cells. Triaxial nanofiber organic solar cells would consist of a conductive core, semiconducting mid-layer, and a conductive outer shell as shown in Figure36.

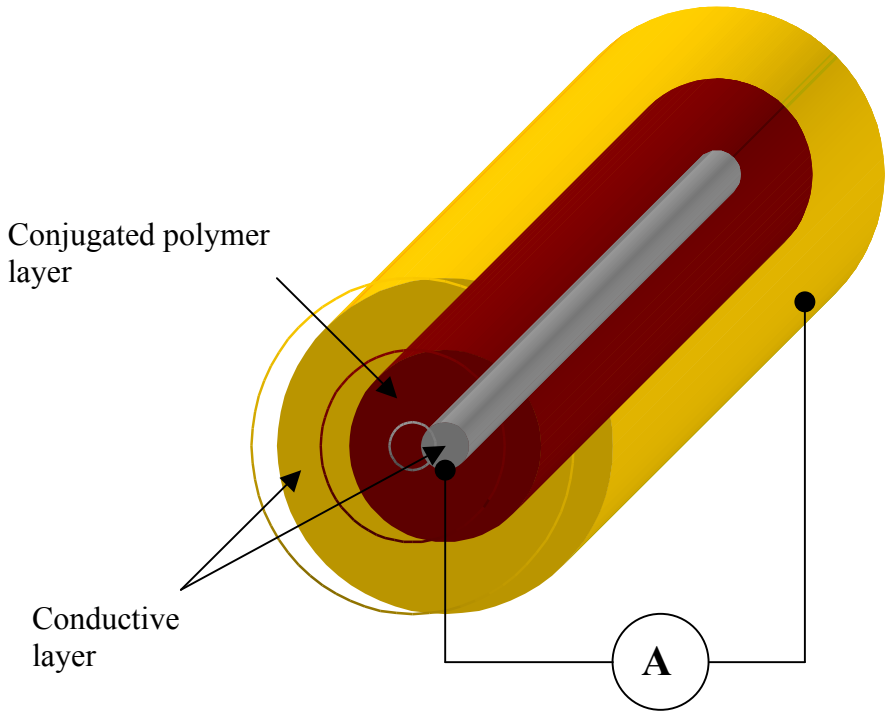

Figure 36: Schematic diagram of Triaxial nanofiber device.

One of the challenges with the polymer-fiber solar cells is in establishing good electrical contact with the conjugated polymer to the two electrodes, and the triaxial fiber has the potential to eliminate the challenges experienced in establishing good electrical contact.

In addition, the device will not require washing for conjugated polymer exposure, will be readily made with true reel-to-reel processing, and it will be significant step from a conventional two-dimensional structure to quasi-one-dimensional devices.

To test the stability of triaxial electrospinning, the core and shell component of the triaxial nanofibers were selected to be an electrospinnable solution of 10% PVP polymer by weight dissolved in 8.5 parts ethanol, and 1.5 parts DI water, and 1:2 ratio of MEH-PPV:PCBM dissolved in chloroform at 1.4% concentration by weight. For the infusion rate, the inner core PVP was set to 10 μl/min, the middle layer MEH-PPV:PCBM solution at 5μl/min, and outer shell PVP solution at 0.3 μl/min. The humidity was recorded at 47.5%, needle tip to substrate distance was 11 cm, and triaxial electrospinning were carried out with a stable polymer fiber jet found at 10.5 kV. Figure 37 shows an optical microscope image of the collected nanofibers at 100× magnification.

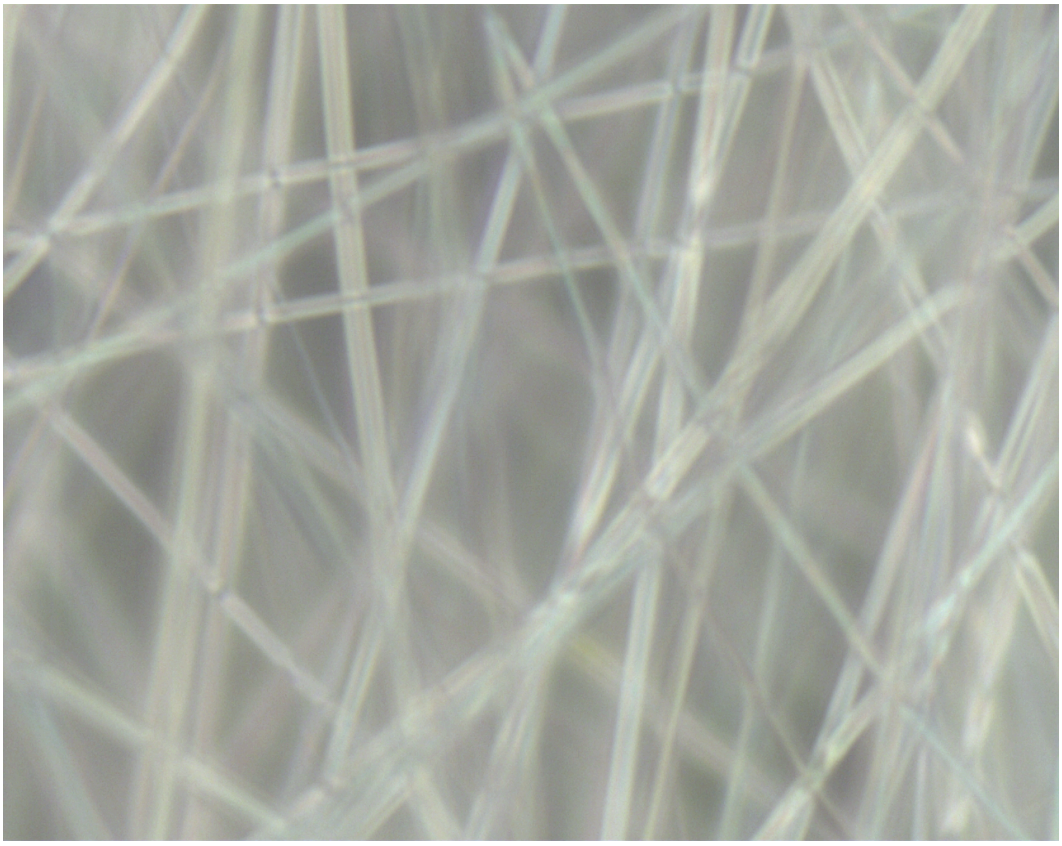

Figure 37: Optical microscope image of a triaxial nanofibers.

From seeing an optical contrast in the triaxial nanofiber, an additional experiment was carried out with the addition of 50.4 mg Aluminum nanoparticles in 1 milliliter of inner core PVP solution, and 59.6 mg Indium Tin Oxide nanoparticles in 1 milliliter outer shell PVP solution. For this experiment, the electrospinning conditions were modified with changes in infusion rate with the inner core solution at 8.5 µl/min, middle layer at 8.5 µl/min, and outer shell solution at 45 µl/min. The humidity was at 46.1%, and a stable fiber jet was observed at 12 kV. The collected nanofibers were observed under a Hitachi scanning electron microscope to further verify the triaxial structure of the collected nanofibers.

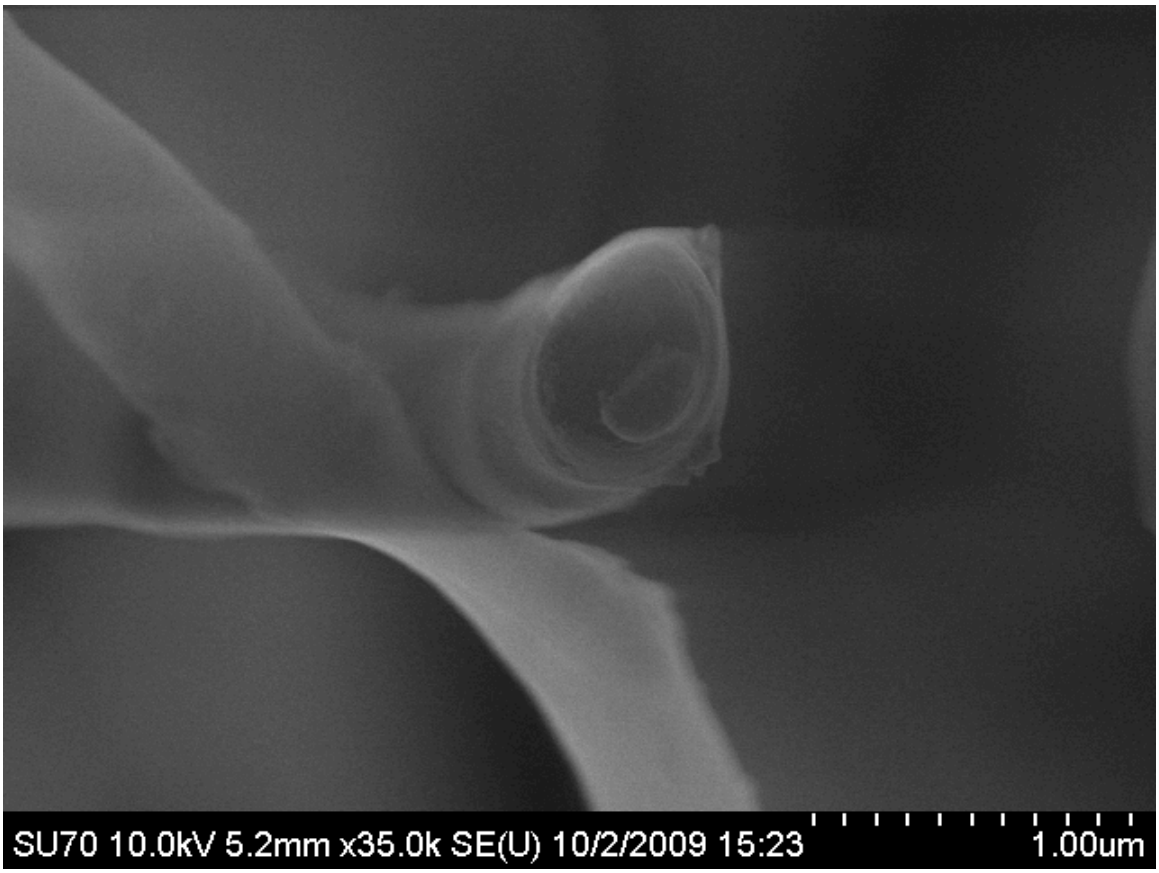

Figure 38: Cross sectional image of triaxially electrospun Al/PVP-MEH-PPV:PCBM-ITO/PVP nanofiber.

From the cross sectional image of the triaxial nanofiber, three different layers from different components of the nanofibers are visible.

For a functional triaxial nanofiber solar cell, the outer shell solution must be conductive, and also transparent for the active middle layer light absorption. In addition, good electrical contact must be established between the active layer, and the two conductive layers. Two other criteria for a functional triaxial nanofiber solar cell are the light absorption, and the work function of the conductive nanofibers. Through our extensive research in synthesis of conductive nanofibers, mixing of Aluminum and Indium tin oxide nanoparticles in a PVP polymer did not result in sufficient conductivity to fabricate a working solar cell. In addition, synthesis of conductive nanofiber has

proven difficult with a work function suitable for the MEH-PPV:PCBM active layer. Because of these challenges encountered in Triaxial electrospinning, other device structure for an electrospun polymer-fiber solar cell have been studied.

5.3 Co-planar bimetallic substrate for electrospun polymer-fiber device

Our first device was successfully prepared with a very simple structure where two metal-coated microscope glass slides were glued adjacent to each other onto another glass slide. Such a device structure allowed easy access to collected nanofibers for nanofiber processing, and mobility of the device will be dependent on electrode separation rather than the fiber matt thickness. A sample image is shown below.

(a)

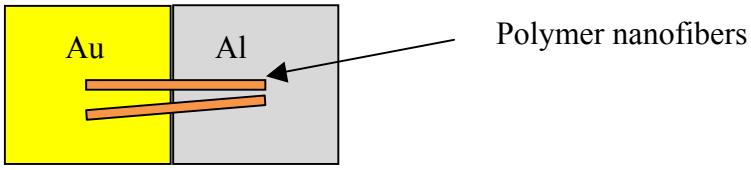

(b)

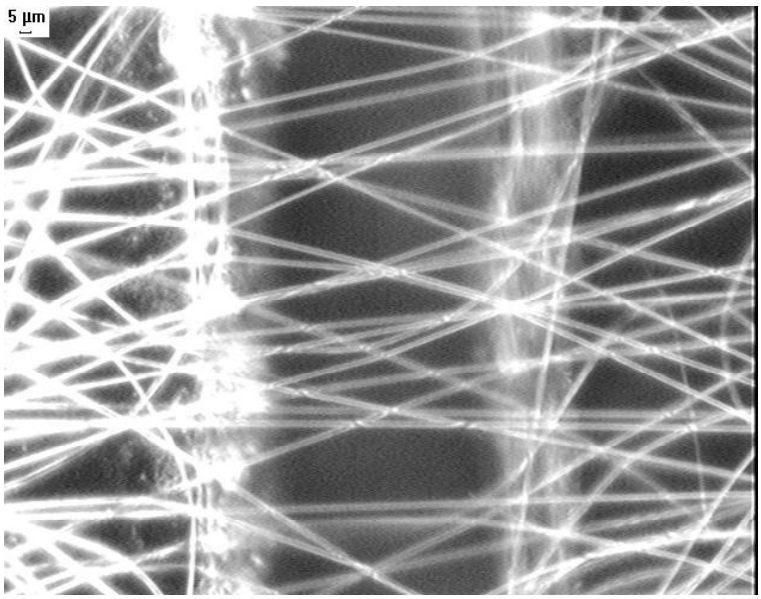

Figure 39: (a) Simple substrates used to produce initial photodiodes. Microscope slides were broken, gold and aluminum were deposited, and the two halves were glued back together with gaps ranging from 3 to 50 µm. (b) Optical microscope image of Electrospun fibers between gold and aluminum gap at 50×.

Aluminum was evaporated onto a glass slide to match the LUMO of PCBM, and gold was sputter coated onto a glass slide to match the HOMO of MEH-PPV. Separation between the two electrodes was reproducible where tight placement of the two slides along side each other always resulted in 3-50 µm separation.

For the first devices, poly[2-methoxy-5-(2-ethylhexoxy)-1,4-phenylenevinylene] (MEH-PPV) was used as an electron donor, and [6,6]-phenyl-C61 butyric acid methyl ester (a soluble form of C_{60} known as PCBM) was used as an electron acceptor. In preparation of MEH-PPV for electrospinning, it was first diluted in a solvent $CHCl_3$ (chloroform) to a concentration of 0.8 %, under continuous stirring for two weeks. PCBM at a concentration of 5.5-8.5% in chloroform was then added to the diluted solution of MEH-PPV for a 1:2 weight ratio mixture of MEH-PPV to PCBM respectively.

For the shell of the coaxial fibers, a polymer solution that is immiscible to chloroform was chosen. Poly(vinylpyrrolidone) (PVP) at a concentration of 10 % in 1.5 parts DI water to 8.5 parts Ethanol is immiscible to chloroform, and was used as an electrospinnable outer solution B. The two solutions were then fed through a coaxial needle, and the PVP coated MEH-PPV/PCBM nanofiber was collected onto an electrically grounded substrate. The collected coaxial nanofibers were then soaked in an ethanol bath for 2 hours to wash away the electrically insulating PVP coating to allow electrical contact between the MEH-PPV/PCBM, and the substrate electrodes.
For these devices, the resulting current-voltage characteristics are shown in Figure 40 below.

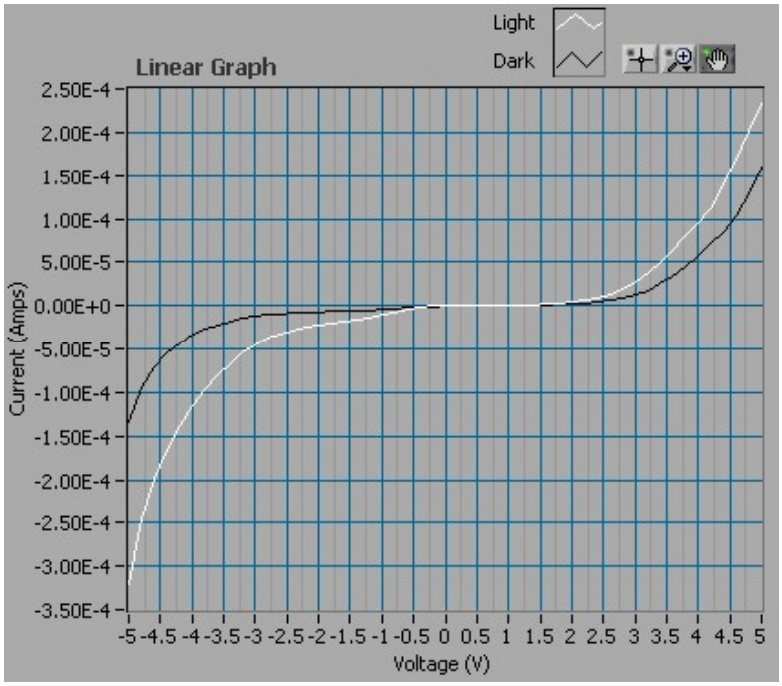

Figure 40: J-U curve for the electrospun fibers on aluminum and gold substrates. The devices demonstrate photodiode characteristics.

The two break-down voltages which are also sensitive to light exposure demonstrate that photodiode were characteristics obtained from an electrospun device prepared with co-

planar bimetallic substrates. In addition, small open circuit voltage (U_{oc}) was recorded at 0.020 V. Based on this successful device fabrication using co-planar bimetallic substrate, it was felt that additional improvements could be made to the device structure to improve the output. We considered reducing the metal separation for more efficient charge collection, and the use of multiple two metal junctions to increase the charge collection area. Such device structure is further discussed in the next chapter for use in electrospun polymer-fiber solar cells.

6. Interdigitated Electrode Substrate

Polymer solar cells typically take the form of a sandwich structure with the active layer placed in between the anode and cathode electrodes. There are several challenges with this design. For example, at least one of the electrodes must be an optically transparent material such as Indium Tin Oxide (ITO) or Fluorinated Tin Oxide (FTO) [84]. These materials typically have lower conductivity than metal electrodes and are often deposited using high temperatures which can be harmful to the polymer. In addition, the device fabrication requires a two-layer coating (at a minimum) with fabrication of the active layer, and the counter electrode.

For use with electrospun fibers, one possible design would make use of co-planar interdigitated electrodes of dissimilar materials. This chapter describes the development of such a structure through photolithography onto a heavily oxidized Si wafer. This device structure offers some potential advantages in comparison to the conventional multilayered sandwich configuration. For example, because transparency is not required, co-planar interdigitated electrodes in organic solar cells allow the use of a wider variety of electrode materials. In addition, the interdigitated structure has an inherent reliability due to the incorporation of multiple junctions for charge collection. Interdigitated electrodes of a single metal have been used in sensors [81], transistors [85], and even in photovoltaic devices [85]. There are limited reports of the use of vertically-oriented two-metal interdigitated electrodes in polymer solar cells [87].

6.1 Experiment

The co-planar two-metal electrode substrates were fabricated on the oxidized surface of silicon wafers using photolithography. Two photomasks were prepared and the masks were used to pattern photoresist using UV light and standard photolithographic techniques.

Aluminum and nickel electrodes with a separation distance of between 1 and 3 μm were deposited at a thickness of approximately 100 nm. Figure 41 shows a schematic and microscope image of a completed interdigitated two-metal electrode substrate. The total device area was 0.11 cm^2.

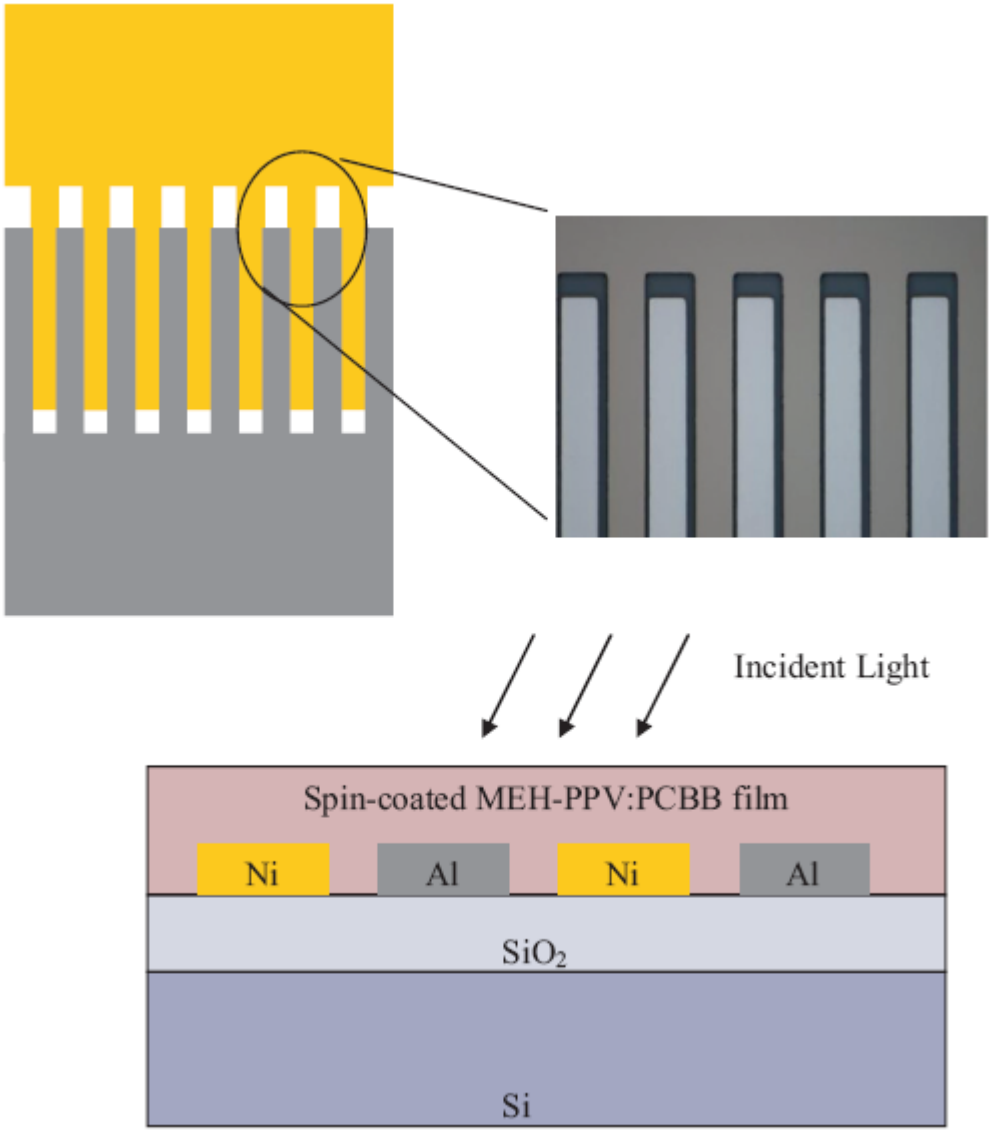

Figure 41: (a) Interdigitated two-metal substrate wafer patterns after two-step photolithography. (b) Side view of interdigitated electrodes showing that electrodes do not block the incident light.

The minimum electrode separation in these devices was limited by our photolithographic capabilities (about 1 μm) and we estimated, based on the short diffusion length of the donor material, that the separation between the two metal electrodes should be closer to 100-200 nm for efficient charge collection. Therefore, relatively poor device efficiency was expected due to incomplete charge collection. However, the primary goal of this

work was to introduce and demonstrate the feasibility of new co-planar electrode geometry and no effort was made to optimize the device efficiency.

A solution was prepared from a mixture of poly[2-methoxy-5-(2-ethylhexyloxy)-1,4-phenylenevinylene] (MEH-PPV) as the electron donor, and [6,6]-phenyl-C_{61} butyric acid butyl ester (PCBB) as the electron acceptor. MEH-PPV was diluted to 0.72 % concentration in chlorobenzene, and stirred for a minimum of 2 weeks. PCBB was then added to the MEH-PPV solution with an additional amount of chlorobenzene to adjust the solution concentration. MEH-PPV:PCBB in a 1:3 wt ratio at 2.44 % total concentration of donor:acceptor solution was prepared, and stirred overnight. The solution was spin-coated over the interdigitated two-metal electrode at 2000 rpm for 40 seconds.

Devices were tested in dark and under AM1.5 illumination of 80 mW/cm^2 intensity. The current density-voltage (*J-U*) curve was measured using a Keithley 236 source generator by varying the applied voltage from -2 to 2 V in 0.04 V steps across nickel and aluminum electrodes. In addition, the resistance of the silicon dioxide substrate film was tested by measuring the illuminated *J-U* characteristics of the electrodes prior to depositing the polymer film in order to make sure the current response was due to that of the donor:acceptor film and not the silicon substrate.

6.2 Results

The actual electrode separations of the co-planar interdigitated bi-metallic substrate used for the experiment were 1.21 μm on one side and 2.42 μm on the other. The electrode fingers were roughly 10 μm wide. Figure 42 shows a 100× magnified image of the co-planar interdigitated bi-metallic electrode used for this experiment.

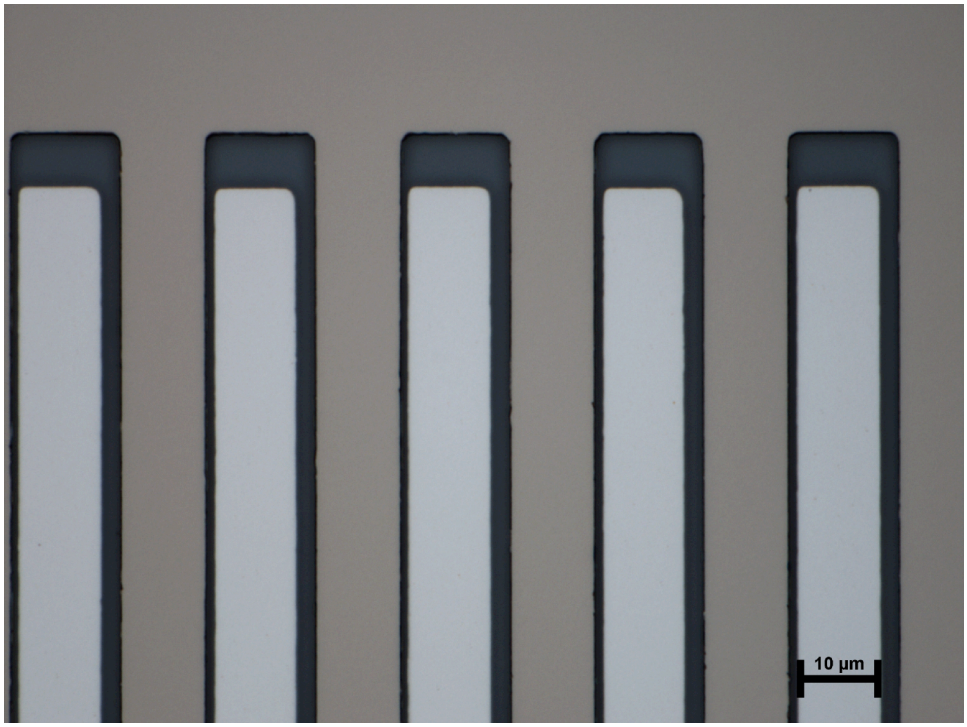

Figure 42: 100x magnified image of the interdigitated 2 metal electrode substrate.

Figure 43 is a plot of the J-U curves with cubic interpolation, obtained from the device after spin coating of MEH-PPV:PCBB donor:acceptor solution. A best-fit line through the experimental data is also included.

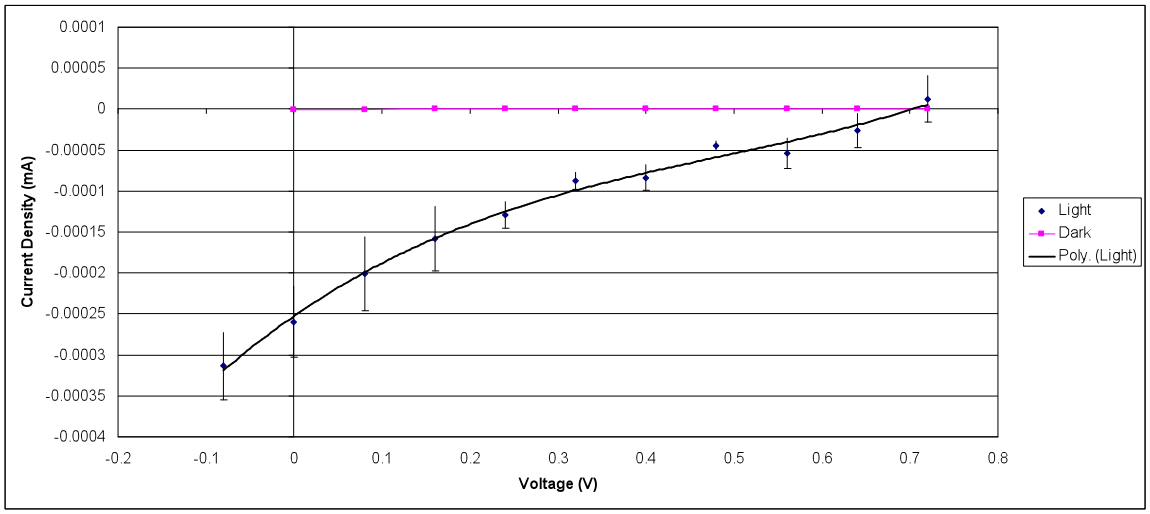

Figure 43: J-U characteristic on 1:3 wt ratio of MEH-PPV:PCBB on interdigitated two metal substrate. The solid line represents a curve fit through the experimental data.

The device showed no response under dark conditions, while a relatively strong response was obtained upon illumination. The typical thickness of the active layer in bulk heterojunction solar cells is near 100 nm, and the separation of our interdigitated bi-metallic electrodes is very large by comparison. Therefore only a very small fraction of the photon generated excitons (i.e. those within about one diffusion length – 20 nm of an electrode) can potentially contribute to the external current. However the device generated a measurable photovoltaic effect even under these less than optimum conditions. The open circuit voltage of the device was 0.704 V, and the short circuit current was 0.252 μA.

The device efficiency was calculated in two ways. It was first calculated using the total area of the co-planar interdigitated electrode device (approximately 0.11 cm^2). By this method, the efficiency was determined to be $3.53x10^{-4}$ %. However, the majority of this total area is occupied by the electrode pads and only the fractional area between the cathode and anode electrodes is expected to contribute to the photocurrent. Neglecting the area of the electrode metal surfaces, the active area of the device was determined to be approximately 15 % of the total illuminated area of the device (approximately 0.017 cm^2), and from this, the estimated total device efficiency was found to be 0.0023 %. It is expected that this efficiency could be further increased by reducing the electrode separation distance and by optimizing the properties (e.g. weight fractions) of the organic solution. With respect to the electrospun polymer-fibers, co-planar bi-metallic interdigitated electrode substrate offers a simple alternative for electrospun polymer-fiber solar cells.

7. Electrospun Polymer-fiber solar cell materials optimization

Co-planar bi-metallic interdigitated electrode substrates were used for testing all electrospun polymer-fiber solar cells. A variety of different materials, solvents, and coaxial shell extraction methods have been tested. The aim of this chapter is to further understand the characteristics of different materials, and compatibility of each experiment for electrospun polymer-fiber solar cells device synthesis.

7.1 P3HT and MEH-PPV

Earlier we have introduced P3HT and MEH-PPV as popular choices for a fabrication of organic photovoltaics due to their good solubility, processability, environmental stability, electroactivity, and other interesting properties [58]. Taking these properties into consideration, P3HT was tested for synthesis of electrospun polymer-fiber solar cells. At 44.8% humidity, the needle tip to substrate distance was set at 11 cm. A 45:55 weight ratio of P3HT:PCBM was dissolved in Chlorobenzene at 1% concentration, and was coaxially electrospun as core solution with an infusion rate of 4μl/min. The infusion rate of the outer 10 wt% PVP solution dissolved in 8.5 parts ethanol and 1.5 parts DI-water was set to 26 μl/min, and a rather unstable jet of coaxial nanofiber jet was found at 7.7 kV. The collected fibers were annealed in 60ºC oven for 30 minutes to promote crystallization of P3HT, and were further washed in ethanol for an immediate removal of PVP shell. The device was then transferred to 130ºC hot plate, and were heated for 2 minutes for improved metal to polymer contact. Figure 44 shows a 50× optical microscope image of the synthesized solar cell device.

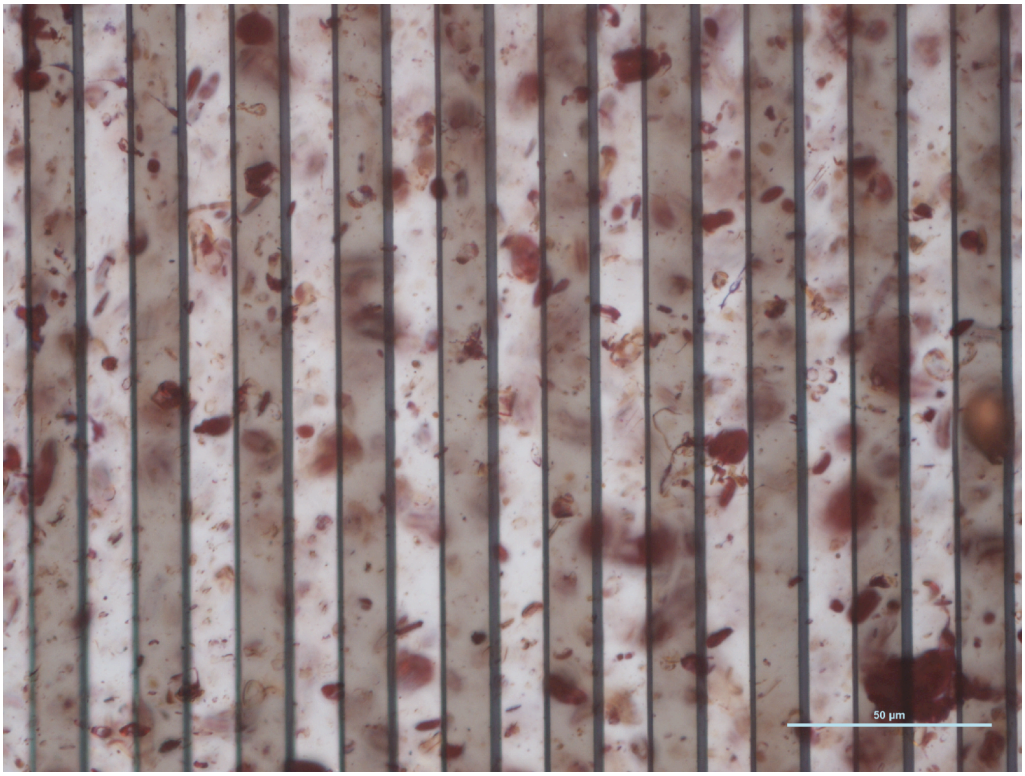

Figure 44: Optical microscope image at 50× magnification for P3HT:PCBM nanofiber after ethanol washing.

As can be seen from the figure, P3HT failed to maintain its nanofiber structure with PVP extraction. Additional experiments were performed using ethanol vapor for the PVP removal in hopes of avoiding destruction of the P3HT nanofibers.. Figure 45 shows the collected coaxial nanofibers of P3HT:PCBM with PVP shell. For this experiment, coaxial nanofiber jets were stable at 7.7-8.5 kV, and the fibers were washed in ethanol vapor at 80ºC.

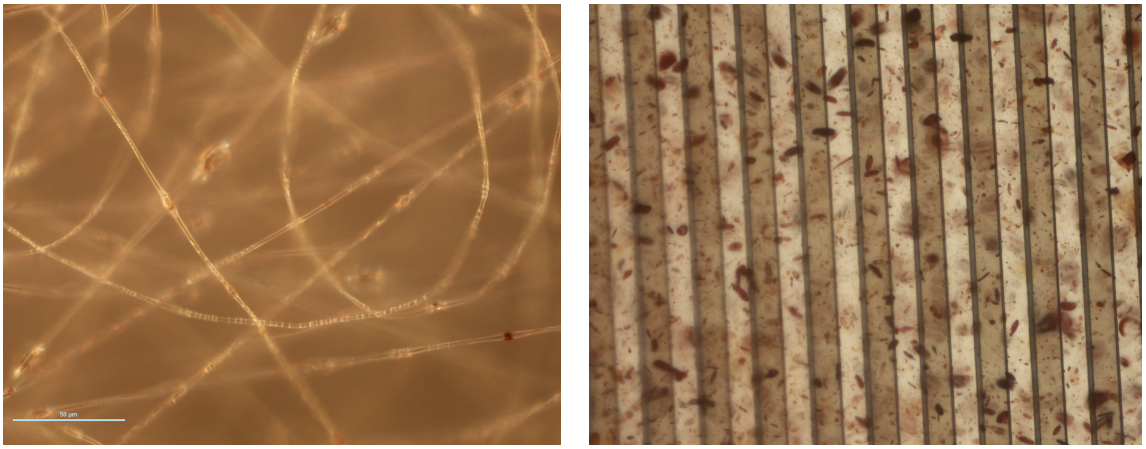

Figure 45: (Left image) Coaxially electrospun P3HT:PCBM nanofibers. (Right image) Coaxially electrospun P3HT:PCBM nanofibers washed in ethanol vapor at 80ºC oven.

Regardless of different PVP extraction methods, P3HT failed to maintain its nanofiber structure. For this reason, MEH-PPV was chosen for further research on electrospun polymer nanofiber solar cells.

7.2 Solvents

Organic photovoltaics are known to have better performance with good film morphology where a choice of solvent is a contributing factor [88]. In electrospinning, undissolved particles can lead to clogging, and particle accumulation that can cause an unstable jet. For electrospinning of a MEH-PPV:PCBM mixture, Chloroform and Chlorobenzene are are known solvents [89]. To determine an ideal solvent for electrospinning, two solutions of 0.5% by weight MEH-PPV dissolved in chloroform and chlorobenzene were prepared for comparison. Figure 46 is a normalized photoluminescence spectrum for comparison of MEH-PPV film using two different solvents.

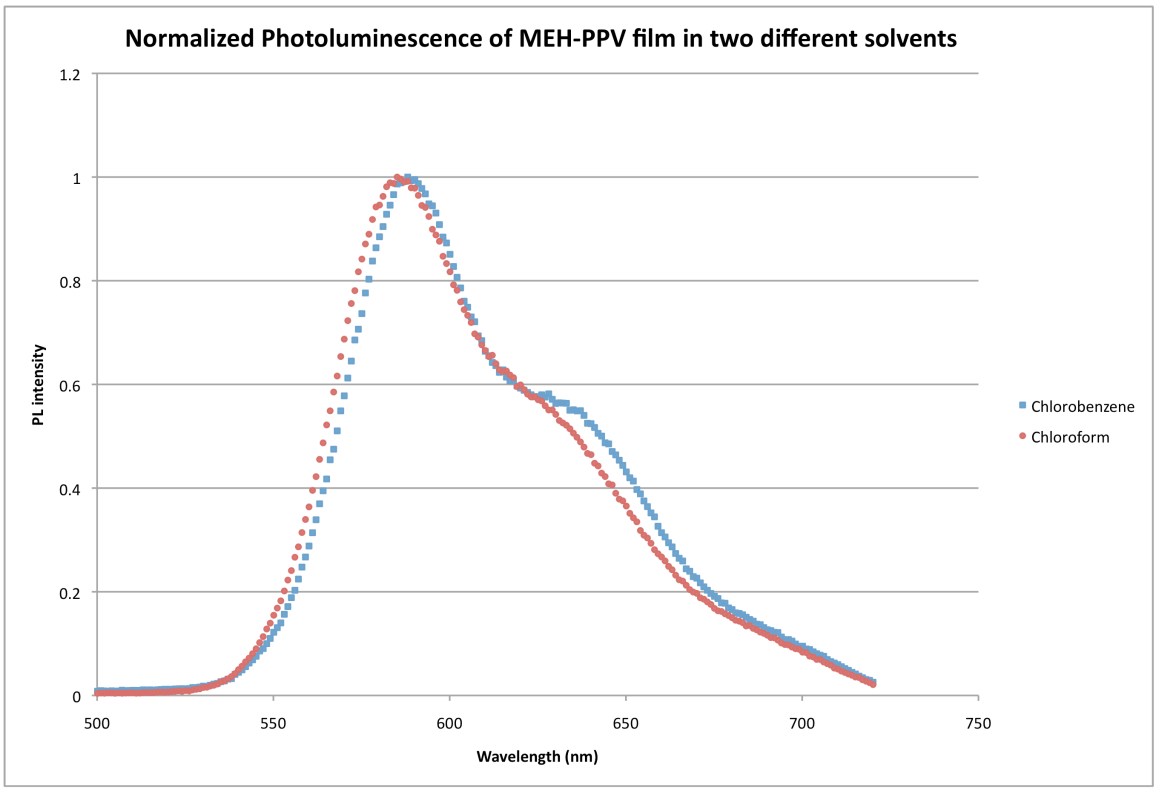

Figure 46: Normalized Phtoluminescence spectrums of 0.5% by weight MEH-PPV in Chloroform and Chlorobenzene.

The photoluminescence spectra compared shows a 4 nm red shift in MEH-PPV solution prepared from chlorobenzene. It has been previously stated that stretching of the polymer chains causes a red shift in MEH-PPV solution. The result indicates better MEH-PPV solution morphology from chlorobenzene solution where more stretching of the polymer chains was observed from low viscosity and spin-coating process. In addition, a study of MEH-PPV in different solvents done by Alsalhi et al shows better quantum yield in a chlorobenzene solution, where quantum yield is a ratio from a number of photons emitted over a number of photons absorbed [90].

Table : Quantum yield of MEH-PPV in different solvents at 1 μM [90].

Solvent	Optical density ±0.01	Quantum yield ±0.01
Benzene	0.6	0.35
Chlorofrom	0.94	0.22
THF	0.42	0.50
Chlorobenzene	0.73	0.34
Toluene	0.4	0.49
Dichlorobenzene	1.2	0.22
Ethylenedichloride	1.1	0.21

For bulk heterojunction solar cell, more charge generation is expected for higher quantum yield, which will lead to better efficiency for a device. Due to the morphology and overall characteristics of MEH-PPV film, chlorobenzene is a better choice for fabrication of electrospun polymer-fiber solar cell.

7.3 MEH-PPV to PCBM ratio

For bulk heterojunction systems, PCBM has two roles for organic photovoltaics to properly function. One is in its role as an electron acceptor assisting in charge separation from the excitons generated from the donors, and the other with the transport of charge to the anode using its percolation network. To understand the ability of PCBM as a charge acceptor, photoluminescence of MEH-PPV:PCBM mixtures were studied as shown in Figure47.

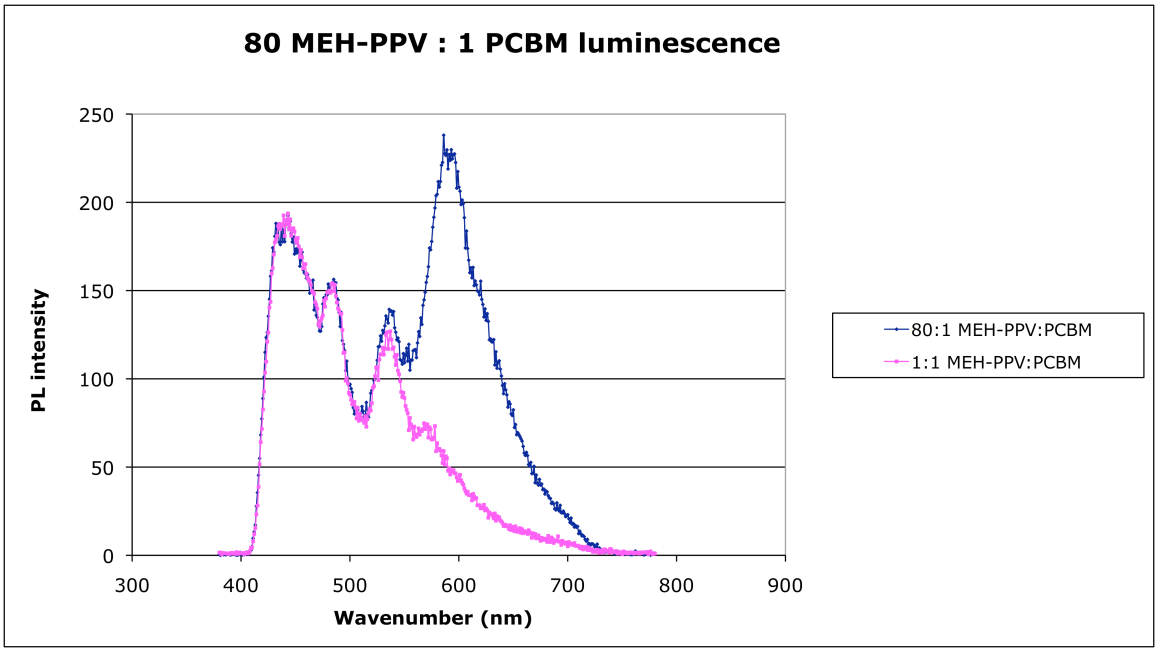

Figure 47: Photoluminescence spectrum of 80:1 MEH-PPV:PCBM, and 1:1 MEH-PPV:PCBM films prepared from chlorofom solution.

Several MEH-PPV:PCBM ratios were tested, and all MEH-PPV fractions less than 80:1 ratio resulted in 586nm MEH-PPV Photoluminescence quenching as indicated for the 1:1 MEH-PPV:PCBM spectra. This shows that PCBM is a strong electron acceptor, and is an indication of efficient charge collection taking place at the PCBM/MEH-PPV interface. As for charge transport to the anodes, a higher PCBM fraction is necessary for the formation of percolation network. The highest performance of a bulk heterojunction film has been observed for a device prepared from 1:4 MEH-PPV:PCBM solution [57]. However for coaxial electrospinning, the electrospun fiber jet loses its stability after 1:3 MEH-PPV:PCBM ratio, and a more stable 1:2.5 MEH-PPV:PCBM solution has been used in synthesis of electrospun polymer-fiber solar cells.

7.4 PCBM and PCBB

PCBB is a PCBM derivative that is known to have slightly better solubility and has resulted in higher performing organic photovoltaic devices [91]. The co-planar bi-metallic interdigitated substrate was tested with an MEH-PPV:PCBB mixture, and demonstrated a photovoltaic characteristics as shown in Chapter 6. However, contrary to its success in thin film structures, PCBB-doped solutions failed to maintain nanofiber structure during coaxial electrospinning. Conjugated polymer solutions of 1.06% concentration of 1:1 MEH-PPV:PCBB, and 1.45% concentration of 1:3 MEH-PPV:PCBB by weight were coaxially electrospun in attempt to synthesize electrospun polymer-fiber solar cells. After multiple experiments with these solutions, a similar morphology was observed after ethanol washing of MEH-PPV:PCBB. The 1:3 MEH-PPV:PCBB nanofibers were collected and were washed through ethanol soaking, and ethanol vapor. In all of these experiments, the collected nanofibers resulted in morphology shown in Figure 48.

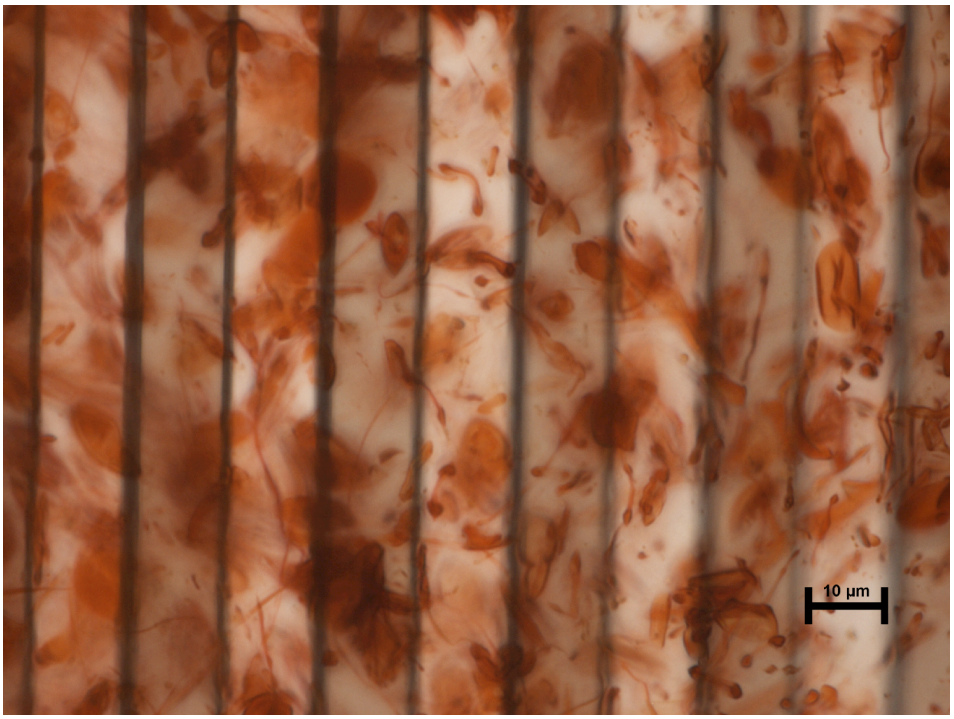

Figure 48: Optical microscope image of a sample MEH-PPV:PCBB solution after ethanol vapor washing at 100× magnification.

Similar to P3HT experiments, PCBB did not maintain its nanofiber structure after PVP extraction. We speculate that due to the improved solubility of PCBB, the polymer is not able to maintain its nanofiber structure. For the purpose of maintaining a nanofiber structure, PCBM is used for synthesis of electrospun polymer-fiber solar cells.

8. Electrospun Polymer-fiber solar cell

Through testing of numerous different materials and electrospinning conditions, an electrospun polymer-fiber solar cell was synthesized using 2.28% by weight concentration of 1:2.5 weight ratio MEH-PPV:PCBM solution prepared from chlorobenzene. In preparation of the MEH-PPV:PCBM solution, a base solution of 0.9% by weight of MEH-PPV in chlorobenzene was first prepared, and stirred for 10 days. Then 24.8 mg of PCBM was added to 1 ml of the 0.9% MEH-PPV base solution to prepare a 1:2.5 weight ratio MEH-PPV:PCBM of 2.28% concentration. The prepared solution was pumped through the inner core syringe, and a 10% by weight concentration of PVP in 8.5 parts ethanol and 1.5 parts DI water was pumped through the outer shell syringe for coaxial electrospinning. The infusion rate for the inner core was at 4 μl/min, and infusion rate of outer shell was set to be at 25 μl/min. Needle to substrate distance was kept at 11 cm, and the humidity was measured to be 16.9%. The electrospun fibers were collected on a gold and aluminum co-planar bi-metallic interdigitated electrode, and the electrode separation between the two gold and aluminum junctions were measured with an optical microscope to be 1.61 μm and 2.34 μm. The collected fibers were quickly dipped in ethanol and taken out after removal of PVP shell, and were dried on a 130ºC hot plate. This resulted in a thin PVP film coating, insulating the surface of electrode contacts. The PVP coatings were further removed by scratching the surface with a wooden stick, and a silver paste was added prior to testing of the electrospun polymer-fiber solar cell device. The current voltage (*J-U*) characteristics were measured using a Keithley 236 source generator by varying the applied voltage from -1 to 1 V in 0.0222 V steps across gold and aluminum electrode.

In our attempt to accurately characterize the performance of electrospun polymer-fiber solar cell, the amount of fibers collected were kept to a minimum with a countable amount of fibers for total active area calculation, while also maintaining the device functionality. Figure 49 is an optical microscope image of the collected coaxial nanofibers at 100×.

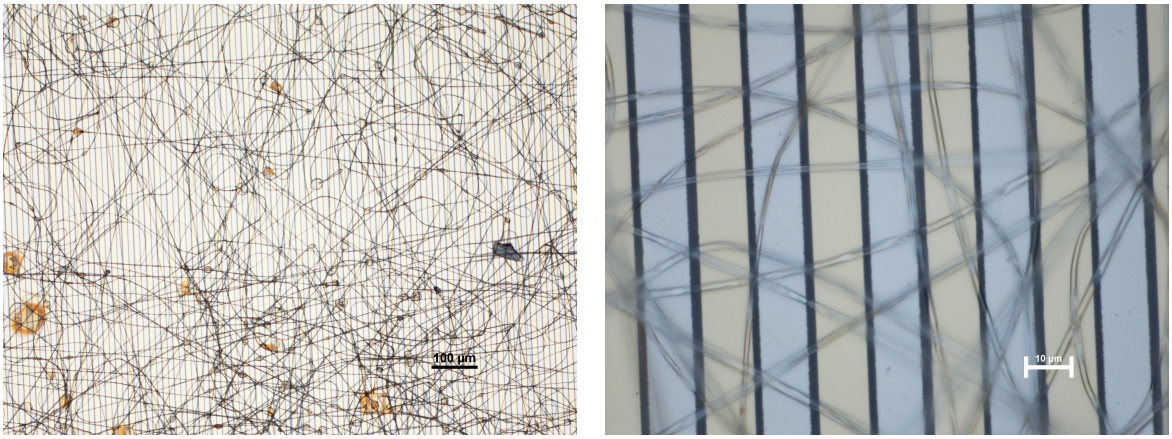

Figure 49: Optical microscope image of the collected coaxial nanofibers on co-planar bi-metallic interdigitated electrode substrate at 10× (Left image), and 100× (Right image).

Before ethanol washing, the collected coaxial nanofibers show some beaded structures from unstable electrospinning jet. Figure 50 below is an optical micrscope image of the collected nanofibers after PVP extraction.

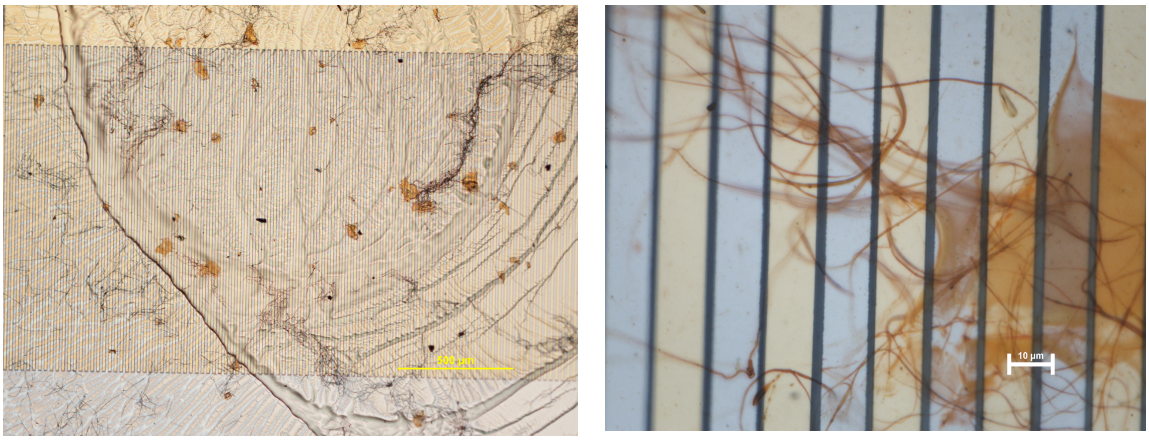

Figure 50: Optical microscope image of the collected coaxial nanofibers on co-planar bi-metallic interdigitated electrode substrate after ethanol washing at 10× (Left image), and 100× (Right image).

The wavy structure observed in the 10× image shows a PVP film, and after ethanol washing, good nanofiber structure is maintained along with some conjugated polymer spots. However, under the dark field, we observe a good nanofiber structure throughout the whole suface of the co-planar bi-metallic interdigitated substrate as shown in Figure51.

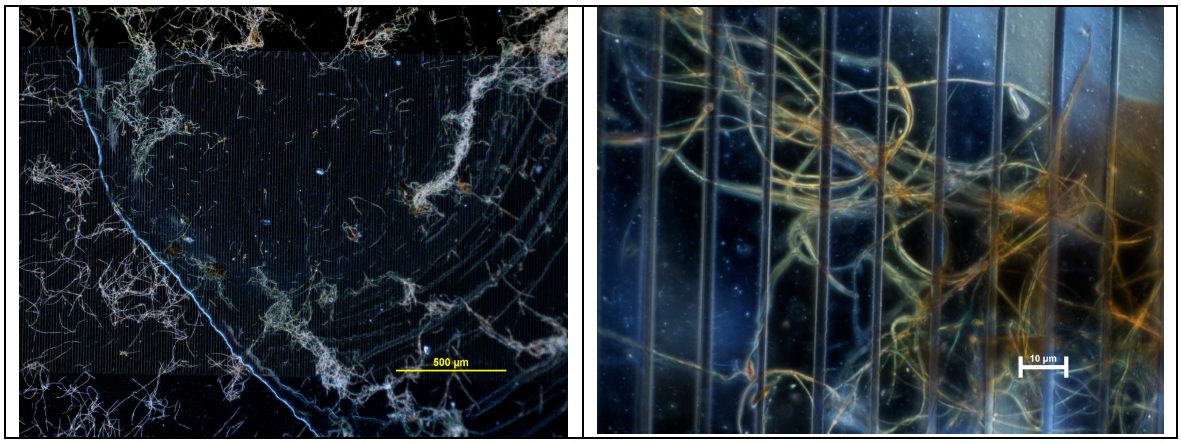

Figure 51: Optical microscope image MEH-PPV:PCBM nanofibers after Ethanol washing in Dark field at 10× (Left image), and at 100× (Right image).

The dark field under an optical microscope filters out directly transmitted light, and is a technique known to be free of artifacts. From this dark field image, we conclude that a good nanofiber morphology is preserved after the ethanol washing of the MEH-PPV:PCBM nanofibers.

The electrospun polymer-fiber solar cell was further evaluated by measuring its J-U curve as shown in Figure 52.

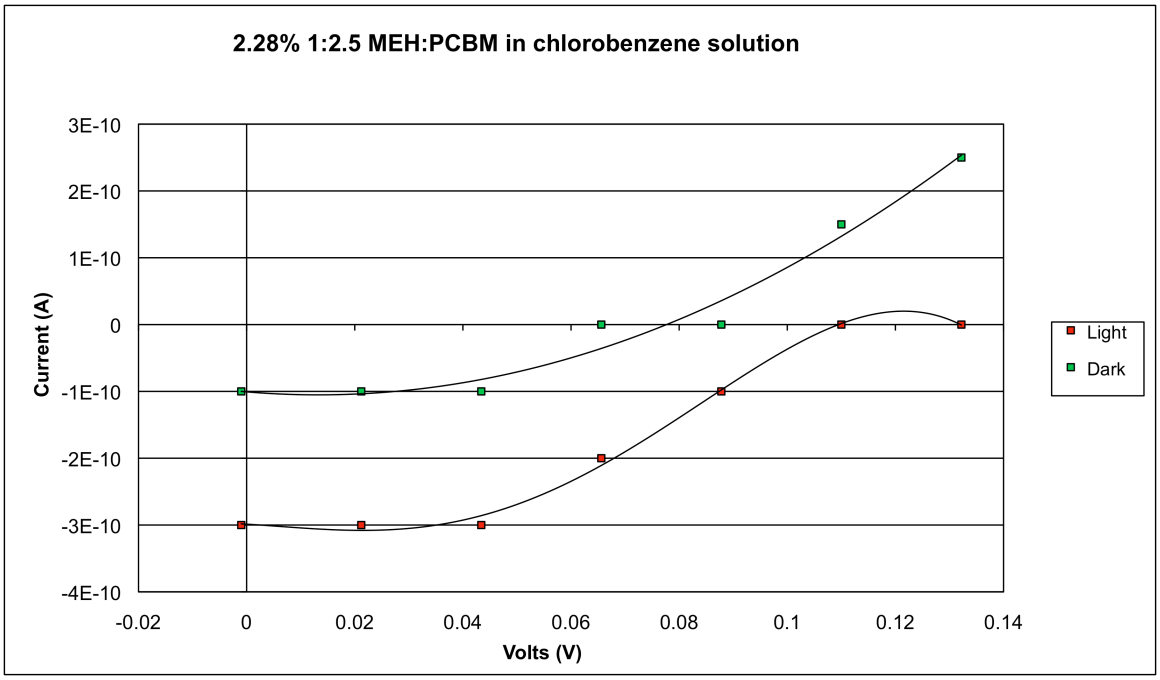

Figure 52: J-U curve measured for MEH-PPV:PCBM nanofibers on co-planar bi-metallic interdigitated electrode. Red squares are the device response with AM1.5 illumination of 80 mW/cm^2, and green squares show the response with the device placed in the dark.

The J-U curve shows a photovoltaic response with a U_{oc} recorded at 0.11 V, and a photovoltage I_{sc} at 3×10^{-7} mA where the total efficiency is then estimated to be 7.92×10^{-10} % based on the total area of the co-planar bi-metallic interdigitated electrode. However, as discussed in detail in Chapter 10, the total area can also be estimated from the number of gold-nanofiber-aluminum junctions given the thickness of electrospun nanofibers. The thickness of the nanofibers are measured to be around 1 μm from optical microscope, and thus the actual efficiency for the electrospun polymer-fiber solar cells may be estimated to as 3.08×10^{-7} % or better considering the potential failure of the nanofibers to establish contact with the electrode junctions. Similar to the earlier device synthesized from MEH-PPV:PCBB film on co-planar bi-metallic interdigitated electrode, the electrospun polymer-fiber solar cells leaves room for improvement with a

smaller electrode separation. With proper adjustments made for electrospun polymer-fiber solar cells, this device may bring significant impact in the field of organic photovoltaics.

9. Characterization of Electrospun Fibers

9.1 Absorption

The electrospun polymer-fiber solar cells were further tested through series of optical characterization methods. The UV-vis spectrometer was used to study the change in absorption of MEH-PPV nanofibers. Various concentrations of MEH-PPV with 0.24, 0.35, 0.47, and 0.7 weight % in chloroform were coaxially electrospun, and their absorptions were measured after PVP extraction with Ethanol. Results of these absorption measurements are presented below.

(a)

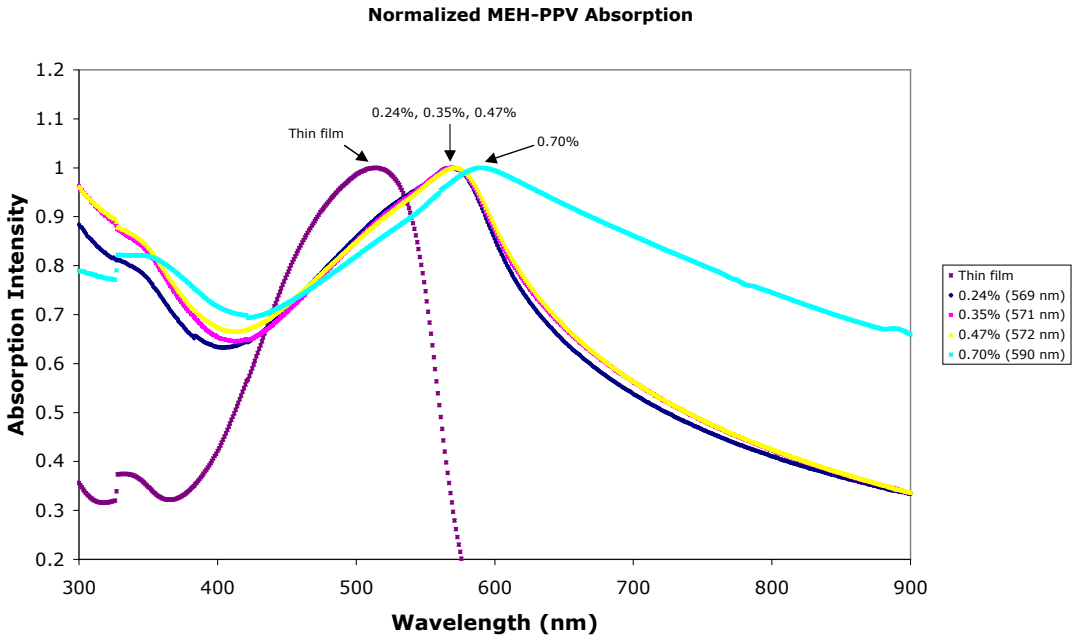

(b)

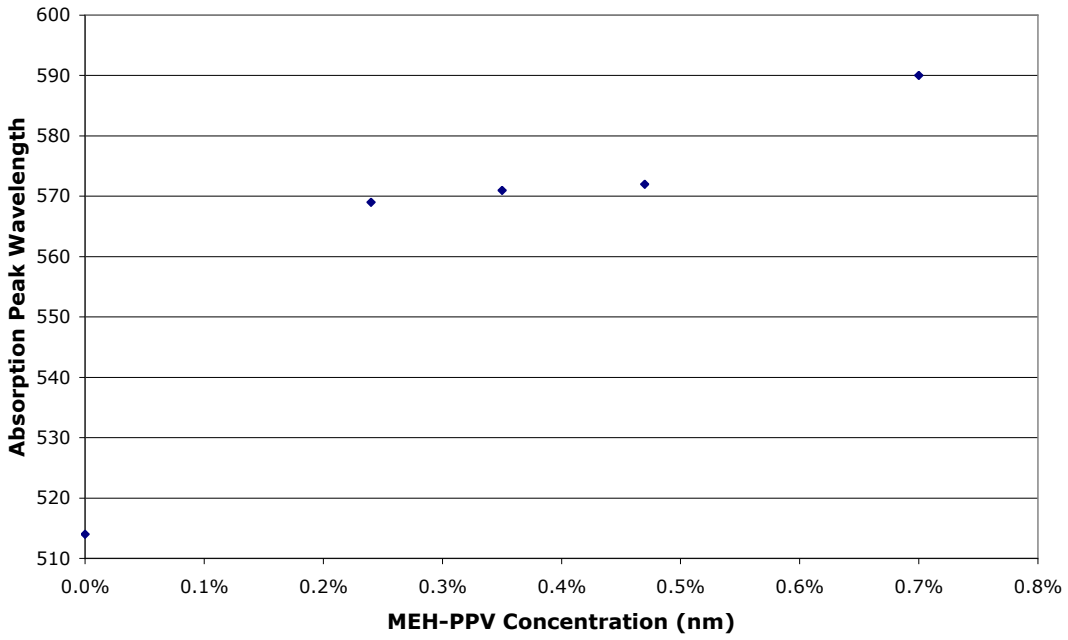

Figure 53: (a) MEH-PPV absorption of 0.24 % (◆), 0.35% (■), 0.45 % (▲), and 0.7 % (×) concentration in chloroform. (b) MEH-PPV absorption peak vs MEH-PPV concentration. 0% is for thin film absorption.

The absorption peak of the MEH-PPV thin film was measured at 514 nm. A significant redshift was observed for all concentrations of MEH-PPV nanofibers. The nanofiber made using a 0.7 % concentration solution was the highest recorded redshift. In addition to this experiment, 1.45% solution of 1:3 weight ratio MEH-PPV:PCBB in chlorobenzene were similarly electrospun and tested for absorption. Figure 54 shows the morphology of the collected nanofibers after PVP extraction with ethanol vapor.

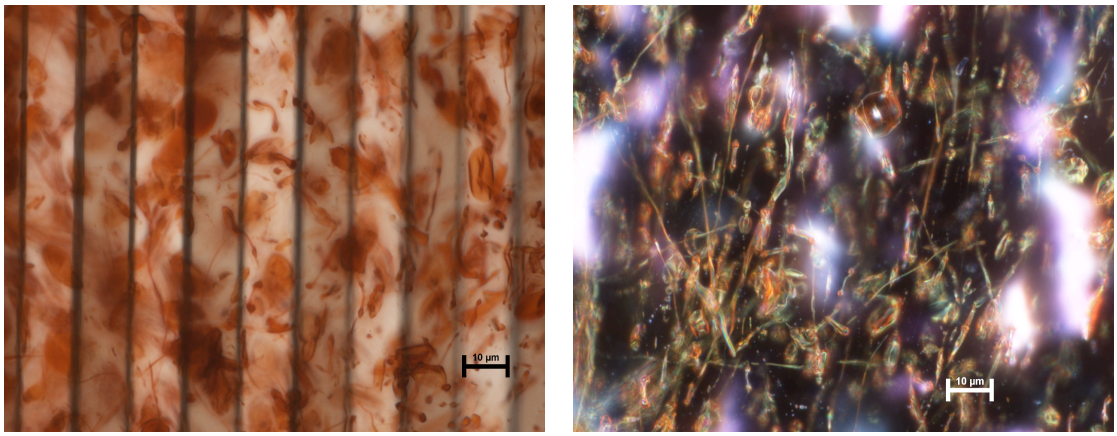

Figure 54: Bright field (Left), and dark field (Right) image of MEH-PPV:PCBB coaxial nanofibers washed with ethanol vapor.

As it was discussed earlier, nanofiber structure is poorly maintained for PCBB mixed MEH-PPV. However, the dark field still exhibits some nanofiber morphology and more importantly, the UV-Vis absorption measurement of the sample showed an absorption peak at 520 nm. This is a small red shift as compared to the MEH-PPV thin film. This experiment shows that the MEH-PPV red shift in nanofiber structures are observed even after a change in its solvent, and it agrees with the explanation that the red shift is mainly due to the stretching of the polymer chains from electrospinning [71].

9.2 Photoluminescence

In this work, MEH-PPV solutions 0.24, 0.30, 0.47, 0.70, 1.00 weight % in chloroform have been studied for absorption changes. From a series of absorption measurements, a red shift in MEH-PPV has been observed. However, these experiments have not been repeated for MEH-PPV in a chlorobenzene solution, and an explicit verification of absorption red shift in MEH-PPV with chlorobenzene needs to be

studied. In addition, photoluminescence(PL) measurementd have been performed for the same chloroform based MEH-PPV nanofibers where Figure 55 below shows a series of measured PL spectra.

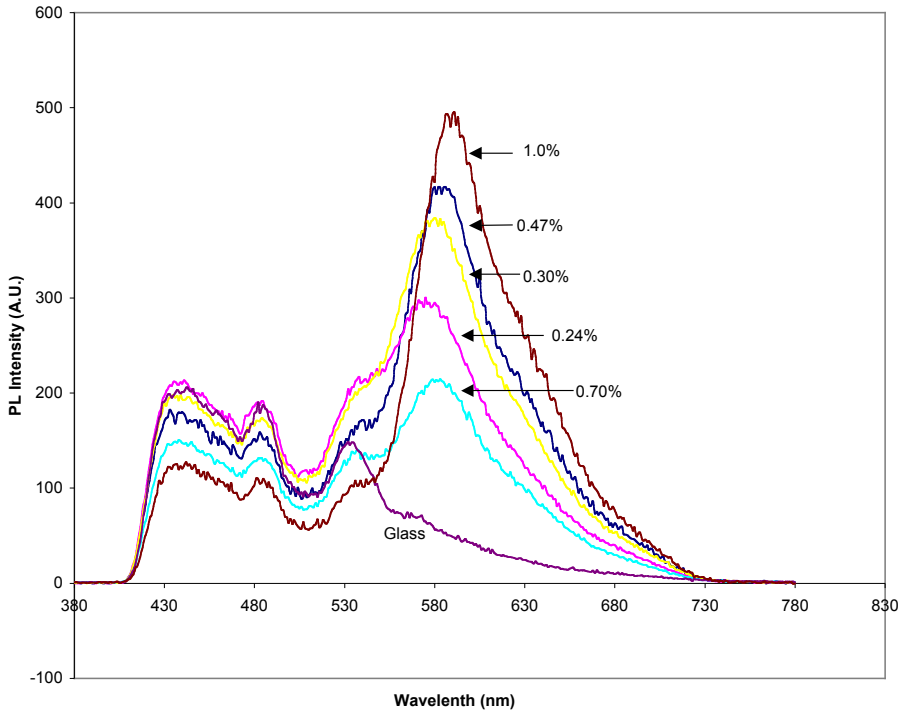

Figure 55: PL of MEH-PPV nanofibers with varying concentration of MEH-PPV solution.

The collected coaxial fibers on microscope glass slide were all soaked in Ethanol for 2 hours to remove the PVP shell followed by PL measurement of the MEH-PPV nanofibers. A consistent increase in PL intensity has been observed excluding nanofibers of 0.7 % MEH-PPV solution. We notice a potential correlation to the low PL intensity of 0.7 % MEH-PPV solution with its absorption measurement resulting in the largest red shift of 76 nm. The cause of inconsistency in 0.7 % PL is not yet understood, and needs further investigation.

10. Discussion and Analysis

The efficiency of the synthesized Electrospun polymer-fiber solar cells has been estimated to be 7.92×10^{-10} %, based on the total substrate area. The unique device structure with the Co-planar bimetallic interdigitated electrode substrate allows further evaluation of its efficiency from the total active nanofiber area. For this chapter, a detailed analysis of an actual efficiency extracted from the electrospun polymer-fiber solar cells is presented.

10.1 Active area of electrospun polymer-fiber solar cells

In preparation of the electrospun polymer-fiber device with the co-planar bimetallic interdigitated electrodes, an increased number of nanofibers on surface of the interdigitated electrodes will yield greater I-V curve response with higher numbers of active electrode-nanofiber-electrode junctions. However, one of the aims for this project is the characterization of the performance of a single electrode-nanofiber-electrode junction. To account for this measurement, a limited amount of nanofibers were collected for statistical analysis of a number of active nanofiber junctions.

There are a total of 638 electrodes in co-planar bimetallic interdigitated electrodes, and this implies 637 bimetallic solar cell junctions. Therefore, an active electrospun polymer-fiber solar cell exists for every nanofiber to bridge the bimetallic electrode separation. To get an estimate for a number of active electrospun polymer-fiber solar cells, the number of nanofibers bridging the electrode separation was recorded for every 10 electrode separation columns under an optical microscope of 100× magnification. An average number of electrode-nanofiber-electrode junctions per 10 electrode separation

columns were estimated after 18 of the 10 electrode separation columns, and the total number of electrode-nanofiber-electrode junctions on the co-planar bimetallic interdigitated electrodes were calculated with a weighted average estimate for every 50 electrode separation columns. As a result, we count a total of 28957.6 electrode-nanofiber-electrode junctions on the surface of the co-planar bimetallic interdigitated electrode. Based on the dimension of the fibers and the electrode separation, the actual efficiency of the electrospun polymer-fiber solar cells is estimated to be 3.08×10^{-7} %.

10.2 Efficiency Validation

With the unique device structure of co-planar bimetallic interdigitated electrode substrate, the 3.08×10^{-7} % efficiency of the electrospun polymer fiber solar cells has been shown to be better than the 8.7×10^{-8} % efficiency of Solar cloth presented by Sundarrajan [69]. Some assumptions have been made in evaluation of the total active area of the electrospun polymer-fiber solar cells, but these assumptions actually yield an overestimate of electrospun polymer-fiber area.

The first assumption made is with regard to the alignment of the nanofibers. For every nanofiber counted, it is assumed to be aligned orthogonally to the electrode surface. For every charge generated from MEH-PPV, charge collection is more likely for a shortest distance to the collector considering the effect of recombination. With this assumption, the active area for a single electrospun nanofiber is a product of 1 μm nanofiber diameter, and the average electrode separation of 1.97 μm. In addition, due to the cylindrical structure of the electrospun nanofibers, the actual point of nanofiber to

electrode contact can be much smaller compared to the diameter of the electrospun nanofiber as indicated in Figure 56 below.

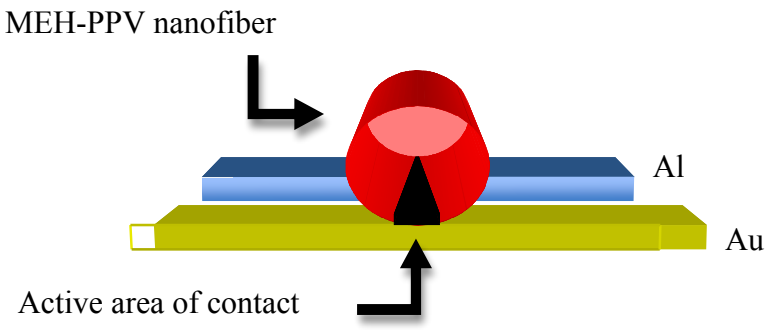

Figure 56Figure : Cross sectional image of an electrospun polymer-fiber solar cells.

The efficiency is inversely proportional to the active area of the device, and this overestimate of an electrospun polymer-fiber solar cells implies the device efficiency to be 3.08×10^{-7} % or better.

Another source of error can be considered from insufficient contact of electrospun polymer-fiber solar cell. The number of electrode-nanofiber-electrode junctions was evaluated from top-down view of the optical microscope, where an electrode to electrode contact was assumed for every nanofiber to bridge the electrode separation. However, if the electrode-nanofiber-electrode junction is viewed in cross section, there is a possibility where even with an apparent nanofiber bridge, no contact will be established as shown in Figure57.

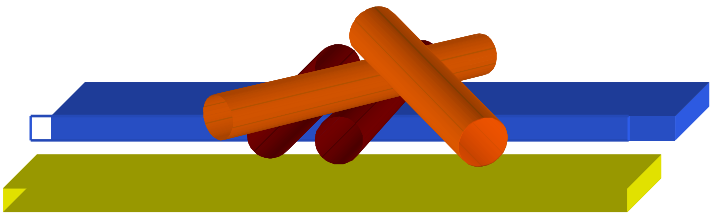

Figure 57: Schematic of electrospun nanofibers at one electrode-nanofiber-electrode junction. The orange cylindars indicate nanofibers with insufficient contact.

Without alignment of electrospun nanofibers, the random orientation of the collected nanofibers will result in nanofiber stacking, and this will prevent the complete formulation of electrode-nanofiber-electrode junctions. However, this incomplete form of electrode-nanofiber-electrode junctions will appear to be complete from the optical microscope, but this potential lack of contact will lead to an over estimate in total number of complete electrode-nanofiber-electrode junctions. With all considerations for errors in the active area measurement, a more likely overestimate of our active area allows us to conclude that the efficiency of our electrospun polymer-fiber solar cell is 3.08×10^{-7} % or better.

10.3 Equivalent Circuit

To further understand the performance of our device, an equivalent circuit analysis has been performed. In a typical solar cell, series resistance (R_s) of a device is the sum of limited conductivity of the material, contact resistance between semiconductor and the electrodes, and other contact resistance with the electrodes to the external circuit. In addition, a solar cells will have shunt resistance (R_{sh}) which is lowered by the leakage

current, and charge carrier recombination. An equivalent circuit for a solar cell is as shown in Figure 58.

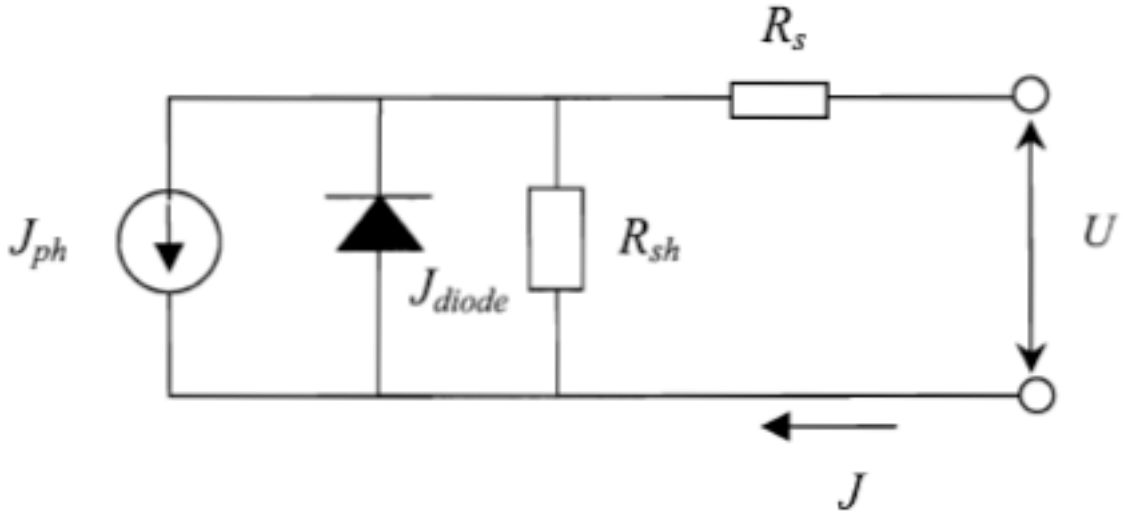

Figure 58: Solar cell Equivalent circuit.

From this equivalent circuit, the current-voltage characteristic for a solar cell is a sum of a diode current, shunt resistance current, and the photo-induced short circuit current that can be expressed as,

$$J = J_0\left[\exp\left(\frac{q}{nkT}(U - JR_sA)\right) - 1\right] + \frac{U - JR_sA}{R_{sh}A} - J_{ph}$$

where J_0 is the diode saturation current, q the elementary charge, n the ideality factor, k the Boltzman constant, T is the temperature, A for the active area, and J_{ph} is the photo-induced short circuit current. For an ideal solar cell, R_s would be 0 Ω with an infinite R_{sh}.

10.3.1 Influence of ideality factor

Ideality factor describes how closely a diode follows the theoretical prediction of an ideal diode. The number typically ranges in 1<n<2 where n=1 is considered for an ideal diode. For our device, assuming R_s=0 Ω and substituting all necessary parameters in the current-voltage characteristic equation with J_0=1.74852×10^{-7} μA/cm^2, T=295.75 K, A=0.057 mm^2, R_{sh}=10 TΩ and J_{ph}= 0.525 μA/cm^2, the voltage is dependent on the ideality factor as shown in Figure59.

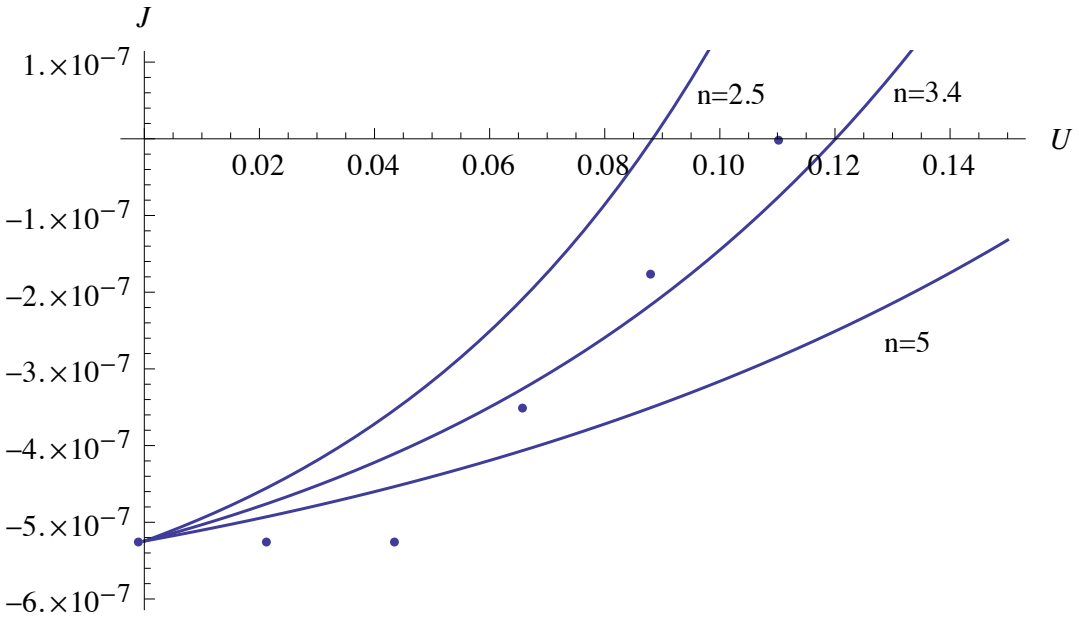

Figure 59: Current voltage characteristics of the electrospun polymer-fiber solar cell with varying Ideality factor. The dots are actual data points collected from the electrospun polyer-fiber solar cell under illumination.

It is evident from figure above that the voltage of the current-voltage characteristic equation is dependent on the ideality factor. With consideration for an open circuit voltage error estimate of 10%, an ideality factor was found to be in the range of 2.84 ≤ n ≤ 3.4. However in comparison with the electrospun polymer-fiber solar cell data, n=3.4

resulted in the best fit for an open circuit voltage U_{oc} of 0.11 V. An estimated ideality factor of n=3.4 has been found to be unusually high for a typical solar cell. High ideality factor generally is an indication of multilevel charge recombination sites. In addition, electrospun nanofibers are known to reduce the depletion width resulting in an increased probability of tunneling along with thermionic emission at the electrode nanofiber junction [92], and thus the ideality factor of n=3.4 for the electrospun polymer-fiber solar cell.

10.3.2 Influence of shunt resistance

To understand the influence of shunt resistance in our eletrospun polymer-fiber solar cell, series resistance R_s= 0 Ω is chosen. Figure 60 are current-voltage characteristics of the elctrospun polymer-fiber solar cell with increasing shunt resistance.

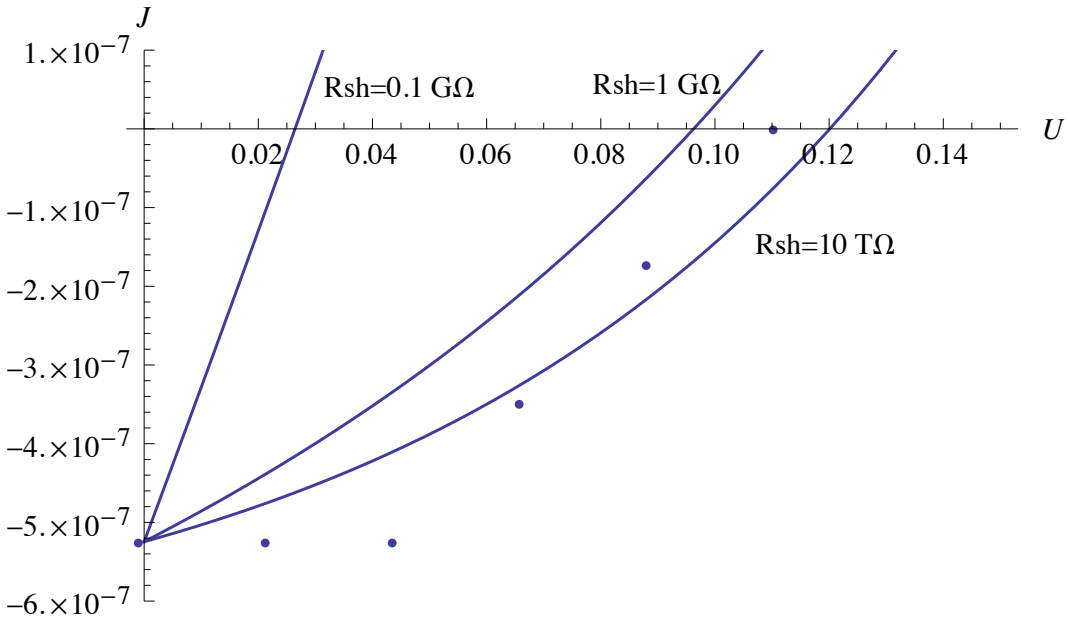

Figure 60: Current-voltage characteristic equation of electrospun polymer-fiber solar cells with increasing shunt resistance where R_s=0.

When the current-voltage characteristic equation is applied in the electrospun polymer-fiber solar cell, all graphs converge at the short circuit current density J_{sc}= -0.525 μA/cm^2, while the open circuit voltage and the Fill factor appears to be proportional to the shunt resistance. After reaching a value of R_{sh}=10 TΩ, further increase in shunt resistance has been found to cause no further improvement in open circuit voltage and fill factor. Applying the current-voltage characteristic equation to the collected data, the shunt resistance of the electrospun polymer-fiber solar cell is found to be approximately 10 TΩ.

10.3.3 Influence of series resistance

To understand the influence of series resistance, we assume infinite shunt resistance. Figure 61 are current-voltage characteristics of the elctrospun polymer-fiber solar cell with increasing series resistance.

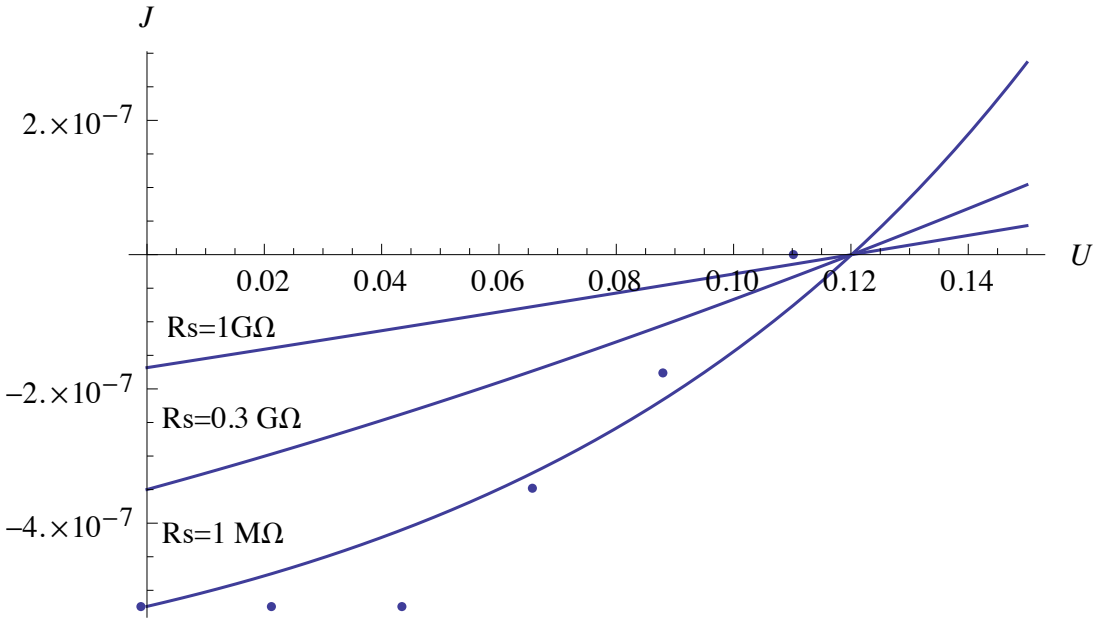

Figure 61: Current-voltage characteristic equation of electrospun polymer-fiber solar cells with increasing series resistance where $R_{sh}=\infty$.

Applying the current-voltage characteristic equation for the electrospun polymer-fiber solar cell shows that the short circuit current and the fill factor is inversely proportional to the series resistance while all current-voltage curve converge at the open circuit voltage of 0.12 V for the ideality factor of 3.4. From careful analysis of our current-voltage characteristics, we find that further decrease in series resistance below 1 MΩ gives no further improvement in short circuit current and fill factor of the device. In application of the current-voltage characteristic equation, we find the series resistance of electrospun polymer-fiber solar cell to be approximately 1 MΩ.

10.3.4 Characteristic of electrospun polymer-fiber devices

From the equivalent circuit analysis, n of 3.4, R_{sh} of 10 TΩ assuming $R_s=0$, and an R_s of 1 MΩ or less assuming $R_{sh}=\infty$ have been found. The high ideality factor for the device has been attributed to the nanofibers structurally induced multi-level recombination sites. An interesting characteristic in the device is the overestimate of its 1 MΩ series resistance. Solar cells are generally known to have better performance under low series resistance, and this is evident from inverse proportionality of series resistance to the fill factor of solar cells. The electrospun polymer-fiber solar cell fill factor reached a limit in its improvement with the series resistance as high as 1 MΩ. The series resistance of the device is 1 MΩ or less, and this is also an implication that an electrospun polymer-fiber solar cells are functional under high series resistance.

Similarly, high shunt resistance of the device implies stable device performance of the circuit. However, the efficiency of the device is relatively small compared with other organic solar cell devices, and further research is needed for better power extraction for an electrospun polymer-fiber solar cell.

Although there is some uncertainty in the exact value of the device parameters, our calculation shows that the device has a high ideality factor because of defects leading to recombination. It also has a high shunt resistance because of limited leakage current to the silicon dioxide substrate, and it has a relatively high series resistance due to long fiber length and poor contact with the electrodes.

11. Conclusion and Future Studies

11.1 Conclusion

In this work, MEH-PPV:PCBM based electrospun polymer-fiber solar cells have been studied. Organic solar cells synthesized with electrospinning offers improved carrier transport, charge transfer, shunt resistance, charge collection, mobility enhancement, and absorption tuning. Improvement in these parameters with proper power extraction will potentially improve device performance, and will add a new device structure to organic solar cells.

Electrospinnable polymer mixing, and multi-layer electrospinning have been discussed for electrospinning of conjugated polymers. MEH-PPV, P3HT, and PTEBS were all considered for electrospun polymer-fiber solar cell device synthesis. Electrospinnable polymer mixing of PTEBS resulted in Bimodal fibers, while P3HT maintained its electrical properties with some degradation. Coaxial electrospinning of PTEBS were unstable showing sensitivity to humidity, and MEH-PPV showed good nanofiber structure and electrical response when coaxially electrospun as a core solution.

Different device structures for an electrospun polymer-fiber solar cell have been considered. A conventional metal-semiconductor-metal device structure was limited by low charge carrier mobility, and a triaxial nanofiber device structure lacked in good conductor solution for the core and outer layer of the conjugated polymer-fiber solar cell. The Co-planar bimetallic interdigitated electrode substrate was developed for simple electrospun polymer-fiber device fabrication. Preliminary tests of the co-planar bimetallic interdigitated substrate using an MEH-PPV:PCBB film resulted in a working

solar cell of $3.53x10^{-4}$ % neglecting non-active area from the electrodes. Successful synthesis of electrospun polymer-fiber solar cells was done with coaxially electrospun fibers collected onto the co-planar bimetallic interdigitated electrode, and further extraction of electrically insulating shell of the coaxial nanofibers.

Materials used for the electrospun polymer-fiber solar cell synthesis were selected based on their electrospinnability, and their absorption properties. Reports of red shift are often observed for MEH-PPV rather than the P3HT polymer, and this is verified from the 76 nm red shift observed in our solution concentration based MEH-PPV nanofiber absorption experiments. In addition, nanofiber morphology after polymer shell extraction was maintained for coaxial electrospinning of MEH-PPV:PCBM mixture instead of P3HT:PCBM mixture. The use of PCBB as an electron acceptor has failed to maintain nanofiber morphology after polymer shell extraction, while a PCBM mixture in MEH-PPV was consistently able to maintain nanofiber morphology. The use of chlorobenzene for MEH-PPV has shown to be a better solvent in comparison to chloroform with a slight red shift in its Photoluminescence spectrum, and from better quantum yield reported from other references. Therefore, an MEH-PPV:PCBM mixture in chlorobenzene solution was chosen for the electrospun polymer-fiber solar cell synthesis. Optimum device performance for the MEH-PPV:PCBM mixture bulk heterojunction solar cell is observed for a weight ratio of 1:4 respectively. However, the MEH-PPV:PCBM solution mixtures were limited to a weight ratio of 1:2.5 due to an induced instability in its coaxial electrospinning for higher PCBM concentrations.

Finally, an electrospun polymer-fiber solar cell was synthesized from an MEH-PPV:PCBM mixture in chlorobenzene solution using coaxial electrospinning. From

acareful estimate of the active area in an electrospun polymer-fiber solar cell, the device achieved a power conversion efficiency of $\eta=3.08 \times 10^{-7}$ %, a short circuit current of J_{sc}= 0.525 μA/cm^2, an open circuit voltage of U_{oc}= 0.11 V, and a fill factor of *ff*= 0.43. From the equivalent circuit analysis, an ideality factor of n=3.4, shunt resistance of R_{sh}=10 TΩ, and a series resistance of R_s= 1 MΩ has been estimated. These parameters show stability with the device being functional under high series resistance, and an advantage of electrospinning leading to a burning of the shunts [73] is also verified with high shunt resistance of the device.

11.2 Future Studies

The electrospun polymer-fiber solar cell prepared in this work is the first device to be prepared from MEH-PPV. The unique device structure, and its device parameters needs further investigation through experiments with absorption, Photoluminescence, and mobility measurements. In addition, other optimization processes may be introduced for better performance, and stability of the device.

11.2.1 Mobility measurement

From generation of excitons, the holes travel to the cathode, and high hole mobility is required for efficient charge transfer in an organic solar cell. Increase in mobility of the generated charges are often reported in electrospinning experiments. With successful synthesis of electrospun polymer-fiber solar cell, change in mobility from the structural change in organic solar cell needs to be investigated. Hall effect is often used for mobility measurements, but low mobility of polymers are often difficult

for measurement [93]. Instead for low mobility materials, Time-of-flight (TOF) [94], field-effect transistor (FET) measurement [95], space-charge limited current (SCLC) measurement [34], and pulse radiolysis time-resolved microwave conductivity (PR-TRMC) [96] technique may be used.

11.2.2 Device optimization

11.2.2.1 Co-planar bimetallic interdigitated electrode

Our electrospun polymer-fiber solar cell was synthesized by nanofiber collection on the surface of Co-planar bimetallic interdigitated electrode. The electrode separations of 1.61 μm and 2.34 μm has been achieved for a functional device using MEH-PPV:PCBM nanofibers. However, this electrode separation much greater than the MEH-PPV exciton diffusion length of 20 ± 3 nm, and this will result in greater charge recombination, and decreased charge collection [27]. By reduction of co-planar bimetallic interdigitated electrode separation, an improved charge collection, increased short circuit current, and an overall improvement in device efficiency are expected. The co-planar bimetallic interdigitated electrode was prepared using photolithography, but a Scanning electron Microscope technique is expected to provide better resolution resulting in smaller electrode separation.

11.2.2.2 Control of fiber diameters

The electrospun polymer-fiber solar cell had a fiber diameter of ~1 μm. This fiber diameter is too large for efficient charge collection to consider for the MEH-PPV hole mobility. With a reduction in the polymer fiber diameter, there will be an improved charge collection. Control of the fiber diameter in electrospinning may be achieved through changing the solution concentration, and other parameters which may effect the resulting nanofiber diameter.

11.2.2.3 P3HT for electrospun polymer-fiber solar cells

P3HT is a conjugated polymer that has been a popular choice for fabrication of organic solar cells with its ability to produce high efficiency organic solar cells. Although the P3HT polymer has shown good photoelectric activity in our experiments, electrospinning of P3HT has continued to fail in maintaining its nanofiber structure through the PVP polymer extraction process of coaxial electrospinning. However with proper optimization of the electrospinning experiment, P3HT nanofibers has been synthesized with it electronic properties maintained [63]. A mixture of PCBM in such polymer may produce a nanofiber of good solar cell performance collected over the co-planar bimetallic interdigitated electrode, and the device parameter maybe compared with those synthesized by Subramanian et al for the difference in their device structure [69].

11.2.2.4 Triaxial nanofiber solar cell

In the earlier chapter, an electrospun polymer-fiber solar cell of triaxial nanofiber structure has been discussed. Synthesis of such device proves to be difficult due to limited choices for the conductive solutions, a need for transparent outer electrode layer, and establishment of electrical contact between the core electrode layer, and the outer electrode layer. However, the triaxial nanofiber structure for a solar cell has many advantages such as its as-spun device preparation process, nanoscale active layer for low polymer diffusion length of polymers, potentially improved mobility, and red shift. Further investigation in synthesis of conductive nanofibers may further the research in triaxial organic solar, and such device will introduce a new device structure to organic solar cells.

References

[1] "I N T E R N A T I O N A L E N E RGY A G E N CY KEY WORLD ENERGY," *Energy*, 2008.

[2] M. K. Hubbert, "Darcy's Law and the Field Equations of the Flow of Underground Fluids," *Hydrological Sciences Journal*, vol. 2, no. 1. pp. 23-59, 01-Mar-1957.

[3] G. Lewis, Nathan S. and Crabtree, *Basic Research Needs for Solar Energy Utilization*. 2005, pp. 1-276.

[4] G. L. Pearson, D.M. Chapin, C.S. Fuller, "A New Silicon p-n Junction Photocell for Converting Solar Radiation into Electrical Power," *Journal of Applied Physics*, vol. 25, pp. 676-677, 1954.

[5] R. H. Fahrenbruch, Alan L, Bube, *Fundamentals of solar cells: photovoltaic solar energy conversion*. New York: Academic Press, 1983, p. 559 p.

[6] C. Goh, M.D. McGehee, *Organic solar cells for low-cost solar cells*. American Institute of Physics, 2008, pp. 978-0-7354-0572-1.

[7] D. E. Carlson, and C. R. Wronski, "Amorphous Silicon Solar Cell," *Applied Physics Letters*, vol. 28, no. 11, pp. 671-3, 1976.

[8] S. Guha, J. Yang, and a Banerjee, "Amorphous silicon alloy photovoltaic research-present and future," *Progress in Photovoltaics: Research and Applications*, vol. 8, no. 1, pp. 141-150, Jan. 2000.

[9] V. H. Marín, L. E. Delgado, and A. Tironi, "World Record: 41.1% efficiency reached for multi-junction solar cells at Faunhofer ISE," *Nature*, vol. 466, no. 7308, p. 815, Aug. 2010.

[10] "NREL News - NREL Solar Cell Sets World Efficiency Record at 40," 2008. [Online]. Available: http://www.nrel.gov/news/press/2008/625.html. [Accessed: 14-Jun-2011].

[11] "UD-led team sets solar cell record, joins DuPont on $100 million project," 2007. [Online]. Available: http://www.udel.edu/PR/UDaily/2008/jul/solar072307.html. [Accessed: 14-Jun-2011].

[12] A. Slaoui and R. T. Collins, "Advanced inorganic materials for photovoltaics," *MRS Bulletin*, vol. 32, no. 3, pp. 211-218, 2007.

[13] Meng Tao, “Inorganic Photovoltaic Solar Cells: Silicon and Beyond,” 2008. [Online]. Available: www.electrochem.org/dl/interface/wtr/wtr08/wtr08_p30-35.pdf. [Accessed: 14-Jun-2011].

[14] J. Goetzberger, Adolf; Knobloch, “Crystalline Silicon Solar Cells,” p. 229, 1998.

[15] S.-S. H. P.H. Fang, *Investigation of Organic Semiconductor for Photovoltaic Application*. 1971, p. 43.

[16] A. K. Ghosh and T. Feng, “Erratum: Rectification, space-charge-limited current, photovoltaic and photoconductive properties of Al/tetracene/Au sandwich cell,” *Journal of Applied Physics*, vol. 45, no. 2, p. 977, 1974.

[17] L. E. and O. M. G. Newman. Lyons, “Photovoltages in Tetracene Films,” *Australian Journal of Chemistry*, vol. 24, no. 1, pp. 13-23, 1970.

[18] T. K. Mukherjee, “Photoconductive and photovoltaic effects in dibenzothiophene and its molecular complexes,” *The Journal of Physical Chemistry*, vol. 74, no. 15, pp. 3006-3014, Jul. 1970.

[19] E. E. Reucroft, P.J.; Kronick, P.L.; Hillman, “Research Directed Toward the Study of Materials for Organic Photovoltaic Cells,” *Journal of the Electrochemical Society*, vol. 114, no. 10, pp. 1054-1057, 1968.

[20] H. Shirakawa and A. G. Macdiarmid, “Electrical conductivity in doped polyacetylene,” *Physical Review*, vol. 39, no. 17, pp. 1098-1101, 1977.

[21] G. A. Chamberlain, “Organic solar cells: a review,” vol. 8, pp. 47 - 83, 1983.

[22] Y. Harima, K. Yamashita, and H. Suzuki, “Spectral sensitization in an organic p-n junction photovoltaic cell,” *Nature*, vol. 45, no. November, pp. 1144-1145, 1984.

[23] W. Tang, “Two-layer organic photovoltaic cell c.,” *Semiconductors*, vol. 14650, no. 1985, pp. 1985-1987, 2011.

[24] W. U. Huynh, X. Peng, and A P. Alivisatos, “CdSe Nanocrystal Rods/Poly(3-hexylthiophene) Composite Photovoltaic Devices,” *Advanced Materials*, vol. 11, no. 11, pp. 923-927, Aug. 1999.

[25] E. Kymakis and G. A J. Amaratunga, “Single-wall carbon nanotube/conjugated polymer photovoltaic devices,” *Applied Physics Letters*, vol. 80, no. 1, p. 112, 2002.

[26] E. Kymakis, I. Alexandrou, and G. a J. Amaratunga, “High open-circuit voltage photovoltaic devices from carbon-nanotube-polymer composites,” *Journal of Applied Physics*, vol. 93, no. 3, p. 1764, 2003.

[27] A Breeze, Z. Schlesinger, S. Carter, and P. Brock, "Charge transport in TiO2/MEH-PPV polymer photovoltaics," *Physical Review B*, vol. 64, no. 12, pp. 1-9, Sep. 2001.

[28] C. J. Brabec, *Organic Photovoltaics: Concepts and Realization*. Springer Series in Materials Science., 2003.

[29] Q. Qiao, "Characteristics of water-soluble polythiophene : TiO_2 composite and its application in photovoltaics," pp. 26-28, 2005.

[30] Q. Qiao, J. Beck, and J. T. Mcleskey, "Photovoltaic Devices from Self-doped Polymers," in *Proceedings of SPIE Vol. 5938*, 2005, vol. 5938, pp. 1-9.

[31] Q. Qiao, W. C. Kerr, J. Beck, E. Corrigan, and J. T. Mcleskey, "Optimization of Photovoltaic Devices from Layered PTEBS and Nanocrystalline TiO_2 ," *ECS Transactions*, vol. 1, no. 33, pp. 1-6, 2006.

[32] Q. Qiao and J. T. McLeskey, "Water-soluble polythiophene/nanocrystalline TiO_2 solar cells," *Applied Physics Letters*, vol. 86, no. 15, p. 153501, 2005.

[33] K. W. Cheng. and W. K. Chan. C Y Kwong, W C H Choy, A B Djurisic, P C Chui, "Poly(3-hexylthiophene):TiO_2 nanocomposites for solar cell applications," *Nanotechnology*, vol. 15, pp. 1156-1161, 2004.

[34] S.S. Sun and N. S. Sariciftci, *Organic Photovoltaics: Mechanisms, Materials, and Devices*. CRC Press, 2005.

[35] B. F. Zhang, E. Perzon, X. Wang, W. Mammo, M. R. Andersson, and O. Inganäs, "Polymer Solar Cells Based on a Low-Bandgap Fluorene Copolymer and a Fullerene Derivative with Photocurrent Extended to 850 nm **," *Advanced Functional Materials*, vol. 15, no. 5, pp. 745-750, 2005.

[36] B. C. J. Brabec et al., "A Low-Bandgap Semiconducting Polymer for Photovoltaic Devices and Infrared Emitting Diodes **," *Advanced Functional Materials*, vol. 12, no. 10, pp. 709-712, 2002.

[37] H.-yu Chen et al., "Polymer solar cells with enhanced open-circuit voltage and efficiency," *Nature*, vol. 3, pp. 649-653, 2009.

[38] A. J. Janssen, M. M. Wienk, and M. P. Struijk, "Low band gap polymer bulk heterojunction solar cells," *Chemical Physics Letters*, vol. 422, pp. 488-491, 2006.

[39] L. M. Campos et al., "Extended Photocurrent Spectrum of a Low Band Gap Polymer in a Bulk Heterojunction Solar Cell," *Chemistry of Materials*, vol. 17, no. 16, pp. 451-452, 2005.

[40] M. M. Wienk, M. G. R. Turbiez, M. P. Struijk, M. Fonrodona, and R. A. J. Janssen, "Low-band gap poly(di-2-thienylthienopyrazine):fullerene solar cells," *Applied Physics Letters*, vol. 88, pp. 3-5, 2006.

[41] X. Wang, E. Perzon, and F. Langa, "Infrared photocurrent spectral response from plastic solar cell with low-band-gap polyfluorene and fullerene derivative," *Applied Physics Letters*, vol. 85, no. 21, pp. 5081-5083, 2004.

[42] X. Wang et al., "Enhanced Photocurrent Spectral Response in Low-Bandgap Polyfluorene and C_{70} -Derivative-Based Solar Cells **," *Advanced Functional Materials*, vol. 15, pp. 1665-1670, 2005.

[43] N. S. Sariciftci, "Photoinduced electron transfer from conducting polymers onto Buckminsterfullerene," *Proceedings of SPIE*, vol. 1852, pp. 297-307, 1993.

[44] Y. Ohsawa and T. Saji, "Electrochemical Detection of $C_{60}^{(6-)}$ at Low Temperature," *Journal of the Chemical Society, Chemical Communications*, p. 781, 1992.

[45] W. U. Huynh, J. J. Dittmer, and a P. Alivisatos, "Hybrid nanorod-polymer solar cells.," *Science (New York, N.Y.)*, vol. 295, no. 5564, pp. 2425-7, Mar. 2002.

[46] N. S. Sariciftci, D. Braun, and C. Zhang, "Semiconducting polymer-buckminsterfullerene photodiodes , and photovoltaic cells heterojunctions : Diodes ," *Applied Physics Letters*, vol. 62, no. 6, pp. 585-587, 1993.

[47] S.G. Chen, P. Stradins, and B. A Gregg, "Doping highly ordered organic semiconductors: experimental results and fits to a self-consistent model of excitonic processes, doping, and transport.," *The journal of physical chemistry. B*, vol. 109, no. 28, pp. 13451-60, Jul. 2005.

[48] A. B. Holmes. R N Marks, J J M Halls, D D C Bradley, R H Friend, "The photovoltaic response in poly(p-phenylene vinylene) thin-film devices," *Journal of Physics-Condensed Matter*, vol. 6, pp. 1379-1394, 1994.

[49] S. Barth and H. Bässler, "Intrinsic Photoconduction in PPV-Type Conjugated Polymers," *Physical Review Letters*, vol. 79, no. 22, pp. 4445-4448, Dec. 1997.

[50] V. D. Mihailetchi et al., "Electron Transport in a Methanofullerene," *Advanced Functional Materials*, vol. 13, no. 1, pp. 43-46, Jan. 2003.

[51] G. Yu, K. Pakbaz, and A. J. Heeger, "Semiconducting polymer diodes : Large size , low cost photodetectors with excellent visible-ultraviolet sensitivity," *Applied Physics Letters*, vol. 64, no. 25, pp. 3422-3424, 1994.

[52] H. Kim, J. Young, K. Lee, Y. Park, Y. Jin, and H. Suh, "Organic photovoltaic cells based on conjugated polymer / fullerene composites.," *Current Applied Physics*, vol. 1, pp. 139-143, 2001.

[53] S. S. Hoppe, Harald Niyazi, "Organic solar cells: An overview," *Journal of Materials research*, vol. 19, no. 7, pp. 1924-1945, 2004.

[54] G. E. Jabbour. Sean E. Shaheen, David S. Ginley, "Organic based photovoltaics toward low cost power generation.," *MRS Bulletin*, vol. 30, pp. 10-19, 2005.

[55] N. Greenham, X. Peng, and A.P. Alivisatos, "Charge separation and transport in conjugated polymer/cadmium selenide nanocrystal composites studied by photoluminescence quenching and photoconductivity*," *Synthetic Metals*, vol. 84, no. 1-3, pp. 545-546, Jan. 1997.

[56] A. P. Alivisatos. N.C. Greenham, X.P., "A CdSe nanocrystal/MEH-PPV polymer composite photovoltaic.," in *First NREL Conference*, 1997.

[57] G. Yu, J. Gao, J. C. Hummelen, F. Wudl, and A. J. Heeger, "Polymer Photovoltaic Cells : Enhanced Efficiencies via a Network of Internal Donor-Acceptor Heterojunctions," *Science*, vol. 270, no. 5243, pp. 1789-1791, 1995.

[58] Z. Huang, "A review on polymer nanofibers by electrospinning and their applications in nanocomposites," *Composites Science and Technology*, vol. 63, no. 15, pp. 2223-2253, Nov. 2003.

[59] W. E. Teo and S. Ramakrishna, "A review on electrospinning design and nanofibre assemblies.," *Nanotechnology*, vol. 17, no. 14, p. R89-R106, Jul. 2006.

[60] J. A. Matthews, E. D. Boland, G. E. Wnek, D. G. Simpson, and G. L. Bowlin, "Compatible Polymers Electrospinning of Collagen," *Journal Of Bioactive And Compatible Polymers*, vol. 18, 2003.

[61] I. Hayati, "Investigations into the mechanisms of electrohydrodynamic spraying of liquids," *Journal of Colloid and Interface Science*, vol. 117, no. 1, pp. 205-221, May. 1987.

[62] T. Subbiah, G. S. Bhat, R. W. Tock, S. Parameswaran, and S. S. Ramkumar, "Electrospinning of nanofibers," *Journal of Applied Polymer Science*, vol. 96, no. 2, pp. 557-569, Apr. 2005.

[63] S. Lee, G. D. Moon, and U. Jeong, "Continuous production of uniform poly(3-hexylthiophene) (P3HT) nanofibers by electrospinning and their electrical properties," *Journal of Materials Chemistry*, vol. 19, no. 6, p. 743, 2009.

[64] Q. Zhao, Y. Xin, Z. Huang, S. Liu, C. Yang, and Y. Li, "Using poly[2-methoxy-5-(2′-ethyl-hexyloxy)-1,4-phenylene vinylene] as shell to fabricate the highly fluorescent nanofibers by coaxial electrospinning," *Polymer*, vol. 48, no. 15, pp. 4311-4315, Jul. 2007.

[65] Y. Zhao, X. Cao, and L. Jiang, "Bio-mimic multichannel microtubes by a facile method.," *Journal of the American Chemical Society*, vol. 129, no. 4, pp. 764-5, Jan. 2007.

[66] V. Joo, Yong Lak, Kalra, J. H. Lee, J. H. Park, and M. Marquez, "Confined Assembly of Asymmetric Block-Copolymer Nanofibers via Multiaxial Jet Electrospinning.," *Small (Weinheim an der Bergstrasse, Germany)*, vol. 5, no. 20, pp. 2323-32, Oct. 2009.

[67] I. D. Norris, M. M. Shaker, F. K. Ko, and A. G. Macdiarmid, "Electrostatic fabrication of ultrafine conducting fibers : polyaniline/polyethylene oxide blends," *Synthetic Metals*, vol. 114, pp. 109-114, 2000.

[68] S. Chuangchote, T. Sagawa, and S. Yoshikawa, "Efficient dye-sensitized solar cells using electrospun TiO_2 nanofibers as a light harvesting layer," *Applied Physics Letters*, vol. 93, no. 3, p. 033310, 2008.

[69] S. Sundarrajan, R. Murugan, a S. Nair, and S. Ramakrishna, "Fabrication of P3HT/PCBM solar cloth by electrospinning technique," *Materials Letters*, vol. 64, no. 21, pp. 2369-2372, Nov. 2010.

[70] S. Berson, R. De Bettignies, S. Bailly, and S. Guillerez, "Poly(3-hexylthiophene) Fibers for Photovoltaic Applications," *Advanced Functional Materials*, vol. 17, no. 8, pp. 1377-1384, May. 2007.

[71] A. Babel, D. Li, Y. Xia, and S. A. Jenekhe, "Electrospun Nanofibers of Blends of Conjugated Polymers : Morphology , Optical Properties , and Field-Effect Transistors," *Macromolecules*, vol. 38, no. 11, pp. 4705-4711, 2005.

[72] T. Nguyen, "Control of Energy Transfer in Oriented Conjugated Polymer-Mesoporous Silica Composites," *Science*, vol. 288, no. 5466, pp. 652-656, Apr. 2000.

[73] F. Padinger, R. S. Rittberger, and N. S. Sariciftci, "Effects of Postproduction Treatment on Plastic Solar Cells," *Advanced Functional Materials*, vol. 13, no. 1, pp. 85-88, Jan. 2003.

[74] G. Li et al., "High-efficiency solution processable polymer photovoltaic cells by self-organization of polymer blends," *Nature Materials*, vol. 4, no. 11, pp. 864-868, Oct. 2005.

[75] C. Wu, S. Nagata, G. C. Tepper, and J. T. McLeskey, "Electrokinetic separation of co-solutes into bimodal fibers by electrospinning," *Applied Physics Letters*, vol. 92, no. 10, p. 101920, 2008.

[76] J. M. Deitzel, J. Kleinmeyer, D. Harris, and N. C. B. Tan, "The effect of processing variables on the morphology of electrospun nanofibers and textiles," *Polymer*, vol. 42, pp. 261-272, 2001.

[77] C.M. Hsu and S. Shivkumar, "N,N-Dimethylformamide Additions to the Solution for the Electrospinning of Poly(ε-caprolactone) Nanofibers," *Macromolecular Materials and Engineering*, vol. 289, no. 4, pp. 334-340, Apr. 2004.

[78] C.M. Hsu and S. Shivkumar, "Nano-sized beads and porous fiber constructs of Poly (ε-caprolactone) produced by electrospinning," *Journal of Materials Science*, vol. 39, pp. 3003 - 3013, 2004.

[79] P. Gupta and G. L. Wilkes, "Some investigations on the fiber formation by utilizing a side-by-side bicomponent electrospinning approach," *Polymer*, vol. 44, no. 20, pp. 6353-6359, Sep. 2003.

[80] R. Kessick and G. Tepper, "Microscale polymeric helical structures produced by electrospinning," *Applied Physics Letters*, vol. 84, no. 23, p. 4807, 2004.

[81] R. Kessick and G. Tepper, "Electrospun polymer composite fiber arrays for the detection and identification of volatile organic compounds," *Sensors and Actuators B: Chemical*, vol. 117, no. 1, pp. 205-210, Sep. 2006.

[82] S. Madhugiri, A. Dalton, J. Gutierrez, J. P. Ferraris, and K. J. Balkus, "Electrospun MEH-PPV/SBA-15 composite nanofibers using a dual syringe method.," *Journal of the American Chemical Society*, vol. 125, no. 47, pp. 14531-8, Nov. 2003.

[83] H. Yang and L. Dong, "Electroluminescent Organic Light Emitting Micro / Nanofibers Fabricated Using Three-fluid Coaxial Electrospinning," in *2009 IEEE Nanotechnology Materials and Device Conference*, 2009, pp. 118-120.

[84] Q. Qiao, J. Beck, R. Lumpkin, J. Pretko, and J. Mcleskey Jr, "A comparison of fluorine tin oxide and indium tin oxide as the transparent electrode for P3OT/TiO_2 solar cells," *Solar Energy Materials and Solar Cells*, vol. 90, no. 7-8, pp. 1034-1040, May. 2006.

[85] E. S. Kolesar Jr. and J. M. Wiseman, "Selective detection of nitrogen dioxide and diisopropyl methylphosphonate with an interdigitated gate electrode field-effect transistor (IGEFET)," *Sensors and Actuators B: Chemical*, vol. 5, no. 1-4, pp. 37-46, Aug. 1991.

[86] D. Josell et al., "Three Dimensionally Structured CdTe Thin-Film Photovoltaic Devices with Self-Aligned Back-Contacts: Electrodeposition on Interdigitated Electrodes," *Journal of The Electrochemical Society*, vol. 156, no. 8, p. H654, 2009.

[87] A. G. M.Niggemann, D. Ruf, B. Blasi, M. Glatthaar, M. Riede, C. Muller, B. Zimmermann, "Functional substrates for flexible organic photovoltaic cells," in *Proceedings of SPIE Vol. 5938*, 2005, vol. 5938, pp. 593802-1-593802-9.

[88] L. Xue, L. Liu, Q. Gao, S. Wen, J. He, and W. Tian, "Planar-diffused photovoltaic device based on the MEH-PPV/PCBM system prepared by solution process," *Solar Energy Materials and Solar Cells*, vol. 93, no. 4, pp. 501-507, Apr. 2009.

[89] J. Kronholm, D.; Hummelen, "Organic electronics," *Material Matters*, vol. 2, no. 3, pp. 1-32, Sep. 2007.

[90] O. A. Yassin. M.S. Alsalhi, K.H. Ibnaouf, V. Masilamani, "Excimer state of a conjugate polymer (MEH-PPV) in Liquid Solutions.," *Laser Physics*, vol. 17, no. 12, pp. 1361-1366, 2007.

[91] L. Zheng, Q. Zhou, X. Deng, M. Yuan, G. Yu, and Y. Cao, "Methanofullerenes Used as Electron Acceptors in Polymer Photovoltaic Devices," *The Journal of Physical Chemistry B*, vol. 108, no. 32. pp. 11921-11926, Aug-2004.

[92] R. Rivera and N. Pinto, "Schottky diodes based on electrospun polyaniline nanofibers: Effects of varying fiber diameter and doping level on device performance," *Physica E: Low-dimensional Systems and Nanostructures*, vol. 41, no. 3, pp. 423-426, Jan. 2009.

[93] A. M. Goodman, "Electron Hall effect in Silicon Dioxide," *Physical Review*, vol. 164, no. 3, pp. 1145-1150, Mar. 1967.

[94] P. Ravirajan, S. a Haque, J. R. Durrant, D. D. C. Bradley, and J. Nelson, "The Effect of Polymer Optoelectronic Properties on the Performance of Multilayer Hybrid Polymer/TiO_2 Solar Cells," *Advanced Functional Materials*, vol. 15, no. 4, pp. 609-618, Apr. 2005.

[95] C. D. Dimitrakopoulos and D. J. Mascaro, "Organic thin-film transistors: A review of recent advances," *IBM Journal of Research and Development*, vol. 45, no. 1, pp. 11-27, Jan. 2001.

[96] R. J. O. M. Hoofman, M. P. D. Haas, L. D. A. Siebbeles, and J. M. Warman, "Highly mobile electrons and holes on isolated chains of the semiconducting polymer poly(phenylene vinylene)," *Nature*, vol. 392, no. March, pp. 54-56, 1998.